2013

STICK-SLIP MECHANICAL MODELS FOR OVERHEAD ELECTRICAL CONDUCTORS IN BENDING
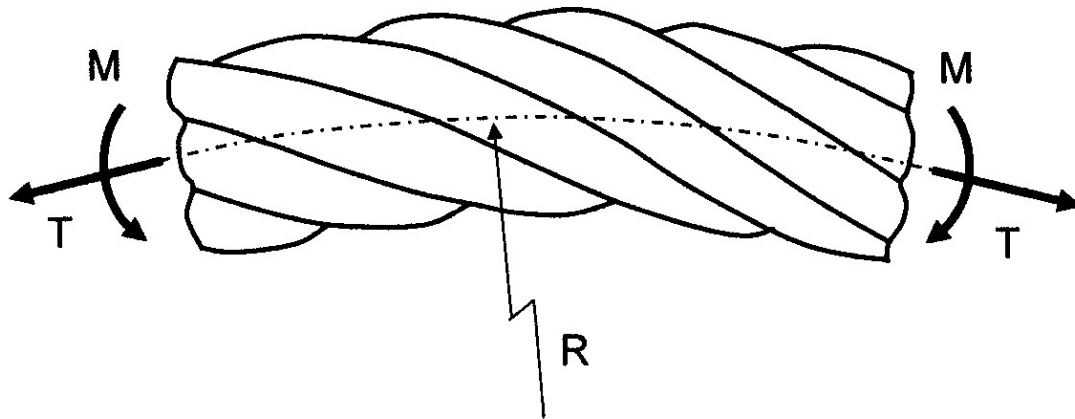
with Matlab® applications

Compared with wire ropes, overhead electrical conductors may seem relatively simple systems. However, when subjected to wind excitation, they undergo so-called Aeolian vibrations, with transverse small amplitude displacements corresponding to conductor bending. In such a motion, individual wire relative slip is restricted, up to a certain point, by friction forces. Thus, beyond a given bending amplitude, microslip occurs at some of the inter-layer contact points. The objective of this report is to present in a unified manner, and to compare, some analytical models which have been proposed in the literature, and which are basically stick-slip models based on Coulomb's laws of friction. These models are used to predict bending stiffness variation for single or multi-layer strands, be they single-strand cables or electrical conductors.

Alain Cardou, Ph.D
GREMCA, Université Laval, Québec
2013

STICK-SLIP MECHANICAL MODELS
FOR
OVERHEAD ELECTRICAL CONDUCTORS
IN BENDING

(with Matlab® applications)

by
Alain Cardou, Ph.D.
GREMCA, université Laval, Québec

2013

STICK-SLIP MECHANICAL MODELS
FOR
OVERHEAD ELECTRICAL CONDUCTORS
IN BENDING

(with Matlab® applications)

by
Alain Cardou, Ph.D.

To my GREMCA colleagues:

Louis, Sylvain and Claude

THE AUTHOR

Dr. Alain Cardou graduated in mechanical engineering from École Nationale Supérieure de Mécanique, now École Centrale de Nantes, France. He received his M.Sc. and Ph.D. degrees in mechanics and materials from the University of Minnesota, Minneapolis. While a professor at Laval University, Quebec City, his general research interests were stress and strength analysis, subjects on which he is author or coauthor of more than 100 papers. For several years, he has been involved in the Canadian Congress of Applied Mechanics (CANCAM) and was elected Fellow of the Canadian Society of Mechanical Engineers (CSME). He is currently adjunct professor at Laval University.

His interest in overhead conductor mechanics dates back to the early eighties when, in association with his colleague Dr. Louis Cloutier, he became involved in a project funded by the Canadian Electrical Association. While some of the work was performed in the Hydro-Quebec laboratories (IREQ), the project led to the creation of a fatigue test laboratory at Laval University, and to a research team now known as GREMCA, which stands for "Groupe de REcherche en Mécanique des Conducteurs Aériens", that is "Research Group on Overhead Conductor Mechanics". Activities of GREMCA are restricted to fatigue problems, which are typically clamp-conductor interaction problems. A number of industrial projects have been conducted in collaboration with various power utilities, Canadian and foreign. Besides standard clamp-conductor performance, they dealt with such systems as OPGW (optical ground wires) cables, trapezoidal wire conductors, spacer clamps etc. They were a source of more fundamental problems, an opportunity for graduate work subjects, experimental, analytical or numerical. For example, the question arises immediately of the applicability of constant amplitude test data to the actual variable amplitude field conditions or, simply put, is it possible to find some kind of cumulative damage law such as Miner's law in machine design? Work is still under way. Also, the fretting fatigue approach has been emphasized, leading to crack propagation studies at contact fret marks. An application was the evaluation of residual life of an actual power line reaching its nominal design life.

GREMCA studies have obtained a wide recognition from relevant technical committees acting within national or international bodies in the field of electric power transmission: Cigré (Conférence internationale des grands réseaux électriques), IEC (International Electrotechnical Commission), IEEE (Institute of Electrical and Electronics Engineers). Most notably, GREMCA members were asked to participate in the updating of EPRI's so-called "Orange Book": *EPRI Transmission Line Reference Book: Wind-Induced Conductor Motion: Second Edition.*EPRI. Palo Alto, CA. 2009. 1018554.

CONTENTS

LIST OF SYMBOLS

Latin alphabet

A_c area of core cross-section

A_i area of individual wire cross-section, layer (i)

(AE)   strand axial stiffness

$a_{c,j}$ parameter in limit tensile force F_{Li} ; $a_{c,i} = F_{Ti} - f_i$

$a_{i,j}$ parameters in limit tensile force F_{Li} ; $j \leq i$

B_c bending stiffness (core); $B_c = E_c I_c$

B_{comp} complementary bending stiffness; $B_{comp} = B_{max} - B_{min}$

B_{compI} complementary bending stiffness in domain (I) (no-slip)

B_{eq} equivalent bending stiffness

B_{max} maximum bending stiffness of strand

B_{minj} minimum bending stiffness of strand, as given by formula (j)

B_w bending stiffness (wire) (single-layer strand); $B_w = E_w I_w$

$B_{w,I}$ bending stiffness (wire) (layer (i)); $B_{w,i} = E_i I_i$

b_i parameter in limit tensile force F_{Li}

c_i parameter in limit tensile force F_{Li} (expression depends on selected model)

D_i diameter of lay cylinder, layer (i)

D_{oi} outer diameter, layer (i)

d_c core wire diameter ("king wire")

d_i wire diameter, layer (i)

d_{Ci} distance between contact points at interface (i), measured on wire of layer (i)

dF_{Li} limit value of dF_i at interface (i), in slip regime

dN_i radial force on a wire element, layer (i), at interface (i)

dN_i' radial force on a wire element, layer (i+1), at interface (i)

dQ_i tangential force on a wire element, layer (i), at interface (i)

dQ_i' tangential force on a wire element, layer (i+1), at interface (i)

ds_i length of wire element, layer (i)

E_c Young's modulus, core material

E_i Young's modulus, layer (i) material

E_w Young's modulus, wire material (single-layer strand)

F   tensile force on layer wire (single-layer strand)

F_c tensile force on core wire

F_{comp} complementary tensile force on layer wire, slip regime (single-layer strand)

F_i tensile force on individual wire of layer (i)

F_L limit tensile force on layer wire, in slip regime (single-layer strand)

F_{Li} limit tensile force on layer wire, in slip regime, layer (i)

F_{xi} axial component of tensile force F_i ; $F_{xi} = F_i \cos \alpha_i$

F_T tensile force on a wire arising from axial force T on strand (single-layer strand)

F_{ti} tangential component of tensile force F_i; $F_{ti} = F_i \sin \alpha_i$

f_i parameter in limit tensile force F_{Li}

h_i length of lay, layer (i)

I_c moment of inertia (core); $I_c = \pi d_c^4 / 64$

I_w moment of inertia (wire); $I_w = \pi d_w^4 / 64$

(i)   layer number (i=1 at outer layer, i=m at innermost layer, in contact with core wire) also interface between adjacent layers (i) and (i+1)

k_B bending stiffness ratio; $k_B = B_{max} / B_{min}$

k_i ratio $k_i = L / d_i \sin \alpha_i$

k_j numerical factor in Eq. (2.7) (j depends on selected model)

k_{bj} numerical factor in Eq. (2.16) (j depends on selected model)

k_{tj} numerical factor in Eq. (2.17) (j depends on selected model)

K   element stiffness in rheological model (one "spring" model)

K_i element stiffness in rheological model ("spring" (i))

L   an arbitrary length of strand, with $L \gg d_i$

M_I bending moment in domain (I)

M_{II} bending moment in domain (II)

M_i bending moment component arising from force F_i , wire (i) in slip regime

M_m median transition moment from domain (I) to domain (II) behaviour

M_{rf} residual bending moment on strand cross-section, in slip regime

M_{rfj} residual bending moment on strand cross-section, in slip regime (model (j))

m   number of layers in strand

N_{Ci} normal contact force at contact points at interface (i)

n_i number of wires in layer (i)

P   transverse force on clamped-clamped strand

q_{Fr} tangential line contact force on helical wire (single-layer)

q_L limit value of tangential contact force; $q_L = \mu q_N$

q_N normal line contact force on helical wire (single-layer)

q_{Ni} normal line contact force on wire of layer (i), interface (i)

q'_{Ni} normal line contact force on wire of layer (i+1), interface (i)

R_{Ci} radius of contact cylinder, interface (i)

R_i radius of lay cylinder, layer (i); $R_i = D_i / 2$

r_c core ("king") wire radius; $r_c = d_c / 2$

r_i wire radius, layer (i); $r_i = d_i / 2$

T   axial force on strand

U   energy

V   shear force in clamped-clamped strand

$\vec{V}_i$ velocity of contact point belonging to wire of layer (i)

$\vec{V}_r$ relative velocity of contacting points

v(x)   clamped-clamped strand transverse displacement

x   Cartesian x-axis, (generally, parallel to unbent strand axis)

Y_b strand bending amplitude (peak-to-peak) at standard distance from supported end

Greek alphabet

α_i lay angle of layer (i), complement of helix angle β_i

α_i' lay angle of layer (i), measured at interface (i)

α_i'' lay angle of layer (i), measured at interface (i-1)

β strand vibration parameter; $\beta = \lambda L / 2$

γ_i ratio $\gamma_i = r_i / R_{Ci}$

$\Delta(.)$ peak-to-peak amplitude of a cyclic quantity

δ_C clamped-clamped strand transverse center point deflection

ε_T wire axial unit strain, due to strand axial force T

ε_c core wire axial unit strain

ε_x strand axial unit strain

ε_{xi} layer unit strain in direction of strand axis

θ polar angle in strand cross-section (Fig. 2.1)

θ_b polar angle in strand cross-section where slip begins (impending slip)

κ bent strand curvature $\kappa = 1/\rho$

κ_b curvature at which slip begins in layer

κ_e "elastic" part of curvature in rheological model

κ_{bj} curvature at which slip begins in layer, model (j)

κ_m median transition curvature from domain (I) to domain (II) behaviour

κ_p "plastic" part of curvature in rheological model

κ_t curvature at which total slip occurs in layer

κ_{tj} curvature at which total slip occurs in layer, model (j)

λ strand vibration parameter; $\lambda^2 = T / B$

λ_i friction parameter at interface (i); $\lambda_i = \mu_i \sin \alpha_i$

μ friction coefficient

μ_i friction coefficient (interface (i))

ν Poisson's ratio

φ angle of bent clamped-clamped strand centerline

ϕ polar angle for curved strand centerline

ρ bent strand radius of curvature

ρ_{hi} helix principal radius of curvature, centerline of wire, layer (i)

σ_a cyclic stress amplitude in vibrating strand

σ_c normal stress on core cross-section

σ_i normal stress on wire cross-section, layer (i)

σ_T normal stress on wire cross-section, due to str

INTRODUCTION

The effect of bending on overhead electrical conductor strength is a technical problem of ongoing interest. It has been described in detail by national (IEEE, CEA) as well as international (Cigré) body publications. In particular, the so-called "Orange Book", published by the Electrical Power Research Institute (EPRI), is a comprehensive presentation of current knowledge on this subject. Its first edition dating from 1979 (EPRI, 1979), it has been updated in 2006 (with a hard-copy edition in 2009), where the Author participated in the revision of its Chapter 3, on conductor fatigue arising from Aeolian vibrations (Cloutier et al. 2006).

The objective of the EPRI book being to give quick, practical answers to the question of conductor fatigue, calculations are based on the simplest mechanical models available, even when knowing the actual behavior is much more complex. Thus, it is of some interest to also develop models that might give a deeper insight into the problem. More realistic models are also useful in the interpretation of experimental data.

Basic aspects of conductor bending are very similar to those of simple wire ropes. It is thus of no surprise that several works relating to these mechanical elements may provide a common approach to what can be called "helical strands". A review of the literature on the available models can be found in Cardou and Jolicoeur (1997). This review has been updated, at least with respect to the bending problem, by Cardou (2006). It will not be repeated here.

Although there have been more recent contributions (e.g. Hong *et al.*, 2005; Foti *et al.*, 2011), the approach on which the present work is based, follows that of Papailiou (1995), with some adjustments. It is to be noted Papailiou's model can be traced back to previous published works on cables, notably those of Lehanneur (1949), in France, and Ernst (1933), in Germany. They might be called "Coulomb models" as they are based on Coulomb's laws of friction applied locally along wire contact lines. Here, they will be referred as "stick-slip" models.

Other models can be found in the cable literature, which are mainly based on purely elastic and geometric considerations (Costello, 1997; Feyrer, 2007). As far as bending is concerned, these models are more technically suited to cables wound on pulleys or on drums, that is, small radius (high curvature) bending. By comparison, Coulomb models should be considered as more appropriate for so-called free-bending, which is the general situation for conductors at or near suspension clamps.

In all cases, simplifying hypotheses have to be made. For example, in the Coulomb models, Poisson's ratio effect is generally neglected. The only internal loads acting on a wire cross-section are assumed to be the normal force (tension) and the small bending moment arising from the strand curvature. In our model, of the six possible internal loads on a wire cross-section, only the normal force plays a role in the strand global behaviour (the wire bending moment being a small correction factor). Also neglected, are the variations in lay angle arising from the axial load. Such variations are considered negligible in the conductor case, in particular for the ACSR (aluminum conductor steel reinforced) because of the steel core high stiffness. Wherever possible, numerical applications are used to show the influence of the simplifications, and the corresponding Matlab$^{®}$ [1] functions are given. They enable the reader to adapt the

---

[1] MATLAB$^{®}$ is a registered trademark of The MathWorks, Inc.

given examples to other conductors than those selected in this report. In most cases, a Matlab® file is given to perform the calculations.

Synopsis
In Chapter 1, basic formulas for a conductor under pure axial load are derived. A special attention is given to an estimation of inter-layer pressure arising from the axial load, as it is assumed to remain unperturbed when the conductor is bent.

In Chapter 2, the elementary case of a single-layer conductor under uniform curvature bending is considered, where the deformed shape is assumed to be circular. As the strand departs from its initially straight state (its axis is assumed to be a straight line), for a large radius of curvature, there is no slip between the wires in the layer and the single ("king") wire core. The strand is assumed to behave as a solid. Then, as curvature increases, a slip region initiates in the vicinity of the section neutral axis. It propagates towards the upper and lower points of the strand cross-section[2]. As these upper and lower points are reached, slip is complete. If the imposed curvature is increased, the strand bending stiffness remains a constant minimum.

In Chapter 3, the model is extended to a multilayer strand. However, simplifications are made. First, as we only consider reverse-lay strands, inter-layer contact consists of a large number of points of contact between wires, a so-called "trellis contact patch". On each wire, discrete contact points are replaced by a contact line. Also, pressure is assumed to be transferred from one layer to the next, starting from the outer one, as if the wires were simple fibers, with no bending stiffness. Bending of the strand is studied as in the single-layer case. Starting from the rectilinear state, curvature is increased, giving a circular shape of decreasing radius to the strand centerline. Slip starts between the two outer layers and propagates along the "contact lines". At some point, slip may start between the second and third layers etc. When slip is complete at every interface, the strand bending stiffness is a minimum.

In Chapter 4, the uniform curvature model is applied to the numerical treatment of a quasi-static free bending problem: the taut clamped-clamped conductor under a center transverse force. Results are compared with published data for typical conductors.

While the previous chapters deal mostly with the problem of strand bending stiffness, in Chapter 5 the question of the maximum bending stress is examined. Comparison is made between theoretical results and available published test data.

Matlab® functions
In order to give the reader a better idea of the order of magnitude of various quantities yielded by each model, each chapter includes a number of numerical examples. For most of these examples, a Matlab® function has been written. The scripts of these functions are available on the Dropbox and Sky Drive websites. Access will be given to interested readers. Requests should be sent to the author: acardou@gmc.ulaval.ca.

---

[2] These " upper" and " lower" points in the bent strand cross-section are sometimes called " extrados" and "intrados " points, as they are located, by definition, on the outer and inner (center of curvature) sides of the strand, as in a wing profile.

CHAPTER 1

CONDUCTOR UNDER AXIAL LOAD

1.1   GEOMETRICAL PROPERTIES

In this chapter, and in the following ones, only the most common case of circular section wire conductors is considered. These conductors are reverse-lay, i.e. stranding takes place in alternating directions from layer to layer. All wires in a given layer are identical. However, there may be differences from layer to layer in wire material and diameter (such as steel and aluminum wires in an ACSR conductor).

The inner-most layer, which contacts the center wire, or "king wire", is made of six wires. If all wires are identical, each following layer has the number of wires of the layer below, plus six. However, this rule needs not apply between layers where wire diameters are different (see Appendix A). Besides, it will be considered that stranding is compact. This means, in a given layer, wires are practically in contact, i.e. they almost fill the available space, with only a small gap between wires.

Packing condition
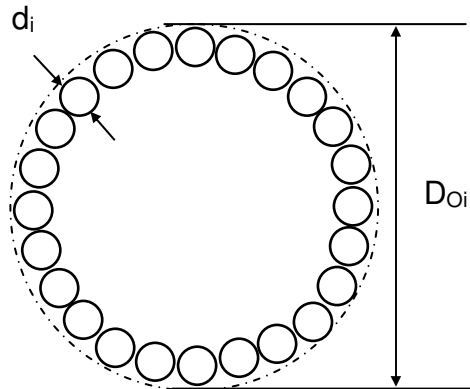
Figure 1. 1

In a conductor, a given layer (i) is made of n_i wires of diameter d_i . The layer outside diameter is D_{Oi} . A wire center line is a circular helix curve wrapped onto a cylinder of diameter $(D_{Oi}-d_i)$, which will be called the lay cylinder. The lay angle α_i is the complementary angle to the helix angle. If α_i is small enough, as it is in practical conductors, a wire section in a plane perpendicular to the conductor axis is practically an ellipse. The wire packing in the layer is compact if adjacent wires are in contact. This occurs for a certain value of α_i . Calling h_i the length of lay of a wire, i.e. the pitch length of the centerline helix, one defines a theoretical lay ratio h_i/D_{Oi}.

In order to have a compact packing, Rawlins (2005) shows that lay angle α_i and lay ratio h_i/D_{Oi} must satisfy two non-linear equations. He also indicates the following equation yields a good approximation of the lay ratio:

$$\frac{h_i}{D_{Oi}} = \frac{1}{1+3/n_i} \frac{\pi}{\sqrt{\left(\frac{n_i^2}{9}-1\right)\tan^2\left(\frac{\pi}{n_i}\right)-1}} \tag{1.1}$$

For a number of wires from 7 to 36, he finds a maximum difference of 0.3% between the theoretical value and the approximate value obtained from Eq. (1.1). This equation does not apply

to the inner-most layer, with $n_i = 6$. In this case it yields an infinite lay ratio, corresponding to $\alpha_i = 0$ deg., i.e. to straight wires.

Preferred lay ratios are given in ASTM standards and are to be used by manufacturers (Rawlins 2005).

However, from a user point of view, for a given conductor, the number of wires in each layer is known, as well as parameters D_{Oi} and d_i. Thus, Eq. (1.1) may be used to obtain the lay ratio for each layer. This leads to the pitch h_i and to the maximum lay angle α_i (corresponding to contacting wires). Indeed, for a circul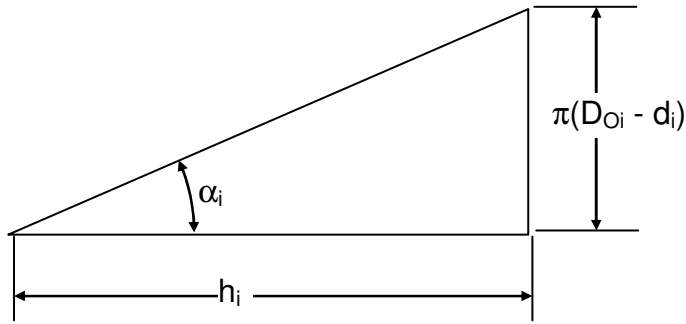ar helix, lay angle α_i, wrapped on a cylinder of diameter $(D_{Oi} - d_i)$, and pitch length h_i, one has the well-known formula:

$$\tan \alpha_i = \frac{\pi(D_{Oi} - d_i)}{h_i} \tag{1.2}$$

While actual lay angles are often smaller than this value (Rawlins 2005), they are not very far from it and this limit value will be used in the numerical examples when the actual lay angle is not known, thus allowing the application of various conductor bending models.

Figure 1. 2

Example 1.1

Geometry and material properties of the Bersimis ACSR conductor are given in Appendix A. It is made of a 1/6 steel core, with three aluminum layers. In the outer layer, there are 20 wires, having a 4.572 mm diameter. The conductor outside diameter is $D_{O1} = 35.05$ mm. Using Eqs (1.1) and (1.2), determine the maximum value for lay angle α_1. Compare with the actual value of 14.14 deg. (Appendix A).

Available Matlab® file: Example_1_1.m

Result: $\alpha_{1max} = 16.7$ deg.

Since the actual value is smaller than α_{1max}, there is a small gap between the wires belonging to this layer. Thus, contact may be considered as a radial contact, between adjacent layers, rather than a "circumferential" or "tangential" one between same layer wires as it is assumed in some models.

Inner-most layer

As seen in Appendix A, the center layer, which is in contact with the core wire, has a non-zero lay angle, with equal nominal wire radii. With this kind of geometry, the layer and the core wire cannot be in contact. Contact occurs between the wires in the layer (tangential contact). In order to have a radial contact, the radius of the core wire has to be slightly larger than the one of the layer wires. A condition has been found by Costello (1997) for this radial contact to occur. For example, consider the case of the Bersimis ACSR (Appendix A) with $r_c = r_4 = 1.27$ mm and $\alpha_4 = 5.33$ deg. Costello's condition requires $r_c/r_4 > 1.00652$ for radial contact to occur. Thus, the core radius has to be such that $r_c > 1.278$ mm, a 0.65% difference with the given value, which is of negligible consequence from the point of view of conductor strength and stiffness. It may have some influence on the slip conditions between the core and inner layer wires when the conductor is bent. This effect will be neglected, and it will be assumed the core wire diameter is such that radial contact is prevailing.

1.2   CONDUCTOR UNDER AXIAL LOAD

An axial load T is imposed on a multilayer conductor. The objective is to determine the axial force in each wire. Depending on the degree of accuracy being sought, the problem can be rather simple or quite complex. A short description of temperature and creep effects is given in Chapter 2 of EPRI's Reference Book (EPRI, 2006). Here, however, it will be assumed the wire material is elastic linear, and undergoes small deformations, so that conductor geometry parameters (lay angles, layer diameters) do not vary appreciably under the imposed load.

Strictly speaking, wires are helical rods (similar to helical springs), whose cross section can be subjected to the usual beam internal loads: normal and shear forces, bending and twisting moments. Such a complete analysis applied to loaded cables has been given by Costello (1997). His analysis is based on Love's theory of curved rods (Love, 1944). However, when wire diameters are small with respect to overall conductor diameter, when lay angles are smaller than 20° (Ghoreishi et al., 2007) and when the conductor unit extension (its equivalent axial strain) is small, which implies a small variation in lay angles, a simpler analysis, such as the one used, among others, by Hruska (1951), is justified. In this approximate analysis, the only internal force being considered in the equilibrium equations is the normal force on a wire cross section (Fig. 1.3). When necessary, a small wire bending moment will eventually be introduced independently.
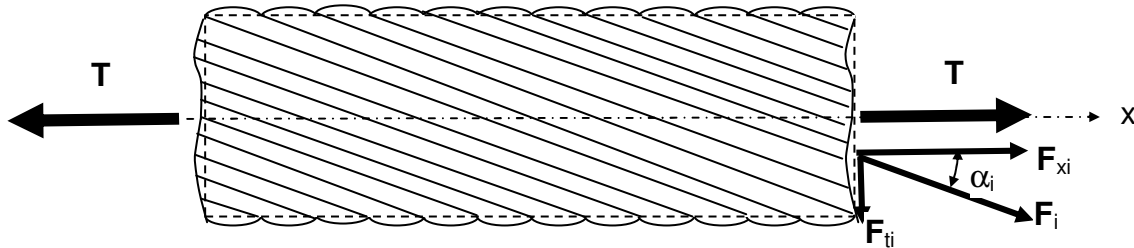

Figure 1. 3

We call F_i the tension in a wire belonging to layer (i). Its component in the conductor axis direction is F_{xi}. Its component in the conductor cross section is F_{ti}. It is tangent to the circle on

5

which lie the wire centers of layer (i) (the cross section of the lay cylinder). Thus, it is called its tangent component.

The total applied force on the conductor is T, parallel to the x-axis. One must have the following static equivalence condition:

$$T = F_c + \sum_{i=1}^{m} n_i F_i \cos \alpha_i \qquad (1.3)$$

in which :

m : number of layers in the conductor (excluding the core wire)
n_i : number of wires in layer (i)
α_i : lay angle in layer (i)
F_c : tensile force on core wire

Tangential components F_{ti} yield a non-zero moment with respect to the x axis. When it is not balanced, it leads to a possible rotation of the layer. Such rotation is minimized by having alternate left and right lay layers (reverse-lay). If the balance is not perfect, and depending on the end conditions, there may be a small rotation due to the axial force T. This coupling effect has been studied by various authors and a comparative study of their results has been made by Jolicoeur and Cardou (1991). Here, this effect will be neglected.

In order to determine the (m+1) forces F_c and F_i , besides the static Eq. (1.3), one has to write m axial strain compatibility equations. Calling ε_x the conductor equivalent unit strain, these equations are:

$$\varepsilon_x = \varepsilon_c = \varepsilon_{xi} \quad (i = 1 \cdots m) \qquad (1.4)$$

Using Hooke's law, they can be written in terms of wire forces F_c and F_i. Indeed, normal stresses acting on wire cross sections are:

$$\sigma_c = F_c / A_c \quad \sigma_i = F_i / A_i \qquad (1.5)$$

Young's Modulus is E_c for the core wire material and E_i for layer (i). In each wire, the corresponding axial unit strain is:

$$\varepsilon_c = F_c / E_c A_c \quad \varepsilon_i = F_i / E_i A_i \qquad (1.6)$$

Compatibility equations (1.4) are related to unit strain in the conductor x-axis, while equations (1.6) apply to wire axis direction. Except for the core wire, these directions make an angle α_i. Thus the well known kinematics strain transformation (also given by Mohr's circle), which is usually derived for a solid bar under axial load, applies:

$$\varepsilon_i = \varepsilon_{xi} \cos^2 \alpha_i \qquad (1.7)$$

6

Thus, compatibility Eq. (1.4) yields:

$$\varepsilon_c = \frac{\varepsilon_i}{\cos^2 \alpha_i} \tag{1.8}$$

Or, in terms of forces:

$$\frac{F_c}{E_c A_c} = \frac{F_i}{E_i A_i \cos^2 \alpha_i} \tag{1.9}$$

Each F_i may be expressed in terms of F_c and put in the statics Eq. (1.3), yielding:

$$T = \frac{F_c}{E_c A_c} \left(E_c A_c + \sum_{i=1}^{m} E_i A_i \cos^3 \alpha_i \right) \tag{1.10}$$

The conductor axial stiffness (AE) is defined as:

$$(AE) = A_c E_c + \sum_{i=1}^{m} n_i A_i E_i \cos^3 \alpha_i \tag{1.11}$$

It can be calculated as soon as conductor geometry and material parameters are known. Once the axial stiffness (AE) is known, wire forces can be calculated for a given tensile load T on the conductor:

$$F_c = \frac{A_c E_c}{(AE)} T \qquad F_i = \frac{A_i E_i \cos^2 \alpha_i}{(AE)} T \tag{1.12}$$

Corresponding stresses are :

$$\sigma_c = \frac{E_c}{(AE)} T \qquad \sigma_i = \frac{E_i \cos^2 \alpha_i}{(AE)} T \tag{1.13}$$

Conductor axial stiffness (AE) given by Eq. (1.11) was obtained by Hruska (1951), Lanteigne (1985) etc., following different ways.

The EPRI formulas
In the EPRI Reference Book (2006), lay angles are neglected and conductor axial stiffness is calculated as if all wires were parallel to the conductor axis. Indeed, lay angles α_i being of the order of 10°, factors $\cos^2 \alpha_i$ and $\cos^3 \alpha_i$ are very close to unity. Eq. (1.13) then reduces to Eqs (2.3-6) and (2.3-7) of EPRI (2006).

Example 1.2

Consider the case of the Cardinal ACSR, whose parameters are given in Appendix A. An axial load T of 25% RTS (Rated Tensile Strength) is applied, which corresponds to T = 37.6 kN. Determine the stresses in the core wire and in each layer. Compare with stress values obtained from the EPRI formulas, in which the lay angles are neglected ($\alpha_i = 0°$).

Available Matlab® file: Example_1_2a.m

Results:
Axial stiffness:	$(AE) = 3.87 \times 10^7$ N.mm^2
Stress in core wire:	$\sigma_c = 203.97$ MPa
Stress in each layer:	$\sigma_i = [59.71 \ 60.83 \ 54.74 \ 169.81]$ MPa

EPRI (2006) equations:
Axial stiffness:	$(AE) = 4.09 \times 10^7$ N.mm^2
Stress in core wire:	$\sigma_c = 193$ MPa
Stress in each layer:	$\sigma_i = [62.94 \ 63.48 \ 57.21 \ 171.73]$ MPa

Curved rod model

It is interesting to compare results obtained with Eqs (1.11) to (1.13) with those obtained from the more rigorous curved rod approach of Costello (1997). For this purpose, we consider the simple 6/1 strand of this author's Example 3.1, a simple single layer, uniform material strand. Its parameters are as follows:

Radius of core wire:	$r_c = 0.103$ in.
Radius of layer wires:	$r_1 = 0.101$ in.
Pitch length of lay:	$h_1 = 9.75$ in.
Material:	$E = 28.5 \ 10^6$ psi (steel)
Applied load:	$T = 18,805$ lb

Assuming a compact packing (as does Costello), Eq. (1.2) yields a lay angle: $\alpha_1 = 7.49$ deg. With zero strand rotation end conditions, stresses obtained by Costello are: $\sigma_c = 85,500$ psi and $\sigma_1 = 83,700$ psi.

Eqs (1.11) to (1.13) have been programmed in the Matlab® file Example_1_2b.m

Results:
Stresses:
Current approximate model:	$\sigma_c = 85,193$ psi and $\sigma_1 = 83,746$ psi
EPRI equations:	$\sigma_c = \sigma_1 = 83,351$ psi

Axial stiffness (AE):
Costello's curved rod model:	6.27×10^6 lb.in^2
Current model Eq. (1.11):	6.29×10^6 lb.in^2
EPRI equations:	6.43×10^6 lb.in^2

8

1.3 PRESSURE BETWEEN LAYERS

It is well known that in a homogeneous, isotropic, bar under axial load, there is no radial stress, while in a conductor under tension, there are clenching forces between layers, i.e. forces at contact points between wires. They can be explained intuitively since the axial force in each wire tends to "straighten up" the helix, and thus induce a decrease of the radius of the lay cylinder. Internal layers block this inward radial motion, thus leading to an interlayer pressure. In fact, such pressure is already present even before the application of force T because of the stranding process. Rawlins (2005) has proposed an evaluation of this residual pressure.

Here, we seek to determine the pressure which is directly related to the axial force T. However, this will require a few simplifying hypotheses. Indeed, stranding being alternate, interlayer contact is a point-wise contact. Also, if one considers layer (i) and adjacent layers (i-1) (interface (i-1)) and (i+1) (interface (i)). One interface (i-1) contact point will be generally located between two interface (i) contact points. The wire element of layer (i) which is situated between these two contact points can be considered as a small beam element loaded at a number of points (several (i-1) layer wires may contact the (i) layer wire between these contact points with layer (i+1)). An "exact" calculation of force transmission from one layer to the other would thus be rather difficult, and not very useful.

An approximate method is devised by considering, firstly that wires have a negligible bending stiffness, and secondly that point contacts are replaced by line contacts. This is equivalent to replacing wires by helical fibres whose diameter is negligible compared with the radius of their lay cylinder. It is the approach used by Hruska (1952), Lanteigne (1985), Papailiou (1995), and Hong et al. (2005).

A model without pressure transmission (Hruska, 1952)
It applies to the conductor outer layer. One considers a wire is equivalent to a string wound on a cylinder whose radius is equal to its center line helix principal radius of curvature (in its osculating plane). With a lay angle α_1, and a cylinder radius R_1, this radius of curvature ρ_{h1} is given by:

$$\rho_{h1} = \frac{R_1}{\sin^2 \alpha_1} \qquad (1.14)$$

With a wire under tension F_1, the unit line contact force is given by:

$$q_1 = \frac{F_1}{\rho_{h1}} = \frac{F_1}{R_1} \sin^2 \alpha_1 \qquad (1.15)$$

Example 1.3

Consider again the case described in Example 1.2. Under the given conditions, calculate the contact force per unit length on the outer layer wires.

Use Matlab® file Example_1_3.m

<u>Result:</u> $q_1 = 1.99$ N/mm

It is interesting to compare this value with the residual contact force calculated by Rawlins (2005) in the case of the Curlew ACSR, which is slightly stronger than the Cardinal ACSR, but with a similar structure. For the outer layer, he finds a 0.33 N/mm residual line force.

Model with pressure transmission
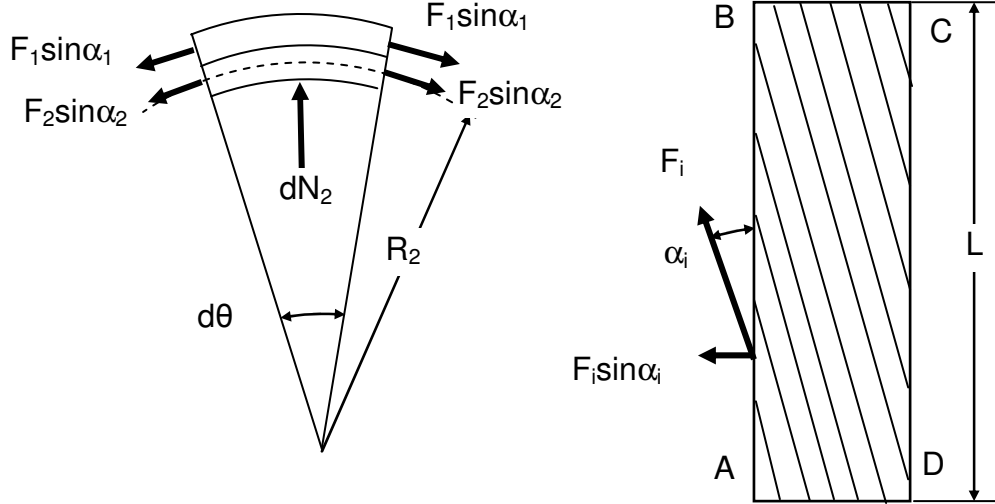
Figure 1. 4

For inner layers, one has to take into account the clenching pressure exerted by the adjacent outer layer. As already indicated, it will be assumed wires can be considered as fibres without any bending stiffness.

A conductor element, length L, is considered. It is limited by two radial planes making a small angle $d\varphi$, and comprising the outermost layers (i=1 and 2). Because of the tension T on the conductor, wires are under tensions F_i (i=1,2). For each wire, the force tangential component, on edges AB and CD is $F_i \sin\alpha_i$. On each layer (2) wire element there is a radial force dN_2. Wire diameter is d_i. (i=1,2). Assuming a compact packing, same layer wires touch each other and the number of wires for each layer, over length L, is k_i given by:

$$k_i = \frac{L}{d_i / \sin\alpha_i} = \frac{L \sin\alpha_i}{d_i} \tag{1.16}$$

Radial equilibrium of the system is given by:

$$k_2 \, dN_2 = 2k_1 F_1 \sin\alpha_1 \frac{d\theta}{2} + 2k_2 F_2 \sin\alpha_2 \frac{d\theta}{2} \tag{1.17}$$

which yields :

$$dN_2 = \frac{d_2}{d_1} \frac{\sin^2 \alpha_1}{\sin \alpha_2} F_1 \, d\theta + \sin \alpha_2 \, F_2 \, d\theta \qquad (1.18)$$

One may easily extend this equation to any layer (i) :

$$dN_i = \sum_{j=1}^{i-1} \frac{d_i}{d_j} \frac{\sin^2 \alpha_j}{\sin \alpha_i} F_j \, d\theta + \sin \alpha_i \, F_i \, d\vartheta \qquad (1.19)$$

which can be written under the more compact form :

$$dN_i = \sum_{j=1}^{i} \frac{d_i}{d_j} \frac{\sin^2 \alpha_j}{\sin \alpha_i} F_j \, d\theta \qquad (1.20)$$

Other expressions can be obtained using the lay length h_i of each layer. Assuming again a compact packing, when $L = h_i$, Eq. (1.16) yields:

$$n_i = \frac{h_i}{d_i / \sin \alpha_i} = \frac{h_i \sin \alpha_i}{d_i} \qquad (1.21)$$

Hence (Papailiou, 1995, his Eq. (3.23) generalized):

$$dN_i = \sum_{j=1}^{i} \frac{h_i}{h_j} \frac{n_j}{n_i} \sin \alpha_j \, F_j \, d\theta \qquad (1.22)$$

Using Eq. (1.2), lay length h_i may be expressed as $h_i = 2\pi R_i / \tan \alpha_i$, in which R_i is the radius of layer (i) lay cylinder. Thus, Eq. (1.22) yields:

$$dN_i = \sum_{j=1}^{i} \frac{R_i}{R_j} \frac{n_j}{n_i} \frac{\tan \alpha_j}{\tan \alpha_i} \sin \alpha_j \, F_j \, d\theta \qquad (1.23)$$

which is the equation found by Hong *et al*. (2005), with the difference, in their paper, that the elementary angle $d\varphi$ is taken as $d\theta_i$, a different value for each layer (apparently, because, in their case, the dN_i was supposed to apply to elements ds_i corresponding to an equal projection ds on the strand axis).

From dN_i , given by Eq. (1.20), one gets the force per unit length (as measured on the layer (i) wire centre line), assuming it is a line contact situation (Lanteigne, 1985):

$$q_{Ni} = \frac{dN_i}{ds_i} = \frac{dN_i}{R_i \, d\varphi} \sin \alpha_i \qquad (1.24)$$

11

$$q_{Ni} = \frac{dN_i}{ds_i} = \frac{\cos \alpha_i}{n_i} \sum_{j=1}^{j=i} \frac{n_j}{R_j} \frac{\sin^2 \alpha_j}{\cos \alpha_j} F_j \qquad (1.25)$$

However, if one is interested on the effect of forces dN_i on the adjacent (i+1) inner layer, it must be applied on the corresponding wire elements. The resultant radial force on layers (i) and (i+1) are $k_i dN_i$ and $k_{i+1} dN'_i$ and the action-reaction principle yields:

$$k_i dN_i = k_{i+1} dN'_i \qquad (1.26)$$

From Eq. (1.16):

$$dN'_i = \frac{d_{i+1}}{d_i} \frac{\sin \alpha_i}{\sin \alpha_{i+1}} dN_i \qquad (1.27)$$

and the force per unit length on wire element ds_{i+1} is obtained as in Eq. (1.24):

$$q'_{Ni} = \frac{dN'_i}{ds_{i+1}} = \frac{dN'_i}{R_{i+1} d\varphi} \sin \alpha_{i+1} \qquad (1.28)$$

yielding:

$$q'_{Ni} = \frac{d_{i+1}}{d_i} \frac{R_i}{R_{i+1}} \frac{\cos \alpha_i}{n_i} \sum_{j=1}^{i} \frac{n_j}{R_j} \frac{\sin^2 \alpha_j}{\cos \alpha_j} F_j \qquad (1.29)$$

or else:

$$q'_{Ni} = \frac{d_{i+1}}{d_i} \frac{R_i}{R_{i+1}} q_{Ni} \qquad (1.30)$$

This equation applies up to interface (m-1), as interface m involves the straight core wire.

Example 1.4

With the same data as in Example 1.2, determine the force per unit length between each layer, calculated either on the outer or on the inner layer.

Available Matlab® file: Example_1_4.m

Result:: q_{Ni} = [1.9949 4.8776 10.377 26.064] N/mm
            q'_{Ni} = [2.6579 7.3055 20.849 26.064] N/mm

At the interface between layer (4) and core wire, there is of course no difference between q_{Ni} and q'_{Ni}.

1.4   POINT CONTACT FORCES

Except for the innermost layer, which is in contact with the core wire, all contacts are point contacts, rather than line contacts. It is possible to obtain an approximate value of the contact forces using the line contact forces given by the above equations. This requires the calculation of the distance between these contact points at a given interface. For example, for layer (i), we need the distance of contact points with layer (i+1).

One can show (Appendix B) this distance, calculated on the contact helix of layer (i) (on a wire outer fiber which is in contact with layer (i+1)), is given by:

$$d_{Ci} = \frac{2\pi R_{Ci}}{n_{i+1}} \frac{\cos \alpha''_{i+1}}{\sin(\alpha'_i + \alpha''_{i+1})} \tag{1.31}$$

where R_{Ci} is the radius of the contact cylinder between layers (i) and (i+1), and angles α'_i and α''_{i+1} are slightly different from the corresponding lay angles as they correspond to the wire "fibre" which is on the contact cylinder and not to the centerline (Appendix B).

This is the same equation as the one obtained by Chouinard (1994), except for his using lay angles α_i and α_{i+1} instead of the present α'_i and α''_{i+1} (which are measured on the contact cylinder). If the difference between lay angles α_i and α'_i is neglected, one gets:

$$d_{Ci} = \frac{2\pi R_{Ci}}{n_{i+1}} \frac{\cos \alpha_{i+1}}{\sin(\alpha_i + \alpha_{i+1})} \tag{1.32}$$

A somewhat different expression has been given by Papailiou (1995). In his work, contact point distance is measured on the centerlines of either layer (i) or (i+1) (his Eqs (3.1) and (3.2)). Using these expressions, one can obtain the distance measured on the contact helix of layer (i):

$$d_{Ci} = \frac{2\pi R_{Ci}}{n_{i+1}} \frac{(1-\gamma_i^2)\cos \alpha_{i+1}}{(1+\gamma_i)\sin \alpha_{i+1} \cos \alpha_i + (1-\gamma_i)\sin \alpha_i \cos \alpha_{i+1}} \tag{1.33}$$

Parameter γ_i is the ratio $\gamma_i = r_i / R_{Ci}$. Eqs (1.32) and (1.33) differ slightly. It can be checked both equations are identical if the γ_i ratio tends to zero, i.e. if wire radius r_i is small with respect to the contact cylinder radius R_{Ci}. In multilayer conductors, this may apply only to the outer layers.

Example 1.5

Considering the same case as in Example 1.2, determine the distances between contact points at interfaces (1,2), (2,3) and (3,4). Compare results obtained with Eqs. (1.31), (1.32) and (1.33).

Use the Matlab® file Example_1_5.m

Results:
Eq. (1.31) d_C = [6.96 6.72 8.33] mm
Eq. (1.32) d_C = [7.09 7.05 8.42] mm
Eq. (1.33) d_C = [9.33 10.14 16.83] mm

Using Eq. (1.32), with the specified lay angles, yields results which are close enough to the "exact" value. When the distance between contact points is known, one can determine the normal contact forces for a tensile force T on the conductor.

Normal contact force due to the axial load on conductor
Calling N_{Ci} the normal point force at interface contact points between layers (i) and (i+1), one gets:

$$N_{Ci} = q_{Ni}d_{Ci} \tag{1.34}$$

where q_{Ni} is given by Eq. (1.25) and d_{Ci} is given either by Eq. (1.31) or its approximate form Eq. (1.32). A specialized form of this equation is given by Chouinard (1994).

Example 1.6

Considering the same case as in Example 1.2, and using Eq. (1.32), determine the normal force at contact points between layers, that is, interfaces (1,2), (2,3) and (3,4).

The line contact forces have been determined in Example 1.4: q = [1.99 4.86 10.35] N/mm.

From Example 1.3, distances between contact points are: d_C = [6.96 6.72 8.33] mm. Thus contact forces are given by the simple product of q and d_C.

Result: N_C = [13.85 32.66 86.22] N

Obviously, from the action-reaction principle, at a given interface, the normal contact forces have to be the same on both contacting layers.

CHAPTER 2

BENDING OF A SINGLE LAYER CONDUCTOR

2.1   INTRODUCTION

Bending of cables and conductors has been studied for many years (see reviews by Cardou and Jolicoeur, 1997; Cardou, 2006) both from the theoretical and experimental point of view. Modelling of a conductor in bending is indeed a much more difficult task than modelling its behaviour under pure axial load. For this reason, the simpler case of a single layer conductor made of a core wire and a six wire layer will be first studied. Two cases are to be considered:
- Constant radius bending
- Free bending

Constant radius bending is found with cables or conductors which are wound on a pulley, a roller, a drum or a turret. **Free bending** occurs whenever a taut cable or conductor is transversely loaded, its centerline undergoing a transverse displacement without contact with another solid (e.g. case of a conductor in the vicinity of a suspension clamp). The resulting deformed centerline has a variable curvature, a fact which renders the analysis quite difficult.

For this reason, most of the available published models are based on the constant radius hypothesis, while at the same time neglecting the contact forces which have to occur in a real case. Nevertheless, it is this approach which will be used here. Firstly, because it leads to explicit results. Secondly, because these "simple" results may be used in the free bending case, which is of course more interesting technically, at least in conductor applications.

2.2   BASIC HYPOTHESES

2.2.1   Contact conditions

Radial contact rather than tangential contact (see Chapter 1) is assumed to prevail between conductor wires. When the single layer conductor is under a simple axial load, its axis is a straight line and the lines of contact between the core wire and the layer wires are circular helices. It is shown in Appendix B that their helix angle is slightly different from the $(90°-\alpha)$ helix angle of the centerline. Here, this difference is neglected. The line contact force arising from the axial load T is uniform and has been evaluated in Chapter 1. It will be noted q_0 . At this stage, the flattening of a wire along the contact helix, which yields a narrow contact "strip", is also neglected. Friction plays an important role in conductor bending. It is assumed Coulomb's law of friction applies.
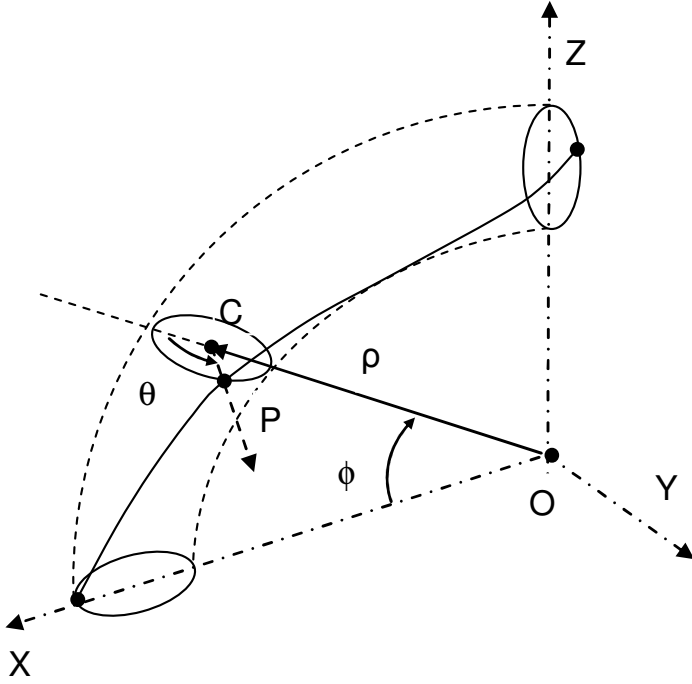
2.2.2 Wire shape in the bent conductor

When a constant curvature ρ is imposed on the conductor, the lay cylinder is deformed into a circular torus. One may wonder what is the shape taken on this torus by a wire centerline. With zero bending stiffness wires, and with no friction, these centerlines would follow the torus geodesic lines. This hypothesis has been used by some authors (e.g. Baticle, 1912). Another hypothesis is to assume the deformed curve, being defined by angles ϕ and θ (Fig. 2.1), is such that ϕ and θ are proportional. In a logical way, this curve is sometimes called a "toroidal helix". This is a widely used assumption. Lehanneur (1949) has shown such a curve is kinematically admissible. When the conductor is rectilinear, principal curvature at any point on the helix curve is the same. On the torus curve, the curvature varies from point to point.

Figure 2. 1

Leider (1977) has calculated the curvature variation for both curves, over a pitch length. He has found the variation is greater for the geodesic curve than for the toroidal helix. This implies the bending deformation energy is larger in the first case than it is in the second case. According to the principle of minimum potential energy (at equilibrium), the actual shape of the deformed wire centerline should be closer to the toroidal helix than to the geodesic curve.

2.3 FRICTIONLESS BENDING BEHAVIOR

A taut single layer conductor under axial tension T is considered. Each wire carries a force F_T, with the corresponding uniform normal stress σ_T on its cross section. This conductor is now given a uniform curvature $\kappa = 1/\rho$. Here, it is assumed there is no friction so that the helical wires can slip freely on the core wire. If taken separately, layer wires and core have a bending stiffness:

$$B_w = E_w I_w \qquad B_c = E_c I_c \tag{2.1}$$

With a circular cross section radius r, $I_w = \pi r^4 / 4$. The conductor minimum bending stiffness is often calculated as if all wires were parallel rods (EPRI, 2006):

$$B_{min1} = 6B_w + B_c \tag{2.2}$$

If the lay angle α is taken into account, the simplest equation is the one given by Papailiou (1995):

$$B_{\min 2} = 6B_w \cos \alpha + B_c \tag{2.3}$$

Eq. (2.3) does not take into account the fact that, when a helical rod undergoes bending (i.e. the axis of the cylinder is "bent"), there is a twisting component. The rod material shear modulus should then appear in the equation. Equivalently, Poisson's ratio ν should be a parameter in the $B_{\min}$ equation. Such a calculation was made by Lehanneur (1949), yielding the following expression (for a 6-wire layer):

$$B_{\min 3} = 6B_w \cos \alpha \left[1 - \frac{\nu}{2(1+\nu)} \sin^2 \alpha \right] + B_c \tag{2.4}$$

Another expression has been obtained by Costello (1997), considering each wire is an independent helical rod (Timoshenko, 1956):

$$B_{\min 4} = 6B_w \cos \alpha \frac{2}{(2 + \nu \sin^2 \alpha)} + B_c \tag{2.5}$$

An expression obtained by Lanteigne (1985) can also be mentioned:

$$B_{\min 5} = 6B_w \cos^3 \alpha + B_c \tag{2.6}$$

Taking Papailiou's Eq. (2.3) as a reference, each one of the above equations for $B_{\min}$ may be written as:

$$B_{\min j} = (6B_w \cos \alpha) \, k_j + B_c \tag{2.7}$$

Taking typical values for α and ν, , e.g. $\alpha = 15^{\circ}$ $\nu = 0.3$, one gets the following k_j values:

k_1 EPRI (2006)	k_2 Papailiou (1995)	k_3 Lehanneur (1949)	k_4 Costello (1997)	k_5 Lanteigne (1985)
1.035	1	0.992	0.990	0.933

Table 2. 1

It is found that the influence of wire twisting stiffness on $B_{\min}$ is rather small. Thus, in the following, Papailiou's simpler Eq. (2.3) will be used. Considering the number of hypotheses and uncertainties, neglecting wire twisting stiffness is a reasonable assumption.

2.4   ZERO-SLIP BENDING

It is now assumed there is some friction between the core and the helical wires. In this section, the coefficient of friction μ is supposed to be large enough to prevent any slip when the conductor is given a uniform curvature κ.

In Chapter 1, it was found tension T generates a normal line contact force q_N. When the curvature is imposed starting from zero, slip between core and helical wires is prevented by friction, and a tangential line force q_{Fr} is generated. According to Coulomb's law, the no-slip condition implies that at each point on the contact lines, $q_{Fr} < \mu q_N$. Hence, the conductor should behave like a solid beam. The Bernoulli-Euler hypothesis is supposed to apply: a plane conductor cross-section remains a plane in the bending process. Thus, helical wire cross section center points, initially in the same plane, stay coplanar.

It is known this model is merely an approximation. In the actual conductor, the state of stress and strain in the contact regions is much more complex than the one in a solid beam. Because of the "tangential elasticity" in the contact region, tangential forces q_{Fr} lead to small tangential displacements of wire section centroid. While this tangential elasticity plays an important role in the analysis of the fatigue process (Leblond and Hardy, 2005), it is neglected in the stick-slip models.

Using the Bernoulli-Euler hypothesis, one gets the tension and compression bending forces as they are merely proportional to the distance from the conductor section neutral axis.

The complementary bending stiffness (Papailiou, 1995; Lanteigne, 1985), for a six wire layer, is:

$$B_{compI} = 3A_w E_w R^2 \cos^3 \alpha \tag{2.8}$$

where $A_w = \pi r^2$ is the helical wire cross section area. The total bending stiffness of the conductor before any slippage occurs must also include the wires own bending stiffness B_{min}. Thus the conductor maximum bending stiffness is:

$$B_{max} = B_{min} + B_{compI} \tag{2.9}$$

Example 2.1

A single layer conductor is made of n=6 helical aluminum wires and a steel core wire (Papailiou, 1995), whose parameters are as follows:

Core wire: $r_c = 1.35$ mm $E_c = 210000$ MPa
Layer wires: r = 1.35 mm   E = 70000 MPa
Lay cylinder: R = 2.7 mm
Lay angle: $\alpha = 10°$

Determine the conductor bending stiffnesses B_{min}, B_{compI}, B_{max}

Available Matlab® file: Example_2_1.m

Results:
$A_c = A_w = 5.73$ mm^2
$I_c = I_w = 2.609$ mm^4
$B_w = 182.6 \ 10^3$ N.mm^2 $B_c = 547.9 \ 10^3$ N.mm^2

Eq. (2.3): $B_{min} = 1626.8 \ 10^3$ N.mm^2
Eq. (2.8): $B_{compI} = 8371.8 \ 10^3$ N.mm^2
Eq. (2.9): $B_{max} = 9998.6 \ 10^3$ N.mm^2

It is found $B_{min} \ll B_{max}$, which explains why the small differences between the various expressions for B_{min} (Eqs (2.2) to (2.6)) can be neglected. For example, the simplest equation (2.2), corresponding to parallel wires, yields in the present case $B_{min} = 1643.7 \ 10^3$ N.mm^2, a difference of about 1% compared with the more exact Eq. (2.3) and a 0.17% difference with respect to B_{max}.

One should notice these results depend neither on the axial force T on the conductor, nor on the coefficient of friction between core and layer wires.

2.5   BENDING IN THE SLIP REGIME

2.5.1   Limit curvatures

In Chapter 1, it was found the axial force T on the conductor induces a uniform line contact force between the core and layer wires, which is given by $q_N = F_T/\rho_h$, where F_T is the force in each helical wire arising from T, and ρ_h is the helical wire centerline radius of curvature in the osculating plane, which is given by $1/\rho_h = \sin^2 \alpha/R$. When the conductor is bent, the centerline curvature varies from point to point, yielding a variation in q_N. It is assumed the curvature is small enough allowing the variation in q_N to be neglected, thus $q_N \equiv q_0$. However, the variation of F in a wire because of the imposed bending will be considered. For example, above the conductor section "neutral axis", $F > F_T$ (Fig. 2.2).
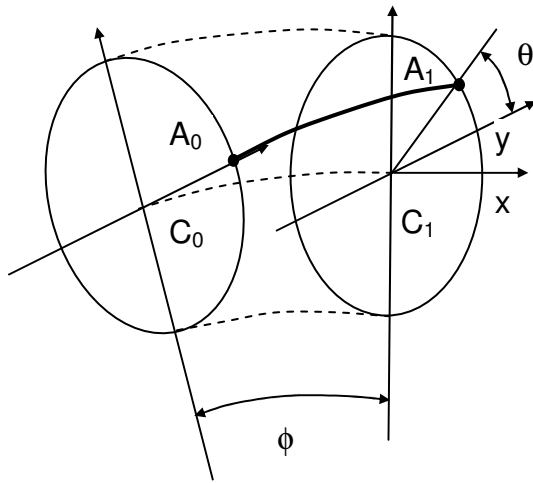
When the imposed curvature is increased, line tangential forces between contacting wires also increase. When curvature reaches a critical value κ_b , the limiting value $q_{Fr} = q_{lim} = \mu q_N$ is attained at one point on each line of contact, and slip starts as soon as $\kappa > \kappa_b$. The slip regime propagates along each line of contact when curvature is increased beyond κ_b. A detailed analysis of this process, based on Coulomb's law was proposed by Rebuffel (1949) and improved by Lehanneur (1949). Their results are summarized here for the special case of a single layer conductor.

Figure 2. 2

Consider one particular wire centerline when it intersects the bending neutral axis at point A_0. Conductor section centroid is C_0. Then, for a section some distance away, the wire centerline is at A_1 on the lay cylinder. Position of A_1 is given by angle θ, measured from neutral axis C_1y (Fig. 2.2). Consider just a half lay length, with $-\pi/2 \le \theta \le \pi/2$. As shown in Fig. 2.2, the tensile side (from the

applied bending), for this particular wire, is assumed to correspond to $0 \le \theta \le \pi/2$, while the compression side corresponds to $-\pi/2 \le \theta \le 0$.

Lehanneur (1949) shows slip will start at angle θ_b given by the condition:

$$\tan \theta_b = -\mu \sin \alpha \tag{2.10}$$

which is slightly below the neutral axis. For example, with typical values $\mu = 0.7$ and $\alpha = 10°$, one finds $\theta_b = -6.9°$. The value of the critical curvature κ_b at which slip starts is given by:

$$\kappa_b = \sigma_T \frac{\mu \sin \alpha}{E_w R \cos^2 \alpha \sqrt{1 + \mu^2 \sin^2 \alpha}} \tag{2.11}$$

where σ_T is the normal stress in each helical wire from the applied tension load T.

Because of the uniform curvature assumption, this applies to all wires in the layer thus, when κ reaches the limit value κ_b, slip will start at all wire sections at an angle θ_b with the neutral axis. On the torus, these sections are on a circle which is a parallel of this surface (Fig. 2.3).
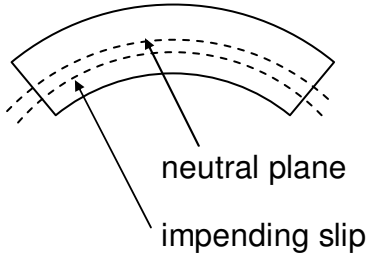
This also applies to the other half layer, which corresponds to $\theta_b' = \pi - \theta_b$. Since $\theta_b < 0$, this is a "parallel" circle with the same radius as the θ_b circle.

neutral plane

impending slip

Figure 2. 3

When κ is increased beyond κ_b, there are two slip zones expanding from these two parallel lines. On one side of the torus, the slip zone is bounded by two parallels given by $\theta_1 < \theta_b$ and $\theta_2 > \theta_b$. The lower parallel reaches the "maximum compression", or "bottom" fibre of the lay cylinder cross section, i.e. $\theta_1 < -\pi/2$ before the upper one reaches the "top" fibre $\theta_2 < +\pi/2$. Because of the symmetry assumption, even if it is in the slip region, there is no wire displacement at $\theta = -\pi/2$ which means wire section displacements take place on both sides of this point towards the bending tension part of the wire. Eventually, curvature κ may be such that the upper parallel $\theta = \theta_2$ reaches the top fibre $\theta = +\pi/2$ The line of contact is everywhere in the slip regime. Total slip occurs for the following curvature:

$$\kappa_{t1} = \frac{\sigma_T}{E_w R \cos^2 \alpha} \frac{1 - (1 - \mu\pi \sin \alpha)e^{\mu\pi \sin \alpha}}{e^{\mu\pi \sin \alpha} - 1} \tag{2.12}$$

Rebuffel (1949) obtains a simpler expression by assuming slip boundaries reach simultaneously the bottom and top fibres. He finds total slip occurs for a curvature:

$$\kappa_{t2} = \frac{\sigma_T}{E_w R \cos^2 \alpha} \frac{e^{\mu \pi \sin \alpha} - 1}{e^{\mu \pi \sin \alpha} + 1} \tag{2.13}$$

Papailiou (1995) proposes an even simpler expression. It is based on the following hypotheses: a) slip always starts on the conductor neutral axis ($\theta = 0$ and π); b) wire stress at those two locations keeps its initial, zero curvature, value σ_T. His expression for slip initiation is then:

$$\kappa_{b3} = \sigma_T \frac{\mu \sin \alpha}{E_w R \cos^2 \alpha} \tag{2.14}$$

And the curvature for total slip is given by:

$$\kappa_{t3} = \frac{\sigma_T}{E_w R \cos^2 \alpha} \left(e^{\mu (\pi/2) \sin \alpha} - 1 \right) \tag{2.15}$$

In order to compare the various expressions, slip initiation curvature can be expressed as:

$$\kappa_{bj} = \sigma_T \frac{\mu \sin \alpha}{E_w R \cos^2 \alpha} k_{bj} \tag{2.16}$$

In the same fashion, total slip curvature can be written as:

$$\kappa_{tj} = \frac{\sigma_T}{E_w R \cos^2 \alpha} k_{tj} \tag{2.17}$$

Using the typical values: $\alpha = 10°$ $\quad \mu = 0.7$, one gets:

j=	1 (Lehanneur, 1949)	2 (Rebuffel, 1949)	3 (Papailiou, 1995)
k_{bj}	0.993	0.993	1
k_{tj}	0.203	0.189	0.210

Table 2. 2

These results indicate that, with respect to Lehanneur's (j = 1) more rigorous, albeit more complex, model, values obtained with both simpler models (j = 2 and 3) differ at most by a few per-cent.

Example 2.2

The same conductor as in Example 2.1 is considered, with the following parameters:
Coefficient of friction: $\mu = 0.7$
Stress from axial load T : $\sigma_T = 10$ MPa

Determine the curvatures corresponding to slip initiation and to total slip. Compare results given by each one of the above three models: 1) Lehanneur's; 2) Rebuffel's; 3) Papailiou's.

Available Matlab® file: Example_2_2.m

Results:

From Eq. (2.11): $\rho_{b1} = 1/\kappa_{b1} = 151.9\,\text{m}$ and $\rho_{b2} = \rho_{b1} = 151.9\,\text{m}$

From Eq. (2.14): $\rho_{b3} = 1/\kappa_{b3} = 150.8\,\text{m}$

From Eq. (2.12): $\rho_{t1} = 1/\kappa_{t1} = 90.3\,\text{m}$

From Eq. (2.13): $\rho_{t2} = 1/\kappa_{t2} = 97.2\,\text{m}$

From Eq. (2.15): $\rho_{t3} = 1/\kappa_{t3} = 87.1\,\text{m}$

The corresponding radii of curvature, even for total slip, are much larger than the conductor outer diameter (8.1 mm). This, in a way, justifies the assumption that wire curvature remains practically a constant in the bending process.

2.5.2 Bending moment

The next step is to determine the bending moments which have to be imposed on the conductor in order to attain these limit curvatures.

As long as $\kappa < \kappa_b$, there is no slip, and the conductor is assumed to behave as a solid beam (called domain (I) of behaviour). The corresponding bending moment is given by the usual expression:

$$M_I = B_{max}\,\kappa \tag{2.18}$$

in which bending stiffness B_{max} is given by Eq. (2.9).

For $\kappa > \kappa_b$, slip occurs over a bounded domain of each contact line. Because of the imposed curvature, normal force on a wire cross section is a function $F(\theta)$. In the no-slip region, F is calculated according to the usual Bernoulli-Euler beam bending theory, which yields a simple sine function. In a slip region, this force becomes an exponential function whose exact form depends on the selected slip model. Taking the simplest one (Papailiou, 1995), it is given by:

$$F = F_L = F_T e^{\mu\theta\sin\alpha} \tag{2.19}$$

It will be noted the normal force at this location along the wire centerline becomes a constant, independent of the conductor curvature. This is because the variation in local wire curvature is neglected. As found in Example 2.2, this is a quite reasonable simplification. Thus, in the slip region, normal force F is equal to the local limit value at which slip initiates.

This normal force includes the zero curvature normal force F_T, due to tension T on the conductor. The component of F due to bending, which we call the complementary force, F_{comp} is given by:

$$F_{comp} = F_T\left(e^{\mu\theta\sin\alpha} - 1\right) \tag{2.20}$$

With Papailiou's assumptions, force F in the slip region, is lower than the ideal beam value on sections located on the tension side (above the neutral axis), and conversely, it is higher on sections located on the compression side. As one would expect, as far as stress is concerned, slip dampens the bending effect.

If, at a certain location, wire (i) is in the slip regime, then its normal force F_i contributes a moment with respect to the neutral axis which is given by:

$$M_i = F_T \left(e^{\mu \theta_i \sin \alpha} - 1 \right) R \sin \theta_i \cos \alpha \tag{2.21}$$

where $R \sin \theta_i$ is the distance of wire (i) centerline from conductor neutral axis at this location. The $\cos \alpha$ term comes from the angle force F makes with the conductor axis.

It is still possible to express the bending moment vs curvature relationship as in Eq. (2.18). However, bending stiffness B is itself dependent on κ, and the (M vs κ) relationship is non-linear.

Rather than considering partial slip, with stick and slip regions, it is more interesting to study the limit case where slip is complete (total), with curvature κ_t. Beyond this value, tension F in each wire is a constant and the complementary moment is also a constant. It is the residual moment of friction M_{rf}. Only the moment coming from each wire bending stiffness B_w (Eq. (2.1)) continues to increase linearly with curvature κ.

Residual moment M_{rf} depends on the selected bending model.

Lehanneur's model (1949) yields:

$$M_{rf1} = \frac{4RF_T \cos \alpha \, e^{\mu \pi \sin \alpha}}{1 + e^{\mu \pi \sin \alpha}} \sum_{i=1}^{3} e^{-\mu(\frac{\pi}{2} - \theta_i) \sin \alpha} \sin \theta_i \tag{2.22}$$

in which summation is carried over wires located on the half circle $-\pi/2 \le \theta_i \le +\pi/2$. There is a factor 2 in order to take into account the moment arising from the wires on the other half-circle.

With Papailiou's model (1995), the residual moment is given by:

$$M_{rf2} = 2RF_T \cos \alpha \sum_{i=1}^{3} \left(e^{\mu \theta_i \sin \alpha} - 1 \right) \sin \theta_i \tag{2.23}$$

The simpler expression (2.23) comes from the already stated simplifying hypotheses: slip always starts at the neutral axis and wire force at this point remains equal to F_T. The following numerical example will show to what extent they differ.

Example 2.3

Using the data of Example 2.2, determine the residual bending moment M_{rf} as derived from Lehanneur's and Papailiou's models.

The calculation will be performed for a conductor section at which the half-circle wire centroid positions are: 0°, +60°, -60°.

Available Matlab® file: Example_2_3.m

Results:
From Eq. (2.22): $M_{rf1} = 66.1$ N.mm
From Eq. (2.23): $M_{rf2} = 67.3$ N.mm

Beyond complete slip curvature κ_t, called domain (II), total moment on the section is:

$$M_{II} = B_{min}\kappa + M_{rf} \tag{2.24}$$

An equivalent secant bending stiffness can be defined in domain (II). It is given by:

$$M_{II} = B(\kappa)\kappa = B_{min}\kappa + M_{rf} \tag{2.25}$$

which yields:

$$B(\kappa) = B_{min} + \frac{M_{rf}}{\kappa} \tag{2.26}$$

Example 2.4

Consider the same conductor as in preceding examples. Results from Papailiou's model are summarized below:

$B_{min} = 1.6268 \times 10^6$ N.mm^2 $B_{max} = 9.9986 \times 10^6$ N.mm^2

$\kappa_d = 6.63 \times 10^{-6}$ mm^{-1} $\kappa_t = 1.15 \times 10^{-5}$ mm^{-1}

$M_{rf} = 67.3$ N.mm

Available Matlab® file: Example_2_4.m

From these data, the $B(\kappa)$ curve can be drawn, except in the partial slip domain (Fig. 2.4). Here, it is sufficient to draw some approximate connecting curve between the B_{max} plateau and the $B(\kappa)$ curve given by Eq. (2.26).
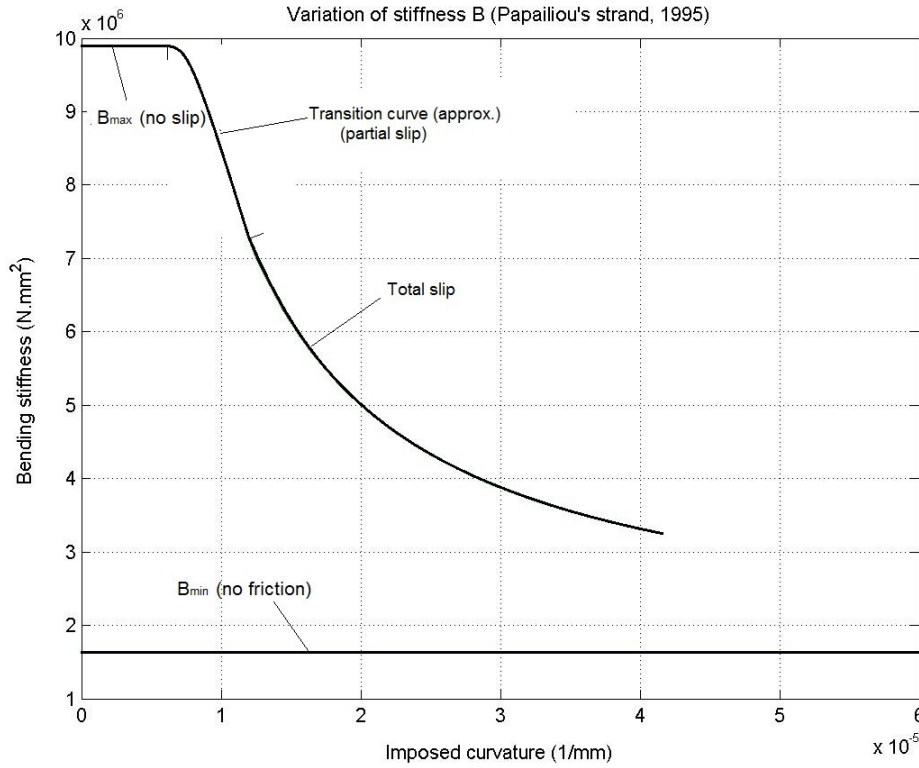
Figure 2. 4

Also of interest is the (M vs κ) curve. Its general shape is shown in Figure 2.5.
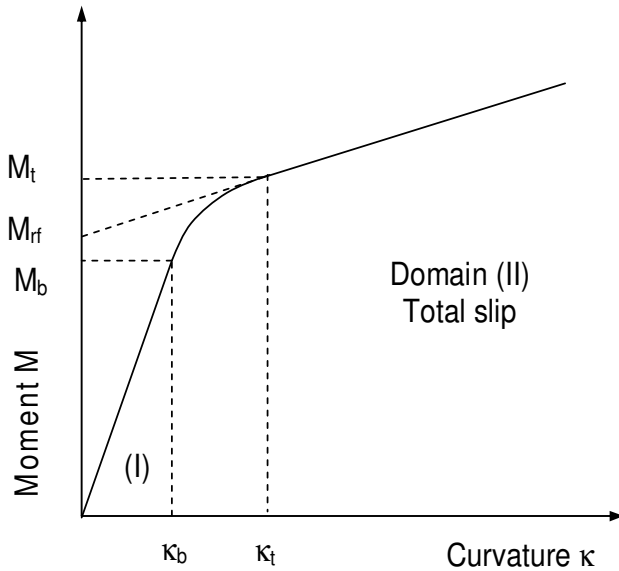
In domain (I), it is a straight line, slope B_{max} (Eq. 2.18). In domain (II), it is also a straight line, slope B_{min} which starts at the total slip point (κ_t, M_t). It intersects the vertical axis at ordinate point M_{rf}, the residual friction moment (Eqs (2.22) or (2.23)). Joining these two straight lines, there is a transition curve corresponding to the partial slip regime.

As suggested by Papailiou (1995), it is simpler to eliminate the non-linear part of the (M vs κ) diagram and replace it with a bilinear one (Fig. 2.6).

Figure 2. 5

25

Curvatures κ_b and κ_t are then replaced with a median transition curvature κ_m which corresponds to the point of intersection of domains (I) and (II) straight lines. The corresponding median transition moment is M_m. Then, the transition domain reduces to a single transition point A.
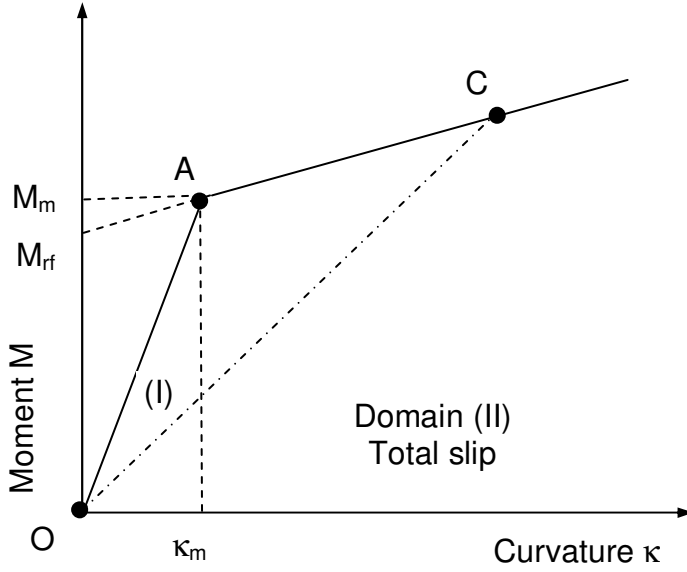
Point A being the point of intersection of the straight lines given by Eqs (2.18) and (2.25), median curvature κ_m is given by:

$$B_{max} \kappa_m = B_{min} \kappa_m + M_{rf} \tag{2.27}$$

Yielding:

$$\kappa_m = \frac{M_{rf}}{B_{max} - B_{min}} = \frac{M_{rf}}{B_{compI}} \tag{2.28}$$

Figure 2. 6

Recall that B_{compI} is the complementary stiffness in the no-slip regime (domain (I)), and is given by Eq. (2.8). Using the simpler form of residual moment M_{rf} given by Eq. (2.23), one gets the following expression for κ_m:

$$\kappa_m = \frac{2}{3} \frac{\varepsilon_T}{R} \cdot \frac{\sum\limits_{i=1}^{3} \left(e^{\mu \theta_i \sin \alpha} - 1 \right) \sin \theta_i}{\cos^2 \alpha} \tag{2.29}$$

in which ε_T is the wire unit strain from axial load T.

Corresponding moment M_m is given by:

$$M_m = B_{max} \kappa_m = \frac{B_{max}}{B_{max} - B_{min}} M_{rf} \tag{2.30}$$

If one lets $B_{max} = k_B B_{min}$:

$$M_m = \frac{k_B}{k_B - 1} M_{rf} \tag{2.31}$$

26

Considering a typical point C, such that $\kappa > \kappa_m$, stiffness $B(\kappa)$ as defined in Eq. (2.26) is the slope of straight line OC, and is called the "secant stiffness" at this particular point. Tangent stiffness at C is the slope of straight line AC, i.e. B_{min}. As seen in Fig. 2.6, and in Fig. 2.4, as $\kappa \to \infty$, then $B(\kappa) \to B_{min}$

Example 2.5

Consider the same conductor as in preceding examples, with the same initial stress $\sigma_T = 10$ MPa. Determine the median values κ_m and M_m. Draw the curves representing curvatures κ_b, κ_t and κ_m vs. σ_T.

Available Matlab® file: Example_2_5.m

Recall the preceding results:
Example 2.1 : $\quad\quad B_{max} = 9.9986 \times 10^6$ N.mm^2 $\quad B_{min} = 1.6268 \times 10^6$ N.mm^2

Thus, $B_{max} = 6.15 B_{min}$ $\quad k_B = 6.15$

Example 2.4 : $\quad\quad M_{rf} = 67.3$ N.mm

Hence, from Eq. (2.28) : $\quad \kappa_m = 8.03 \times 10^{-6}$ mm^{-1} $\quad\quad$ and from Eq. 2.31 : $\quad M_m = 80.4$ N.mm

Curvatures κ_d, κ_t et κ_m are all proportional to σ_T (see Eqs (2.14), (2.15), (2.29)).
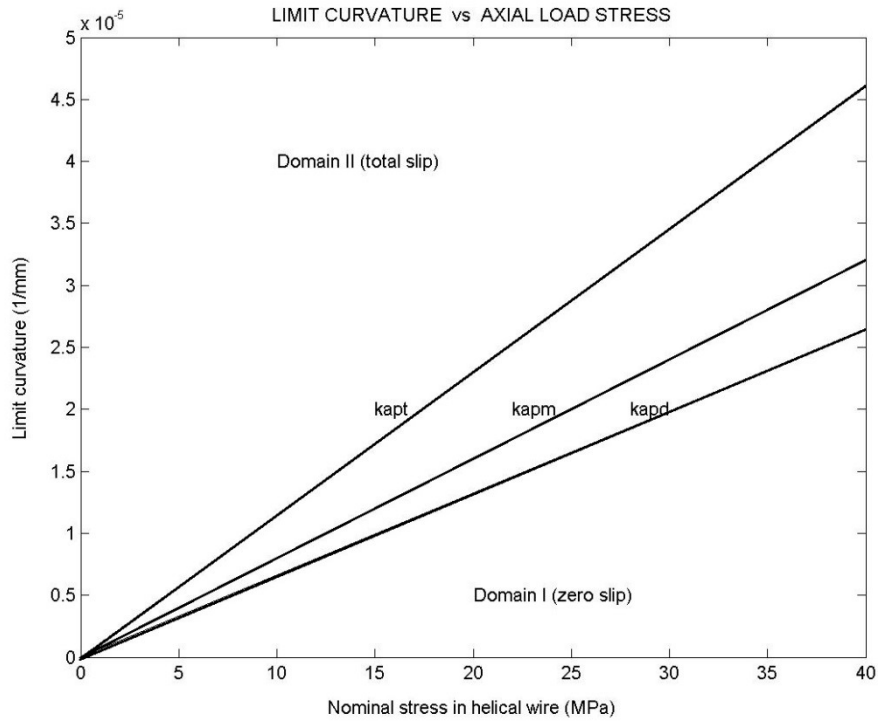
Limit curvatures: $\kappa_d = $ kapd ; $\kappa_m = $ kapm ; $\kappa_t = $ kapt

Figure 2. 7

27

2.5.3 Note on the calculation of residual friction moment M_{rf}

M_{rf} is obtained from Eqs (2.22) and (2.23). This requires positioning each wire centroid by its angle θ_i. Calculations have been made using one particular configuration in which two wires are centred on the conductor "neutral axis". Such sections are at a distance h/6 from each other. For intermediate sections, one should add some angle $\Delta\theta$ such that $0 < \Delta\theta < \pi/3$. This would modify slightly the value of M_{rf}. In fact, M_{rf} is not a constant but, rather, a periodic function along the conductor axis, period h/6. The maximum is reached when the top wires reach the top of the section, a rotation of 30°. For the case of Example 2.3, Papailiou's residual moment becomes 83.5 N.mm (compared with 67.3 N.mm in the initial position).

Physically, this indicates that in the total slip regime (domain II), the total moment which must be imposed on the conductor to obtain a constant curvature varies from section to section. In terms of Strength of Materials, this variable moment will need some shear force, which could come from transverse forces on the conductor, such as reaction forces coming from a pulley.

However, the objective of studying a single layer conductor is to introduce concepts which can be used in multilayer conductors. In such conductors, the number of wires in the outer layer may be much larger than 6, as it is in the single layer. For example, with a 30 wire layer, the angular difference between wires is 12°, and the variation in M_{rf} becomes negligible. Thus, as in Lehanneur (1949) and Papailiou (1995), M_{rf} will be considered a constant.

2.6 RHEOLOGICAL MODEL OF A STRAND IN BENDING (see Appendix C)

The (M vs κ) diagram in Fig. 2.6 shows the bending behaviour of the single layer conductor is similar (or analogous) to the stress-strain behaviour of some materials. Indeed, materials showing an elastic domain, a yield stress, and a subsequent strain hardening domain are often represented by a simple bilinear model, which leads to a stress-strain diagram similar to the diagram in Fig. 2.6. Such a bilinear model is often represented by a rheological system which is constituted by linear springs and frictional slider elements which are put in series or in parallel (Dowling, 1993). These elements are symbolically sketched as in Fig. 2.8.

Figure 2. 8

For a material under stress σ, which leads to strain ε, the element parameter is its Young's modulus E. In the frictional slider element, which is a stick-slip element, it is rigid up to its yield stress S_y, $|\sigma| < S_y$, at which point there is slip, with the applied stress remaining constant and equal to S_y. Strain ε is then undetermined.

For a conductor in bending, the analogy between parameters is as follows:

$$\sigma \to M \quad \varepsilon \to \kappa \quad E \to K \quad S_y \to M_m$$

Parameter K is a bending stiffness which may or may not be equal to B. Thus, the elements of the rheological model are:

Figure 2. 9

The bilinear diagram shown in Fig. 2.6 can be obtained with the spring-slider arrangement of Fig. 2.10.
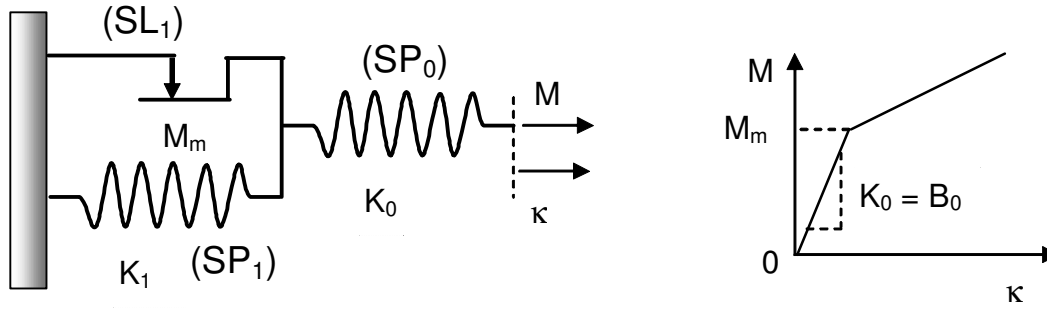
Figure 2. 10

Thus, the state equations are:

$$M < M_m \quad \kappa = \frac{M}{K_0}$$

$$M \geq M_m \quad \kappa = \frac{M_m}{K_0} + \frac{M - M_m}{K_1} = \kappa_e + \kappa_p \tag{2.31}$$

For small curvature, conductor has a linear elastic behaviour which comes entirely from spring element (SP_0). Slope of (M vs κ) diagram is $K_0 = B_{max}$. When $M = M_m$, incipient slip occurs in slider (SL_1), which allows spring (SP_1) to elongate. Total curvature κ has two components, one, κ_e, coming from element (SP_0), and the other, κ_p, from element (SP_1). Curvature κ_e is the "elastic" component, as it is reversible: it is brought back to zero when moment M is reversed to zero (unloading of conductor in bending). Curvature κ_p is a "permanent" curvature when $M = 0$. It is easily shown that the slope of the "strain hardening" line, which is $B_1 = B_{min}$ (Eq. (2.25)) is related to stiffness K_1 of spring element (SP_1) by:

$$\frac{1}{B_{min}} = \frac{1}{B_1} = \frac{1}{B_0} + \frac{1}{K_1} \tag{2.32}$$

from which one gets spring (SP$_1$) stiffness:

$$K_1 = \frac{B_1 B_0}{B_0 - B_1} = \frac{B_{min} B_{max}}{B_{max} - B_{min}} \tag{2.33}$$

Example 2.6

Consider the same conductor as in preceding examples, with the same initial stress $\sigma_T = 10$ MPa. It is to be modelled using the three-element rheological model of Fig. 2.10. Determine the corresponding parameters.

Available Matlab® file: Example_2_6.m

Results:
Spring (SP$_0$) : stiffness $B_0 = B_{max} = 9.9986 \times 10^6$ N.mm^2
Spring (SP$_1$) : stiffness $K_1 = 1.9429 \times 10^6$ N.mm^2
Slider (SL$_1$) : slip limit $M_m = 80.4$ N.mm $\quad \kappa_m = M_m / B_{max} = 8.04 \times 10^{-6}$ mm^{-1}

An advantage of using this rheological model is the easy recovery of various properties in load-unload-load cycles which have been described by Papailiou (1995) through an *ad hoc* approach.

a) Elastic cycle
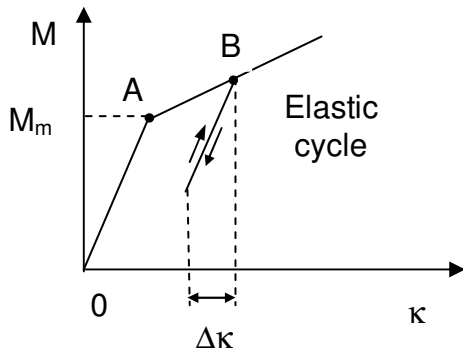
Figure 2. 11

The strand is loaded in bending up to $M > M_m$, corresponding to point B on the (M vs κ) diagram. Then, bending moment is decreased slightly of ΔM. Such decrease comes entirely from spring (S$_0$), with its stiffness B_{max}. Indeed, frictional slider (SL$_1$) prevents any reversal in the extension of spring (SP$_1$) as long as $\Delta M \leq 2M_m$. Thus, curvature variation can only come from spring (SP$_0$). The resulting unloading curve is thus a straight line which is parallel to the loading curve OA, slope B_{max}, and corresponds to a curvature variation $\Delta \kappa = \Delta M / B_{max}$

As a practical application, consider small amplitude vibrations of a taut conductor which has undergone an initial static bending. For these small variations in the bending moment, it is the bending stiffness B_{max} which must be considered. Because of the tangential elasticity at contact points, this is not quite true. However, here we restrict the analysis to the usual stick-slip Coulomb's law between rigid solids.

The stiffness which applies to small load-unload cycles is quite different from the secant stiffness as defined by Eq. (2.26), which is the slope of line OC in Fig. 2.6.

b) Hysteresis cycle

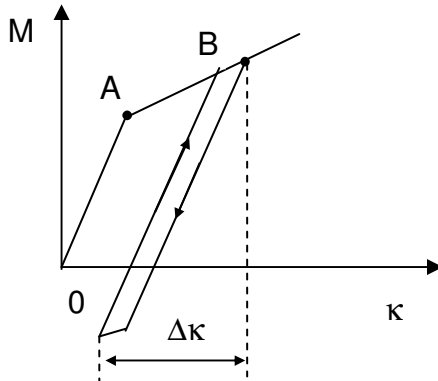Consider now a load-unload-reload cycle for which $\Delta M > 2M_m$. The resulting variation in curvature is $\Delta\kappa > 2\kappa_m$. Such cycle will bring a reverse slip of frictional slider (SL_1). Physically, this corresponds to a reverse slip of the helical wires on the core wire, and to some energy dissipation which is represented by the area of the cycle in Fig. 2.12.

Figure 2. 12

Example 2.7

Consider the same conductor as in preceding examples, with the same initial stress $\sigma_T = 10$ MPa. It undergoes a curvature cycle of amplitude $\Delta\kappa = 2 \ 10^{-5}$ mm^{-1}. Using the preceding rheological model, determine the dissipated energy ΔU at each cycle (per unit length of conductor).

This energy is given by the area of the parallelogram such as the one shown in Fig. 2.12.

Available Matlab$^{®}$ file: Example_2_7.m

Result:: $\Delta U = 1.6 \times 10^{-3}$ N (or mJ / mm)

2.7   FURTHER REMARKS

2.7.1   Variation of wire curvature

As already mentioned, slip limit is based on the line contact force, which is determined from wire tension F and local wire curvature. When the conductor is straight and wire centerline a true helix curve, this curvature is uniform (it has the same value everywhere along the wire). When the conductor is bent, local curvature varies from point to point. Lehanneur (1949) and Papailiou (1995) neglect this variation and consider the radius of curvature (in the osculating plane) remains equal to the initial value $\rho_h = R/\sin^2\alpha$. The variation in wire curvature has been considered by authors who were mostly interested in the calculation of bending stresses (such as the ones arising from winding a cable on a pulley), and in situations where friction is neglected. Leider (1975) has published a comparative study of the variation of wire curvature.

2.7.2   Free bending – variable strand curvature

Conductors are generally in a state of free bending rather than forced bending such as found in cables wound around pulleys or drums. In conductors, forced bending occurs at suspension clamps when the clamp keeper forces the conductor into the clamp.

Cable free bending, taking friction forces into account, has been studied by Ernst (1933) in the context of ropeway applications. However, with variable cable curvature, the analysis does not lead to explicit results, such as those obtained with the uniform curvature hypothesis.

Rather than going directly to the variable curvature case using an analytical approach, it seems more practical to use Papailiou's approach (1995) which consists in starting with a uniform curvature analysis, leading to explicit results, followed by a numerical extension to the variable curvature case. This is the approach used in the following chapters.

CHAPTER 3

BENDING OF A MULTILAYER CONDUCTOR

3.1   HYPOTHESES

Here, the cases under study are restricted to ordinary multilayer conductors with circular section wires and reverse lay. In a given layer, wires are identical, with the same radius and material, either steel or aluminum.

A conductor is made of m layers, numbered starting from the outer layer, which is always layer (1), to the innermost layer, layer (m), in contact with the core wire. In layer (i), there are n_i wires, with cross-section radius r_i. Initially, the wire centerline is a circular helix with lay angle α_i and lay cylinder radius R_i. Assumptions made for a single layer conductor still hold.

3.1.1   Contact conditions

It is assumed again that contact between wires is radial, i.e. between adjacent layers. This means possible contact between same layer wires can be neglected when studying a conductor bending behaviour. Because of the reverse lay, contact between layers is a "trellis" of contact points, except for layer (m) which is in line contact with the core wire.

It is also assumed the contact fibre on a wire, on which contact points with the adjacent layer are located, has the same lay angle α_i as the wire centerline, even if the radius of the contact cylinder is different. Contact forces are now point forces except for layer (m). Normal force N_{Ci} between layers (i) and (i+1) depend on the applied axial force T. As shown in Chapter 1, its value depends not only on the wire tension force F_i, but also on the clenching pressure from layers (i-1), (i-2) etc. Also neglected, in this chapter, is the flattening in the contact zones, which gives an elliptical contact, instead of a point contact, or a strip contact rather than a line contact. Friction forces between wires (including core wire) are assumed to follow Coulomb's law.

3.1.2   Wire shape in a bent conductor

In a bent conductor, when a radius of curvature ρ is imposed to the conductor centerline, wire centerlines are curves on a torus with a cross section radius R_i. These curves are again assumed to be "toroidal helices" as defined in the single layer case (Chapter 2).

3.2   NO-FRICTION CASE

Assuming a zero coefficient of friction, wires are free to bend with respect to their own individual neutral axis. Global conductor bending stiffness is a minimum. It is calculated in the same fashion as in the single layer case. Thus, Eqs (2.2) to (2.5) are easily generalized. For example, Papailiou's Eq. (2.3), in which wire torsion is neglected, yields:

$$B_{min} = \sum_{i=1}^{m} n_i B_{w,i} \cos \alpha_i + B_c \qquad (3.1)$$

where $B_{w,i}$ is a single wire bending stiffness in layer (i):

$$B_{w,i} = E_i I_i \qquad \text{with} \qquad I_i = \frac{\pi r_i^4}{4} \tag{3.2}$$

3.3 ZERO-SLIP BENDING

As in the single layer case, it is assumed there is some friction between wires in contact. Here, the coefficient of friction μ is assumed to be large enough to prevent any slip when the conductor is imposed a uniform curvature κ.

Then, the conductor should behave like a solid beam. The Bernoulli-Euler hypothesis is supposed to apply: a plane conductor cross-section remains a plane in the bending process. Thus, helical wire section center points, initially in the same plane, stay coplanar. Conductor bending stiffness takes its maximum value B_{max}. It is given by:

$$B_{max} = B_{min} + B_{compI} \tag{3.3}$$

Complementary bending stiffness B_{compI} is given by Eq. (2.8) generalized as:

$$B_{compI} = \sum_{i=1}^{m} \frac{n_i}{2} A_i E_i R_i^2 \cos^3 \alpha_i \tag{3.4}$$

in which the identity $\sum_{k=1}^{n_i} \sin^2 \varphi_k = n_i/2$ with $\varphi_{k+1} - \varphi_k = 2\pi/n_i$ for any layer (i) has been used (see proof in Appendix B).

Example 3.1a

Parameters of conductor Bersimis ACSR are given in Appendix A.
Determine its bending stiffnesses B_{min}, B_{compI} et B_{max}.

Available Matlab® file: Example_3_1.m :

Results:
From Eq. (3.1): $\qquad B_{min} = 63.48 \times 10^6$ N.mm^2
From Eq. (3.4): $\qquad B_{compI} = 3.4198 \times 10^9$ N.mm^2
From Eq. (3.3): $\qquad B_{max} = 3.4832 \times 10^9$ N.mm^2

Note that B_{compI} is the main contributing term in B_{max}. Ratio between maximum and minimum bending stiffness is : $B_{max}/B_{min} = 54.9$, or approximately 55.

When lay angles are neglected (parallel straight wires), the following "approximate" values are obtained:

$$B_{min,ap} = 65.02 \times 10^6 \text{ N.mm}^2 \qquad B_{max,ap} = 3.7865 \times 10^9 \text{ N.mm}^2$$

The error on B_{max} is seen to be of an order of magnitude larger than B_{min} itself.

Example 3.1b

Parameters of conductor Cardinal ACSR are given in Appendix A.
Determine its bending stiffnesses B_{min}, B_{compI} et B_{max} .

Available Matlab[®] file: Example_3_1.m :

Results:

From Eq. (3.1):	$B_{min} = 27.75 \times 10^6 \text{ N.mm}^2$
From Eq. (3.4):	$B_{compI} = 1.7569 \times 10^9 \text{ N.mm}^2$
From Eq. (3.3):	$B_{max} = 1.7846 \times 10^9 \text{ N.mm}^2$

Here, ratio B_{max}/B_{min} is approximately 64.

3.4 BENDING IN THE SLIP REGIME

3.4.1 Qualitative analysis of the process

Conductor is initially straight and under axial load T. A uniform curvature κ is imposed in a monotonous way, starting from zero. In the current model, tangential elasticity is neglected. Thus, the conductor behaves initially like a solid beam, with bending stiffness B_{max}. Then, when $\kappa = \kappa_{b1}$, incipient slip will appear on wires in the outer layer. As in the single layer case, slip propagates while κ is increased. At curvature κ_{t1} slip is complete in layer (1). The same process is to be expected at inner layers: (κ_{b2}, κ_{t2}) in layer (2) etc.

Because inter-layer pressure is higher between inner layers, and also because the maximum tensile force in wires (due to bending) is smaller due to their closeness to the neutral axis, slip phases start sequentially, from the outer layer to the inner ones.

Rebuffel (1949), Lehanneur (1949), Lanteigne (1985) and Papailiou (1995) all assume there is no overlap of the slip phases, meaning total slip is achieved in one layer before the next one starts slipping and $\kappa_{b1} < \kappa_{t1} \leq \kappa_{b2} < \kappa_{t2} \leq \kappa_{b3} < \cdots$. In the paper by Hong *et al.* (2005), there seems to be a problem in the boundary conditions between stick and slip zones, and complete slip is never reached in any layer.

3.4.2 Pressure transmission between layers

As shown in Chapter 1, because of the clenching effect due to the applied axial load T, each layer (i) exerts a pressure on the adjacent layer (i+1). In the single layer case (Chapter 2), this pressure is applied on the core wire. This direct contact pressure is easily determined. However, it also affects the contact pressure between layers (i+1) and (i+2) etc.

Assuming this pressure is integrally transmitted, it was shown in Chapter 1 that the total line load between layers (i) and (i+1) on a wire of layer (i) is given by Eq. (1.25):

$$q_{Ni} = \frac{dN_i}{ds_i} = \frac{\cos\alpha_i}{n_i} \sum_{j=1}^{j=i} \frac{n_j}{R_j} \frac{\sin^2\alpha_j}{\cos\alpha_j} F_j \qquad (3.5)$$

which may be rewritten as:

$$q_{Ni} = \frac{dN_i}{ds_i} = \sum_{j=1}^{j=i} \frac{r_i}{r_j} \frac{\sin^2\alpha_j}{R_i} F_j \qquad (3.6)$$

where ds_i is the arc length element on the corresponding line of contact of layer (i).

3.4.3 Point and line contact

An important difference between single layer and multiple layer conductors is the occurrence of point contacts between adjacent layers because of the alternate lays. These contact points render the analysis of stick-slip conditions much more complex.

Papailiou (1995) has shown that the discrete problem arising from the contact points could in fact be replaced by an equivalent continuous line contact problem. This approach will be used in the following analysis, although possible problems arising from this simplification will also be mentioned.

3.4.4 Slip conditions on a wire element
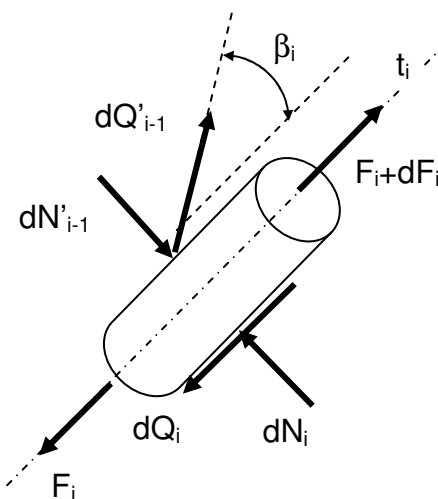
In Fig. 3.1, free body diagram for a wire element ds_i of layer (i) is shown when curvature κ is imposed on the conductor. Here, a wire is considered to be a simple fibre where the only internal force on the cross-section is the tensile force F_i. Because of the imposed conductor bending, this force undergoes a variation dF_i along the wire element. The external forces on the element arise from the contacts with layer (i-1) (on the outer fibre of the helical wire) and with layer (i+1) (wire inner fibre). As mentioned above, point contacts are replaced by line contacts.

It is assumed wire slip on the inner adjacent layer (i+1) will occur in direction (t_i), which is the local direction of the tangent to the wire centerline. It is also assumed layer (i+1) is still sticking to layer (i+2). Tangential force dQ_i is parallel to direction (t_i). However, if layer (i-1) is already slipping on layer (i), tangential

Figure 3. 1

force dQ'_{i-1} makes an angle β_i with respect to direction (t_i). In fact, angle β_i depends on the relative motion of the material points in contact.

If wire element ds_i is still in the stick regime with respect to layer $(i+1)$, relative velocity of contacting points at the $(i-1, i)$ interface is in the (t_{i-1}) direction and $\beta_i = \alpha_i + \alpha_{i-1}$. Elementary tangential force dQ'_{i-1} is parallel to the (t_{i-1}) direction. However, as soon as element ds_i enters the slip regime, relative speed of contacting points at the $(i-1, i)$ interface deviates from this direction and one has $\beta_i > \alpha_i + \alpha_{i-1}$ (Fig. 3.2).
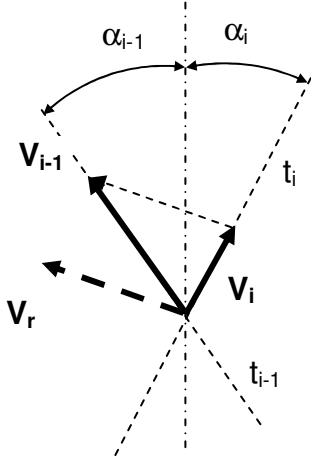

According to Coulomb's law, tangential force dQ'_{i-1} is parallel to the relative velocity $\vec{V_r}$ of contacting points and it is in the opposite direction.

In order to express the equilibrium equation of element ds_i in the (t_i) direction, projection of the elementary tangential force dQ'_i onto this direction has to be taken. At the incipient slip stage, it is merely $dQ'_i \cos(\alpha_i + \alpha_{i-1})$. However, as the slip zone propagates on the $(i, i+1)$ interface, angle β_i varies from point to point along the line of contact.

It is thus difficult to write down an explicit equilibrium equation for any element ds_i in the slip zone. This explains why all published solutions are based on the following simplifying assumptions.

Figure 3. 2

3.4.5 Slip conditions (SC1) from Rebuffel-Lehanneur (1949)

Rebuffel (1949) and Lehanneur (1949) assume tangential force dQ'_{i-1} is parallel to direction (t_i) and in the same direction as the slip velocity $\vec{V_i}$ (Fig. 3.2), since the slip of layer $(i-1)$ on layer (i) is itself an inducing factor for the slip of layer (i) on layer $(i+1)$.

As already mentioned, at interface between layers (i) and $(i+1)$, the normal line contact force on a layer (i) wire is given by Eq. (3.6). However, from Eq. (1.29), the line contact force at interface $(i, i-1)$, acting on this same wire is:

$$q'_{N,i-1} = \frac{r_i}{r_{i-1}} \frac{R_{i-1}}{R_i} \sum_{j=1}^{i-1} \frac{r_{i-1}}{r_j} \frac{\sin^2 \alpha_j}{R_{i-1}} F_j \tag{3.7}$$

These two expressions differ by the term $j = i$, which corresponds to the line contact force arising from tension F_i in a wire of layer (i), but also, the terms coming from the outer layers are not identical. They are close when wire radii are equal and for outer layers, where R_i and R_{i-1} are not too different.

Neglecting these differences, the only tangential force available to equilibrate the variation dF_i due to bending comes from the normal force due to F_i in that same wire, as in the outer layer. Thus, with this

hypothesis, the same slip condition applies to all layers, and it is independent from the pressure coming from the upper (i.e. outer) layers.

This condition is the same as the one obtained with the single layer conductor. It yields the same equations for the limit curvatures, in which the parameters are those pertaining to each layer (i). Thus, for layer (i), the incipient slip curvature is given by the modified Eq. (2.14):

$$\kappa_{bi} = \sigma_{Ti} \frac{\mu_i \sin \alpha_i}{E_i R_i \cos^2 \alpha_i} \tag{3.8}$$

In layer (i), total slip curvature is also given by Eq. (2.15):

$$\kappa_{ti} = \frac{\sigma_{Ti}}{E_i R_i \cos^2 \alpha_i} \left(e^{\mu_i (\pi/2) \sin \alpha_i} - 1 \right) \tag{3.9}$$

When total slip state has been reached in layer (i), the friction residual moment between layers (i) and (i+1) is given by Eq. (2.23):

$$M_{rfi} = 2 R_i F_{T_i} \cos \alpha_i \sum_{j=1}^{n_i/2} \left(e^{\mu_i \theta_j \sin \alpha_i} - 1 \right) \sin \theta_j \tag{3.10}$$

where it is assumed the wire numbers n_i are even numbers. The same remark as in section 2.5.3 should be made regarding the calculation of M_{rfi}. It is performed in one particular section and varies slightly for adjacent sections adjacent. The convention for the calculation of M_{rfi} is as follows. If the integer $(n_i/2)$ is odd (n_i itself is assumed to be an even number), one wire centroid is assumed to be located on the conductor neutral axis. If $(n_i/2)$ is an even number, wires are assumed to be symmetrical with respect to the neutral axis. Note that in the no-slip regime, this problem does not arise.

Example 3.2a

In the Bersimis ACSR, coefficient of friction between layers is assumed to have the uniform value $\mu_i = 0.7$. An axial load T = 30% RTS is applied. Based on contact hypotheses (SC1), determine:

- The limit curvatures κ_b and κ_t for each of the four layers
- The residual friction moment at each interlayer.

Available Matlab® file: Example_3_2.m

From Eq. (3.8) : κ_b = [1.018 1.302 1.528 2.321] 10^{-5} (1/mm)
From Eq. (3.9) : κ_t = [1.834 2.312 2.605 3.839] 10^{-5} (1/mm)

It is found that Lehanneur's hypothesis, that slip is complete on a layer before the next one starts slipping, is not satisfied. One may still assume that the slip zone in layer (i+1) is in contact with a slip zone in layer (i), which would justify, up to a certain point, the hypothesis that the tangential force component due to the outer layers vanishes.

38

Result:
Residual moment of friction (Eq. (3.10)) : M_{rf} = [3.116 1.385 0.309 0.054] 10^4 N.mm

Example 3.2b

In the Cardinal ACSR, coefficient of friction between layers is assumed to have the uniform value $\mu_i = 0.7$. An axial load T = 30% RTS is applied. Based on contact hypotheses (SC1), determine:

- The limit curvatures κ_b and κ_t for each of the four layers
- The residual friction moment at each interlayer.

Use Matlab$^®$ file : Example_3_2.m

From Eq. (3.8) : κ_b = [1.389 1.670 2.541 2.579] 10^{-5} (1/mm)
From Eq. (3.9) : κ_t = [2.478 2.942 4.484 4.295] 10^{-5} (1/mm)

It is found that layer (4) reaches complete slip state before layer (3). This shows that slip conditions (SC1) are not valid in this case, as layer (3) will tend to be put into slip by layer (4), and slip in layer (4) would be restrained by layer (3). Direction of tangential forces shown in Fig. 3.4 should then be reversed.

Result:
Residual moment of friction (Eq. (3.10)) :M_{rf} = [1.9549 1.0132 0.4093 0.1591] 10^4 N.mm

3.4.6   Slip conditions (SC2) from Papailiou (1995)

While conditions (SC1) neglect completely the effect of outer layers on layer (i) slip, Papailiou (1995) and other authors (e.g. Hong et al. 2005), assume that the components of tangential friction forces dQ'_i acting on a wire element and related to outer layer pressure all act opposite to the slip direction. Besides, they are supposed to be identical on the inner and outer wire (i) fibres, that is at the (i, i+1) and (i, i-1) interfaces. This is equivalent to applying a coefficient of friction ($\mu_i + \mu_{i-1}$), that is $2\mu_i$, in general, to the normal contact force (Eq. (3.6)) coming from the layers on top of layer (i). Obviously, conditions (SC1) and (SC2) differ drastically.

Conditions (SC2) are difficult to justify physically. And this is the more so, as the slip phases are assumed to occur sequentially, without any overlap, from one layer to the next. It is difficult to understand why layer (i-1), being in the slip state, would oppose layer (i) slip. Thus, conditions (SC2) tend to have a strong retardation effect on inner layer slip. An advantage, for the mechanical motel, is that slip from one layer to the next is then clearly sequential, with no overlap. That is, slip is complete on one layer, before it starts on the next. As more general equilibrium equations are needed, numerical applications of these slip conditions will be shown later on.

3.4.7   Slip conditions (SC3)

With slip conditions (SC1) tangential friction forces arising from pressure exerted on layer (i) by outer layers (1) to (i-1) are assumed to be equal and opposite. The conductor lay being alternate (reverse), we have seen that this is not the case. At incipient slip of layer (i-1), elementary force dQ'_{i-1} is directed

parallel to the corresponding wire local tangent (practically the same as the wire centerline). Thus, because of the alternate lay, dQ'_{i-1} makes an angle close to $(\alpha_i + \alpha_{i-1})$ with the outer fibre of the layer (i) wire, lay angles being taken as absolute values (Fig. 3.3).
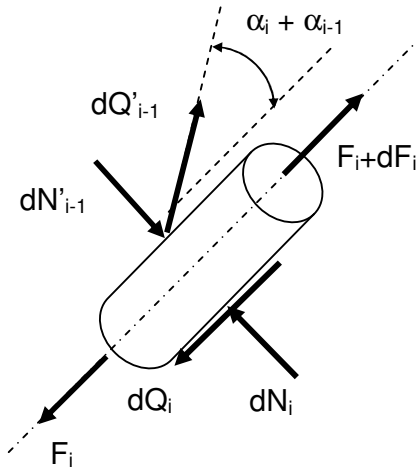

Figure 3. 3

When layer (i) wire starts slipping on layer (i+1), the counteracting friction force is oriented along the local tangent to the virtual contact line between these two layers. Slip of layer (i) slightly modifies the relative motion with respect to layer (i-1). Thus, the corresponding friction force direction is also slightly modified. We shall neglect this effect, which vanishes at incipient slip (Fig. 3.3).

For a wire element ds_i , the corresponding equilibrium equation is :

$$dF_i + dQ'_{i-1} \cos(\alpha_i + \alpha_{i-1}) - dQ_i = 0 \tag{3.11}$$

It is assumed that, when slip occurs at interface (i, i+1), it has already started at interface (i-1, i). Thus, dF_i takes the limit value:

$$dF_i = dF_{Li} = \mu_i dN_i - \mu_{i-1} dN'_{i-1} \cos(\alpha_i + \alpha_{i-1}) \tag{3.12}$$

Normal line contact force at interface (i, i+1) is given by Eq. (3.6), while at interface (i, i-1), it is given by Eq. (3.7).

And, using the same transformation as in Eq. (1.23) :

$$dN_i = \sum_{j=1}^{i-1} \frac{r_i}{r_j} \frac{\sin^2 \alpha_j}{\sin \alpha_i} F_j \, d\varphi + \sin \alpha_i \, F_i \, d\varphi$$

$$dN'_{i-1} = \frac{r_i}{r_{i-1}} \frac{\sin \alpha_{i-1}}{\sin \alpha_i} dN_{i-1} \tag{3.13}$$

Again, it is assumed that layer (i) slip occurs after it has occurred in the outer layers (1) through (i-1). Thus, forces F_i take their limit value F_{Li} and Eq. (3.12) becomes:

$$dF_i = \mu_i \left(\sum_{j=1}^{i-1} \frac{r_i}{r_j} \frac{\sin^2 \alpha_j}{\sin \alpha_i} F_{Lj} \, d\theta + \sin \alpha_i \, F_{Li} \, d\theta \right)$$

$$-\mu_{i-1} \frac{r_i}{r_{i-1}} \frac{\sin \alpha_{i-1}}{\sin \alpha_i} \left(\sum_{j=1}^{i-2} \frac{r_{i-1}}{r_j} \frac{\sin^2 \alpha_j}{\sin \alpha_{i-1}} F_{Lj} \, d\theta + \sin \alpha_{i-1} \, F_{L,i-1} \, d\theta \right) \cos(\alpha_i + \alpha_{i-1}) \tag{3.14}$$

which yields:

$$\frac{dF_{Li}}{d\theta} - \mu_i \sin \alpha_i \, F_{Li} = \frac{r_i}{\sin \alpha_i} \left[\mu_i - \mu_{i-1} \cos(\alpha_i + \alpha_{i-1}) \right] \sum_{j=1}^{i-1} \frac{\sin^2 \alpha_j}{r_j} F_{Lj} \tag{3.15}$$

These differential equations have to be integrated layer after layer, starting with the outer one. The first integral yields:

$$F_{L1} = F_{T1} e^{\mu_1 \sin \alpha_1 \theta} \tag{3.16}$$

This equation for wire tension F_1 is valid only in the slip zone. For the next layer, it is again assumed slip starts on the conductor section "neutral axis". Function (3.16) can now be used in the right hand member of Eq. (3.15). And the solution of this equation for the second layer ($i = 2$) is easily obtained. However, this solution is valid in layer (1) slip zone only.

Papailiou (1995) assumes slip occurs sequentially: e.g., it starts in layer (2) only after it has been completed in layer (1). Besides, he simplifies the equations by replacing functions $F_{Lk}(\varphi)$ by their initial constant value F_{Tk}. His calculations show this approximation has but a small influence on the resulting value for $F_{Li}(\varphi)$. Hong *et al.* (2005), however, do not use this simplification, and this leads to rather different results.

It has also been found, using slip conditions (SC1), in which layers are independent, that slip in layer (i) may start even before it has started in layer (i-1) (Example 3.2b).

Slip conditions (SC3): a study of slip propagation from one layer to the other
For each layer (i), the following parameters are defined:

$$\lambda_i = \mu_i \sin \alpha_i \tag{3.17}$$

$$b_i = \frac{\sin^2 \alpha_i}{r_i} \tag{3.18}$$

$$c_i = \frac{r_i}{\sin \alpha_i} \left(\mu_i - \mu_{i-1} \cos(\alpha_i + \alpha_{i-1}) \right) \tag{3.19}$$

Eq. (3.15) may then be expressed as:

$$\frac{dF_{Li}}{d\theta} - \lambda_i F_{Li} = c_i \sum_{j=1}^{i-1} b_j F_{Lj} \tag{3.20}$$

These equations are then easily integrated, layer after layer, starting with the outer layer (i =1). In each case, Papailiou's hypothesis is used: wire force F_i is assumed to remain constant (independent of conductor curvature) at the section "neutral axis" ($\varphi = 0$ or π) and it stays equal to the initial force F_{Ti} arising from the applied axial force T on the conductor. Solutions given below correspond to the half-layer [-π/2 +π/2]. They are:

For i = 1 :

$$F_{L1} = a_{1,1} e^{\lambda_1 \theta} \quad \text{with} \quad a_{1,1} = F_{T1} \tag{3.21}$$

For i = 2 :

$$F_{L2} = a_{2,1} e^{\lambda_1 \theta} + a_{2,2} e^{\lambda_2 \theta} \tag{3.22}$$

41

where:

$$a_{2,1} = \frac{c_2}{\lambda_1 - \lambda_2} b_1 a_{1,1} \qquad a_{2,2} = F_{T2} - a_{2,1} \tag{3.23}$$

For i = 3 :

$$F_{L3} = a_{3,1} e^{\lambda_1 \theta} + a_{3,2} e^{\lambda_2 \theta} + a_{3,3} e^{\lambda_3 \theta} \tag{3.24}$$

where:

$$a_{3,1} = \frac{c_3}{\lambda_1 - \lambda_3} (b_1 a_{1,1} + b_2 a_{2,1}) \qquad a_{3,2} = \frac{c_3}{\lambda_2 - \lambda_3} b_2 a_{2,2} \qquad a_{3,3} = F_{T3} - (a_{3,1} + a_{3,2}) \tag{3.25}$$

For i = 4 :

$$F_{L4} = a_{4,1} e^{\lambda_1 \theta} + a_{4,2} e^{\lambda_2 \theta} + a_{4,3} e^{\lambda_3 \theta} + a_{4,4} e^{\lambda_4 \theta} \tag{3.26}$$

where:

$$a_{4,1} = \frac{c_4}{\lambda_1 - \lambda_4} (b_1 a_{1,1} + b_2 a_{2,1} + b_3 a_{3,1}) \qquad a_{4,2} = \frac{c_4}{\lambda_2 - \lambda_4} (b_2 a_{2,2} + b_3 a_{3,2})$$

$$a_{4,3} = \frac{c_4}{\lambda_3 - \lambda_4} b_3 a_{3,3} \qquad a_{4,4} = F_{T4} - (a_{4,1} + a_{4,2} + a_{4,3}) \tag{3.27}$$

etc.

These equations are easily put in a general form. In layer $i \leq m$, wire force in the slip zone is given by :

$$F_{Li} = \sum_{j=1}^{i} a_{i,j} e^{\lambda_j \theta} \tag{3.28}$$

in which coefficients $a_{i,j}$ are given by :

$$a_{i,j} = \frac{c_i}{\lambda_j - \lambda_i} \sum_{k=j}^{i-1} b_k a_{k,j} \quad \text{for} \quad j < i \leq m$$

$$a_{i,i} = F_{Ti} - \sum_{k=1}^{i-1} a_{i,k} \tag{3.29}$$

In each sum, a negative or null index corresponds to a vanishing term.

Slip initiation in layer (i)
Once again, it is assumed slip always starts on wire sections located on the conductor "neutral axis". Before the occurrence of slip, the complementary stress in a wire is given by the usual sine function:

$$\sigma_i = E_i \kappa (R_i \sin \theta) \cos^2 \alpha_i \tag{3.30}$$

Thus, in the no-slip domain (domain I), the total wire force is given by:

$$F_{Ii} = F_{Ti} + A_i E_i \kappa (R_i \sin \theta) \cos^2 \alpha_i \qquad (3.31)$$

The slope of this sine function at $\varphi = 0$ is:

$$\left. \frac{dF_{Ii}}{d\theta} \right|_{\theta=0} = A_i E_i \kappa R_i \cos^2 \alpha_i \qquad (3.32)$$

In layer (i), the limit force, which is independent of the imposed curvature, is given by Eq. (3.28). Its derivative at $\varphi = 0$ is :

$$\left. \frac{dF_{Li}}{d\theta} \right|_{\theta=0} = \sum_{j=1}^{i} \lambda_j a_{i,j} \qquad (3.33)$$

Incipient slip in layer (i) occurs at curvature κ_{bi} , when both slopes are equal. Thus, this yields an equation for κ_{bi} :

$$\kappa_{bi} = \frac{\displaystyle\sum_{j=1}^{i} \lambda_j a_{i,j}}{A_i E_i R_i \cos^2 \alpha_i} \qquad (3.34)$$

Total slip in layer (i)

Slip is complete in layer (i) when the slip zone reaches the "extrados"section ($\theta = \pi/2$), that is, the contact points located further away from the section "neutral axis", on the convex side . This occurs for curvature κ_{ti} . At this stage, one has $F_{Ii}\left(\dfrac{\pi}{2}\right) = F_{Li}\left(\dfrac{\pi}{2}\right)$. From Eqs (3.28) and (3.31), this yields

$$F_{Ti} + A_i E_i \kappa_{ti} R_i \cos^2 \alpha_i = \sum_{j=1}^{i} a_{i,j} e^{\lambda_j \pi/2} \qquad (3.35)$$

From which the limit curvature κ_{ti} is obtained:

$$\kappa_{ti} = \frac{\displaystyle\sum_{j=1}^{i} a_{i,j} e^{\lambda_j \pi/2} - F_{Ti}}{A_i E_i R_i \cos^2 \alpha_i} \qquad (3.36)$$

Residual moment of friction on layer (i)

When slip of layer (i) on layer (i+1) is complete, force $F_{Li}(\theta)$ in each wire of layer (i) is now independent of conductor curvature. Let M_{rfi} be the moment of these forces with respect to the conductor section "neutral axis". As in the single layer case, it is called the "residual moment of friction". Here, it is given by:

43

$$M_{\text{rfi}} = 2\cos\alpha_i \sum_{j=1}^{n_i/2} \left(F_{\text{Li}}(\theta_j) - F_{\text{Ti}}\right) R_i \sin\theta_j \qquad (3.37)$$

Here again, a factor 2 is needed as the summation is made on half of the wires, those located in the $\left[-\pi/2 + \pi/2\right]$ domain. It is not absolutely necessary to subtract F_{Ti} from F_{Li} since, in principle, one has the identity $\sum_{j=1}^{n_i/2} \sin\theta_j = 0$. It is shown in the equation in case a certain positioning of the wires in the cross section would not exactly yield a zero moment from the F_{Ti} forces.

Example 3.3

In the Bersimis ACSR, coefficient of friction between layers is assumed to have the uniform value $\mu_i = 0.7$. An axial load $T = 30\%$ RTS is applied. Based on slip conditions (SC3), determine:

- The limit curvatures κ_b and κ_t for each of the four layers
- The residual friction moment at each interlayer.

Available Matlab® file: Example_3_3.m (with case No 1)

Results:
Limit curvatures
From Eq. (3.34) : $\kappa_b = [1.018 \ 1.548 \ 2.233 \ 3.171] \ 10^{-5}$ (1/mm)
From Eq. (3.36) : $\kappa_t = [1.834 \ 2.810 \ 3.984 \ 5.448] \ 10^{-5}$ (1/mm)

With these slip conditions, slip of layer (2) initiates before complete slip in layer (1). This also applies to layers (3) and (4).

Residual moment of friction (Eq. (3.37)) :
They are calculated with the original (SC3) hypotheses. However, while the value of the fourth moment is questionable, its relative influence is very small.

$M_{\text{rf}} = [3.1160 \ 1.65 \ 0.4533 \ 0.074] \ 10^4$ N.mm

3.4.8   Slip conditions (SC4)

In Eq. (3.15), limit forces F_{Lj} from outer layers which appear in the right hand member of the differential equations are exponential functions. Papailiou (1995) makes the integration simpler by replacing the exponential by a constant term. This term is taken as the initial wire tension F_{Tj}, that is, when the conductor is bent, wire tension at $\varphi = 0$. With this simplification, differential equations (3.15) are uncoupled. They are now expressed as:

$$\frac{dF_{\text{Li}}}{d\theta} - \mu_i \sin\alpha_i \, F_{\text{Li}} = \frac{r_i}{\sin\alpha_i}\left[\mu_i - \mu_{i-1}\cos(\alpha_i + \alpha_{i-1})\right]\sum_{j=1}^{i-1}\frac{\sin^2\alpha_j}{r_j}F_{\text{Tj}} \qquad (3.38)$$

44

And, using the same notations as above:

$$\frac{dF_{Li}}{d\theta} - \lambda_i F_{Li} = c_i \sum_{k=1}^{i-1} b_k F_{Tk} \tag{3.39}$$

All right hand members being constant, all solutions can be written as:

$$F_{Li} = a_{c,i} e^{\lambda_i \theta} + f_i \tag{3.40}$$

where:

$$i > 1 \quad f_i = -\frac{c_i}{\lambda_i} \sum_{k=1}^{i-1} b_k F_{Tk} \quad et \quad a_{c,i} = F_{Ti} - f_i$$

$$i = 1 \quad f_1 = 0 \quad et \quad a_{c,1} = F_{T1} \tag{3.41}$$

Thus:

$$F_{Li} = (F_{Ti} - f_i) e^{\lambda_i \theta} + f_i \tag{3.42}$$

Limit curvatures are now expressed as:

$$\kappa_{bi} = \frac{\lambda_i (F_{Ti} - f_i)}{A_i E_i R_i \cos^2 \alpha_i} \tag{3.43}$$

$$\kappa_{ti} = \frac{(F_{Ti} - f_i) \left(e^{\lambda_i \pi/2} - 1 \right)}{A_i E_i R_i \cos^2 \alpha_i} \tag{3.44}$$

Residual moment of friction for each layer is still given by Eq. (3.37). However, limit forces F_{Li} are now given by Eq. (3.42). Thus, residual moment of friction on layer (i) is given by:

$$M_{rfi} = 2R_i \cos \alpha_i (F_{Ti} - f_i) \sum_{j=1}^{n_i/2} \left(e^{\lambda_i \theta_j} - 1 \right) \sin \varphi_j \tag{3.45}$$

where it is assumed, as before, that the n_i are even numbers.

Example 3.4

In the Bersimis ACSR, coefficient of friction between layers is assumed to have the uniform value $\mu_i = 0.7$. An axial load T = 30% RTS is applied. Based on slip conditions (SC4), determine:

- The limit curvatures κ_b and κ_t for each of the four layers
- The residual friction moment at each interlayer.

Available Matlab® file: Example_3_4.m (select case No 1)

Results:
Limit curvatures

45

From Eq. (3.43) : $\kappa_d = [0.989\ 1.504\ 2.171\ 3.082]\ 10^{-5}$ (1/mm)
From Eq. (3.44) : $\kappa_t = [1.782\ 2.671\ 3.7\ 5.097]\ 10^{-5}$ (1/mm)

Residual moment of friction (Eq. (3.45)) :
$M_{rf} = [3.028\ 1.6\ 0.4391\ 0.0722]\ 10^4$ N.mm

It is found conditions (SC3) and (SC4) yield very similar results, thus showing the validity of Papailiou's simplification.

3.4.9   Slip conditions (SC5)

As shown in Fig. 3.2, relative velocity $\vec{V}_r$ tends to deviate more and more from the $\vec{t}_i$ direction, that is, the local tangent to the layer (i) wire centerline, it seems another set of plausible slip conditions, which are intermediate between (SC1) and (SC3), would be conditions (SC5), where the effect of the outer layer (i-1) on layer (i) is neglected, and only the retaining effect of layer (i+1) is considered. Eqs (3.20) or (3.38) still apply, except that in the right hand member, coefficient of friction μ_{i-1} vanishes. Thus, the c_i parameters are now expressed as:

$$c_i = \mu_i \frac{r_i}{\sin \alpha_i} \tag{3.46}$$

Example 3.5a

In the Bersimis ACSR, coefficient of friction between layers is assumed to have the uniform value $\mu_i = 0.7$. An axial load T = 30% RTS is applied. Based on slip conditions (SC5), determine:

- The limit curvatures κ_b and κ_t for each of the four layers
- The residual friction moment at each interlayer.

Available Matlab$^{®}$ file: Example_3_5.m (case No 1)

Results:
Limit curvatures:
From Eq. (3.34) : $\kappa_b = [1.02\ 2.90\ 8.90\ 23.01]\ 10^{-5}$ (1/mm)
From Eq. (3.36) : $\kappa_t = [1.83\ 5.56\ 17.85\ 47.34]\ 10^{-5}$ (1/mm)

Residual moment of friction (Eq. (3.37)) :
$M_{rf} = [3.1160\ 3.1118\ 1.8257\ 0.5478]\ 10^4$ N.mm

The last three residual moments are of course slightly higher than with conditions (SC3). An interesting feature yielded by conditions (SC5) is that layer slip phases are clearly sequential and well separated, as assumed Lehanneur (1949) and Papailiou (1995), as well as by Lanteigne (1985).

With conditions (SC5), the (M vs κ) diagram is made of linear segments connected by non-linear curves which correspond to phases of slip propagation in each layer.

46

Example 3.5b

In the Cardinal ACSR, coefficient of friction between layers is assumed to have the uniform value $\mu_i = 0.7$. An axial load $T = 40$ kN is applied. Based on slip conditions (SC5), determine:

- The limit curvatures κ_b and κ_t for each of the four layers
- The residual friction moment at each interlayer.

Available Matlab® file: Example_3_5.m (case No 2)

Results:
Limit curvatures:
From Eq. (3.34) : $\quad \kappa_b = [1.23 \quad 3.27 \quad 7.61 \quad 11.86] \, 10^{-5}$ (1/mm)
From Eq. (3.36) : $\quad \kappa_t = [2.20 \quad 6.16 \quad 15.25 \quad 24.08] \, 10^{-5}$ (1/mm)

In this case, slip in layer (4) would start before slip in layer (3) is complete.

Residual moment of friction (Eq. (3.37)) :
$M_{rf} = [1.7336 \quad 1.9937 \quad 1.2403 \quad 0.7429] \, 10^4$ N.mm

3.4.10 Slip conditions (SC2) revisited

In section 3.4.6, conditions (SC2), used by Papailiou (1995), have been qualitatively described. They are based on the assumption that both layers (i-1) and (i+1) restrain layer (i) slip and that the corresponding friction forces are equal and oriented in the $\vec{t}_i$ local tangent direction. This may now be easily implemented in the previous equilibrium equations. For example, in Eq. (3.15), $\cos(\alpha_i + \alpha_{i-1})$ needs to be replaced by 1, and μ_{i-1} needs to be replaced by $-\mu_{i-1}$. Thus, in Eq. (3.19), parameter c_i becomes:

$$c_i = (\mu_i + \mu_{i-1}) \frac{r_i}{\sin \alpha_i} \tag{3.47}$$

Using the simplification described with conditions (SC4), of a constant force, Eqs (3.38) have to be modified accordingly.

$$\frac{dF_{Li}}{d\theta} - \mu_i \sin \alpha_i \, F_{Li} = \frac{r_i}{\sin \alpha_i} (\mu_i + \mu_{i-1}) \sum_{j=1}^{i-1} \frac{\sin^2 \alpha_j}{r_j} F_{Tj} \tag{3.48}$$

Solutions take the same form as in Eqs (3.40) to (3.45). As seen in the following example, numerical results are of course quite different.

Example 3.6a

In the Bersimis ACSR, coefficient of friction between layers is assumed to have the uniform value $\mu_i = 0.7$. An axial load $T = 30\%$ RTS is applied. Based on slip conditions (SC2), determine:

- The limit curvatures κ_b and κ_t for each of the four layers
- The residual friction moment at each interlayer.

Available Matlab[®] file: Example_3_6.m (with case No 1)

Results
Limit curvatures
From Eq. (3.34) : $\kappa_b = [1.02\ \ 4.51\ \ 16.28\ \ 43.71]\ 10^{-5}$ (1/mm)
From Eq. (3.36) : $\kappa_t = [1.83\ \ 8.00\ \ 27.75\ \ 72.28]\ 10^{-5}$ (1/mm)

Residual moment of friction (Eq. (3.37)) :
$M_{rf} = [3.12\ \ 4.80\ \ 3.29\ \ 1.02]\ 10^4$ N.mm

Of course, results are unchanged for the first layer (limit curvatures and residual moment of friction). As might be expected, it is found conditions (SC2) yield clearly sequential slip phases and higher residual moments of friction (for layers 2 to 4).

Example 3.6b

In the Cardinal ACSR, coefficient of friction between layers is assumed to have the uniform value $\mu_i = 0.7$. An axial load T = 40 kN is applied. Based on slip conditions (SC2), determine:

- The limit curvatures κ_b and κ_t for each of the four layers
- The residual friction moment at each interlayer.

Available Matlab[®] file: Example_3_6.m (select case No 2)

Results:
Limit curvatures:
From Eq. (3.34) : $\kappa_b = [1.23\ \ 5.05\ \ 12.96\ \ 21.44]\ 10^{-5}$ (1/mm)
From Eq. (3.36) : $\kappa_t = [2.20\ \ 8.90\ \ 22.87\ \ 35.71]\ 10^{-5}$ (1/mm)

In this case, slip in layer (4) would start slightly before slip in layer (3) is complete.

Residual moment of friction (Eq. (3.37)) :
$M_{rf} = [1.734\ \ 3.065\ \ 2.087\ \ 1.323]\ 10^4$ N.mm

3.5   MOMENT-CURVATURE DIAGRAM WITH SLIP

Assuming slip phases from one layer to the next are truly sequential (for layer (i), between curvatures κ_{bi} et κ_{ti}), the (M vs κ) diagram is made of straight segments connected with curves corresponding with slip zone extension between two layers.

The slope of a straight line corresponds to the residual bending stiffness B_i : B_0 corresponds to B_{max}, B_1 corresponds to the (n-1) sticking layers plus layer (1) minimum bending stiffness when total slip has been reached etc. At this stage moment the (M vs κ) relationship is :

$$M = B_1 \kappa + M_{rf1} \qquad \kappa_{t1} \le \kappa \le \kappa_{b2} \tag{3.49}$$

where M_{rf1} is the residual moment of friction between layers (1) and (2).

Beyond curvature κ_{t2}, B_2 is the new bending stiffness, and the (M vs κ) relationship is given by:

$$M = B_2 \kappa + M_{rf1} + M_{rf2} \qquad \kappa_{t2} \le \kappa \le \kappa_{b3} \tag{3.50}$$

Defining moment M_{r2} as the sum :

$$M_{r2} = M_{rf1} + M_{rf2} \tag{3.51}$$

M_{r2} is the total residual moment of friction when layers (1) and (2) are in the complete slip stage. Thus:

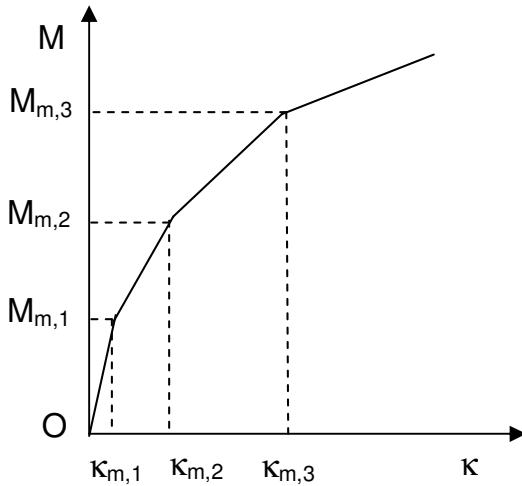$$M = B_2 \kappa + M_{r2} \qquad \kappa_{t2} \le \kappa \le \kappa_{b3} \tag{3.52}$$

After layer (i) has reached the complete slip stage, the (M vs κ) relationship is :

$$M = B_i \kappa + M_{ri} \qquad \kappa_{ti} \le \kappa \le \kappa_{b,i+1} \tag{3.53}$$

in which the residual moment of friction is :

$$M_{ri} = \sum_{j=1}^{i} M_{rfj} \tag{3.54}$$

Linearization of the (M vs κ) diagram

As in the single-layer case, the actual (M vs κ) diagram can be replaced with a simpler polygonal curve. Each partial slip domain (κ_{bi}, κ_{ti}) is replaced with a median transition curvature $\kappa_{m,i}$, which is obtained at the point where lines of slope B_{i-1} and B_i intersect. Thus, this median curvature is given by:

$$\kappa_{m,i} = \frac{M_{r,i} - M_{r,i-1}}{B_{i-1} - B_i} \tag{3.55}$$

The (M vs κ) diagram can now be represented as in Fig. 3.4.

Figure 3.4

Example 3.7

In the Bersimis ACSR, coefficient of friction between layers is assumed to have the uniform value $\mu_i = 0.7$. An axial load T = 30% RTS is applied. Based on slip conditions (SC5), determine:

- Bending stiffness B_i after each slip phase is complete
- Residual moment of friction $M_{r,i}$
- Median transition curvature $\kappa_{m,i}$ and corresponding moment $M_{m,i}$

Available Matlab® file: Example_3_7.m

Results:
Bending stiffness B_i after layer (i) slip is complete
$B = [1.0842 \ 0.2458 \ 0.0828 \ 0.0635] \ 10^9 \ \text{N.mm}^2$

Residual moment of friction after layer (i) slip is complete
$M_r = [3.1160 \ 6.2278 \ 8.0535 \ 8.6013] \ 10^4 \ \text{N.mm}$

Median transition curvatures
From Eq. (3.55) : $\quad \kappa_m = [1.30 \ 3.71 \ 11.20 \ 28.29] \ 10^{-5} \ (1/\text{mm})$

Median transition moments
From Eq. (3.53) : $\quad M_m = [4.524 \ 7.140 \ 8.982 \ 10.397] \ 10^4 \ \text{N.mm}$

This example is based on the case given by Lanteigne (1985). For the same conductor, under the same axial load T, this author gives the first two transition curvatures. According to his own model, these curvatures are 2.22×10^{-5} and 3.28×10^{-4} (1/mm). Here, they are found to be 1.30×10^{-5} and 3.71×10^{-5} , showing the current model (with the (SC5) conditions) predicts slip occurring at a much earlier stage in the bending process.

Example 3.8

In the Cardinal ACSR, coefficient of friction between layers is assumed to have the uniform value $\mu_i = 0.7$. An axial load T = 40 kN is applied. Based on slip conditions (SC2), determine:

- Bending stiffness B_i after each slip phase is complete
- Residual moment of friction $M_{r,i}$
- Median transition curvature $\kappa_{m,i}$ and corresponding moment $M_{m,i}$

Available Matlab® file: Example_3_8.m

Results:
Bending stiffness B_i after layer (i) slip is complete:
$B = [6.8280 \ 2.0612 \ 0.7873 \ 0.2775] \ 10^8 \ \text{N.mm}^2$

Residual moment of friction after layer (i) slip is complete:
$M_r = [1.734 \ 4.799 \ 6.886 \ 8.209] \ 10^4 \ \text{N.mm}$

Median transition curvatures:
From Eq. (3.55) : $\kappa_m = [1.57\ \ 6.43\ \ 16.38\ \ 25.95]\ 10^{-5}$ (1/mm)

Median transition moments:
From Eq. (3.53) : $M_m = [2.808\ \ 6.124\ \ 8.176\ \ 8.929]\ 10^4$ N.mm

This example is based on the case treated by Papailiou (1995). Unfortunately, transition curvatures are not given in the report.

Secant bending stiffness
As in Chapter 2 (Figs 2.4 and 2.6), a secant stiffness $B(\kappa)$ can be defined. It is simply the slope of the straight line from the origin to a given point (κ, M) on the (M vs κ) curve. In the Matlab$^{®}$ function Example_3_8.m, there is an option to draw the $B(\kappa)$ curve. Functions Example_3_8a.m to Example_3_8c.m are specific applications to the Bersimis ACSR case, allowing a comparison with Lanteigne (1985) results for the three axial loads presented in his paper: a) 20% ; b) 40% ; c) 100% of RTS. It is found that his staircase type curves are indeed a crude approximation of the secant $B(\kappa)$ curve obtained with the current model (based on the (SC2) conditions, although the same is found with other conditions).

Rheological modelling
As in the single layer case (section 2.6), the above linearized model for a multiple layer conductor in bending can be represented by a rheological model made of springs and friction sliders. A four-layer conductor will need four spring-slider couples plus a single spring. Such model may be useful to analyze more complex load-unload cycles, such as the ones considered in (Papailiou, 1995). Details are given in Appendix C.

CHAPTER 4

APPLICATION TO VARIABLE STIFFNESS PROBLEMS (FREE BENDING)

4.1   INTRODUCTION

So far, only the purely theoretical situation of uniform curvature bending has been considered. The objective of this chapter is to examine how the previous stick-slip models may be applied to free-bending situations (that is, a conductor without contact with another solid), in which conductor curvature varies from point to point.

In many instances, uniform curvature theoretical models of a conductor or cable bending behaviour have been proposed without any accompanying experimental justification. This observation applies to the papers by Rebuffel (1949) and Lehanneur (1949), Lanteigne (1985) and Hong et al. (2005).

In several cases, the experimental evidence is limited to local strain measurements on some of the outer strands: Raoof (1992), Claren and Diana (1969), Poffenberger and Swart (1965) etc. Often, these tests are small amplitude dynamic tests which yield a kind of information which cannot be used to check the validity of the quasi-static bending models.

Here, two free-bending situations are examined. Firstly, the clamped-clamped taut conductor specimen under a transverse load. Because it has been used in several studies, it will be given a detailed account. Secondly, it will be seen how these results apply to the free field small amplitude vibrations of a conductor near a suspension clamp.

4.2   STATIC SYMMETRIC BENDING TESTS ON A TAUT CONDUCTOR SPECIMEN

As already mentioned, imposing a uniform curvature to a conductor under axial load, in free bending is a purely theoretical situation which cannot be practically implemented. One method which is often used to evaluate the bending stiffness of a taut conductor is schematized in Fig. 4.1.
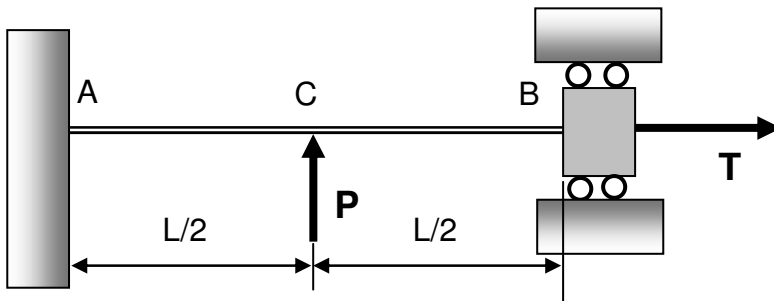

Figure 4. 1

Conductor specimen AB, length L, is put under tension T. At center point C, a transverse force P is applied, increasing monotonously from zero. Tension T is kept constant while this transverse loading is applied. Ensuing transverse displacement δ_C is recorded as a function of force P. From this record, one tries to obtain an equivalent conductor bending stiffness by comparison with a standard beam having a uniform stiffness B.

Among others, this test method has been used by Monroe and Templin (1932), McConnell and Zemke (1980), Zeitler (1994), and by Papailiou (1995). In the first two papers, the test specimen is considered to be similar to a clamped-clamped beam, having a uniform bending stiffness B. Thus, the usual Bernoulli-Euler beam theory is applied, assuming small displacements, and an equivalent bending stiffness B_{eq} is obtained for the conductor. This value has to be different from the stiffness B defined in the preceding chapters. Indeed, the experimental set-up shown in Fig. 4.1 obviously yields a variable curvature for the transverse deflection. The absolute value of the curvature is maximum at points A, B and C, and it vanishes at two intermediate points of inflexion. As shown in Chapters 2 and 3, beyond a certain value, such variable curvature will correspond to a variable stiffness. Thus, the relationship between B_{eq} and the local stiffness B of the conductor under test is not clear.

This drawback has been recognized by Papailiou (1995). Thus, instead of the analytical model based on a uniform stiffness beam, he uses the finite element analysis method (FEA) in which the specimen is discretized into a number of constant stiffness beam elements. For each element, it is assumed the uniform curvature results of Chapters 2 and 3 apply. Thus, for a given curvature κ of the element, the corresponding stiffness $B(\kappa)$ may be obtained (given the axial load T). His tests, performed on a set up such as the one in Fig. 4.1, were not used to obtain a particular equivalent stiffness B_{eq}. His objective was merely to check the uniform curvature model may be applied to a variable curvature situation. Papailiou's numerical results (mostly, the specimen center point deflection vs applied transverse force P) do seem to predict rather well his test data.

With the same experimental set up, Zeitler (1994) uses a different approach. In order to obtain an analytical relationship (δ_C,P,T), he uses an empirical equation, in which the stiffness is not a required parameter. In his paper, the conclusion is that bending behaviour of the conductor specimen cannot be represented by the standard beam bending theory. However, it is easily shown his mathematical model is flawed. Once corrected, his test data may be adjusted to equations obtained by Monroe and Templin (1932), and by McConnell and Zemke (1980) (which are in fact the same).

The various approaches are detailed in the following.

4.3   UNIFORM STIFFNESS CLAMPED-CLAMPED TAUT BEAM

Here, the well known theory of a beam under axial load and subjected to a central transverse force is recalled.
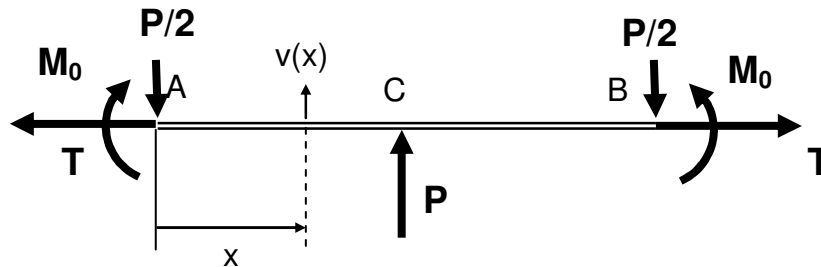

Figure 4. 2

The shear force in the AC and CB regions is V(x). Each beam cross-section undergoes a transverse displacement v(x). The free body diagram for beam segment $0 \le x < L/2$ is shown in Fig. 4.3.
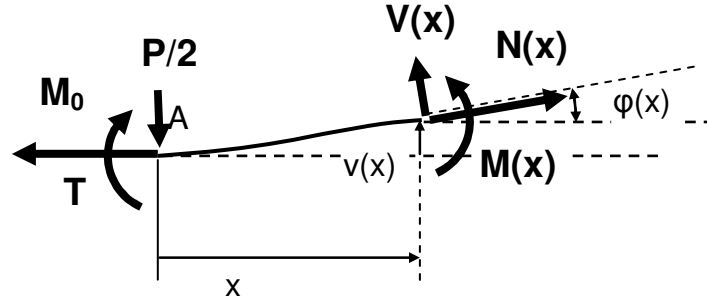

Figure 4. 3

Each cross-section undergoes a rotation $\varphi(x) \simeq dv/dx$. Thus, equations of equilibrium are as follows:

$$N(x)\cos\varphi - V(x)\sin\varphi = T$$

$$N(x)\sin\varphi + V(x)\cos\varphi = \frac{P}{2} \tag{4.1}$$

$$M(x) - M_0 - N\cos\varphi\, v(x) + N\sin\varphi\, x + V\cos\varphi\, x + V\sin\varphi\, v(x) = 0$$

From the first two equations, internal forces N(x) and V(x) can be expressed in terms of T and P. Then, they are used in the third equation to get M(x). Results are:

$$N = T\cos\varphi + \frac{P}{2}\sin\varphi$$

$$V = -T\sin\varphi + \frac{P}{2}\cos\varphi \tag{4.2}$$

$$M(x) = M_0 + Tv(x) - \frac{P}{2}x$$

The usual moment-curvature relationship is supposed to apply, yielding:

$$B\frac{d^2v}{dx^2} = M(x) = M_0 + Tv(x) - \frac{P}{2}x \tag{4.3}$$

where B = EI is the uniform beam bending stiffness.

This equation may be written as:

$$B\frac{d^2v}{dx^2} - Tv = M_0 - \frac{P}{2}x \tag{4.4}$$

Another expression is:

$$v'' - \lambda^2 v = \frac{M_0}{B} - \frac{P}{2B} x \tag{4.5}$$

in which the λ parameter is defined as:

$$\lambda^2 = \frac{T}{B} = \frac{T}{EI} \tag{4.6}$$

One particular solution to Eq. (4.5) is:

$$v_p = \frac{P}{2T} x - \frac{M_0}{T} \tag{4.7}$$

and the general solution to ODE Eq. (4.5) is:

$$v(x) = C_1 \sinh \lambda x + C_2 \cosh \lambda x + v_p(x) \tag{4.8}$$

This equation contains three as yet undefined constants: C_1, C_2, M_0. They can be found using the three following boundary conditions:

At point A ($x = 0$), assuming a perfect clamp condition: $\qquad v(0) = 0 \quad v'(0) = 0$
At point C ($x = L/2$), by symmetry, tangent must be horizontal: $\qquad v'(L/2) = 0$

These two conditions yield:

$$M_0 = \frac{P}{2\lambda} \left[\frac{\cosh \dfrac{\lambda L}{2} - 1}{\sinh \dfrac{\lambda L}{2}} \right] \tag{4.9}$$

The deflection $v(x)$ given by Eq. (4.8) becomes:

$$v(x) = \frac{P}{2\lambda T} \left[(\lambda x - \sinh \lambda x) + \frac{\cosh \dfrac{\lambda L}{2} - 1}{\sinh \dfrac{\lambda L}{2}} (\cosh \lambda x - 1) \right] \tag{4.10}$$

In particular, mid-point C deflection is given by $\delta_C = v(L/2)$ (here, $v(x) \geq 0$). A new, non-dimensional, parameter $\beta = \lambda L/2$ is defined, yielding:

$$\delta_C = \frac{P}{2\lambda T} \left[\beta - \frac{2(\cosh \beta - 1)}{\sinh \beta} \right] \tag{4.11}$$

This expression is similar to the non-dimensional expression given by McConnell and Zemke (1980):

$$\frac{4T\delta_C}{PL} = 1 + \frac{2(1-\cosh\beta)}{\beta\sinh\beta} \qquad (4.12)$$

It can easily be checked the point of inflexion is located at $x = L/4$ (and, by symmetry, at $x = 3L/4$). This result also coincides, under a slightly different form, with the equation given by Monroe and Templin (1932).

Example 4.1

In the case of the Cardinal ACSR, it was found (Chapter 3) that $B_{min} = 27.75 \times 10^6$ N.mm^2 and $B_{max} = 1.7846 \times 10^9$ N.mm^2. It is assumed beam AB is made of this same conductor. Its length is $L = 1$ m, and it is subjected to axial load $T = 40$ kN and transverse force $P = 4$ kN, which acts at mid-point C. Assuming this specimen may be considered as a standard uniform stiffness B beam, determine the deflection δ_C at point C for these two stiffness limit values.

Available Matlab$^{\circledR}$ file: Example_4_1.m (select case No 1)

Results:
Using Eq. (4.11), it is found:
With $B = B_{min}$ $\delta_C = 22.366$ mm
With $B = B_{max}$ $\delta_C = 7.499$ mm

These are indeed the values found by Papailiou (1995) for the same given parameters.

It should be noted that, while the stiffness ratio is $B_{max}/B_{min} = 64.3$, the ratio between corresponding deflections is only 2.98.

Example 4.2

With the same data as in Example 4.1, determine the extreme values for the β parameter as well as for the right-hand member RHM of Eq. (4.12).

Available Matlab$^{\circledR}$ file: Example_4_2a.m.

With $B = B_{min}$ $\beta_1 = 19.16$ RHM = 0.8956
With $B = B_{max}$ $\beta_2 = 2.367$ RHM = 0.2999

Now, let us assume a test has been performed on that specimen and the measured center deflection is $\delta_C = 17$ mm. Determine the equivalent bending stiffness of the conductor.

Use Matlab$^{\circledR}$ file Example_4_2b.m.
In this function, the corresponding left-hand member LHM of Eq. (4.12) is first calculated. Then, the interval (β_1-β_2) is divided into small steps $\Delta\beta = (\beta_1$-$\beta_2)/10000$ (say). Starting at $\beta = \beta_2$, parameter β is increased step by step, and RHM is calculated and compared with the LHM value. Process terminates when RHM > LHM.

Results:
$\beta = 6.071$

$B_{eq} = 2.713 \times 10^8$ N.mm^2 or $B_{eq} = 9.96\,B_{min}$

Variation of curvature

Curvature $\dfrac{d^2 v}{dx^2} = v''(x)$ is easily obtained from Eq. (4.10):

$$v''(x) = \frac{\lambda P}{2T}\left[-\sinh \lambda x + \frac{\cosh \beta - 1}{\sinh \beta}\cosh \lambda x\right] \qquad (4.13)$$

The maximum curvature occurs at the clamped ends A and B, and at mid-point C. It is easily checked it has the same absolute value at each one of these points. It is given by:

$$v''(0) = \left|v''\left(\frac{L}{2}\right)\right| = \kappa_{max} = \frac{\lambda P}{2T}\frac{\cosh \beta - 1}{\sinh \beta} \qquad (4.14)$$

When beam AB is a conductor specimen, it has been shown that, beyond a certain value of curvature κ, layers start slipping, and bending stiffness becomes a variable. Curvature κ_{max} being directly proportional to the ratio (P/T), the maximum value of this ratio for which the constant stiffness solution holds is easily found.

Example 4.3

The same specimen as in Example 4.1 is considered: Cardinal ACSR, L = 1 m, axial load T = 40 kN. For the given conductor, it was found in Example 3.5b that, under T = 40 kN, and with a coefficient of friction $\mu = 0.7$, under SC5 slip conditions, outer layer slip starts at curvature $\kappa_{b,1} = 1.23 \times 10^{-5}$ mm^{-1}. For a system such as the one shown in Fig. 4.1, determine the maximum value of transverse force P which can be applied before any slip occurs in the test specimen AB.

Available Matlab$^{®}$ file: Example_4_3.m

Result: P = 250.8 N

Above this force level, bending stiffness decreases in the high curvature regions and the uniform curvature solution is no longer valid. However, this limit value is based on the assumption that interlayer slip is unrestrained, and it is obvious this condition is not truly fulfiled in the present experimental set up, where both ends of the specimen are assumed to be perfectly clamped. This question will be re-examined further on.

4.4   VARIABLE BENDING STIFFNESS

As proposed by Papailiou (1995), an approximate solution to the variable stiffness problem may be obtained using the uniform curvature solutions found in Chapter 3. Again, the (M,κ) curve is replaced

by a polygonal diagram. Now, transverse load P has to be applied step by step in order to follow slip propagation firstly on a given interface, and secondly within the conductor cross-section.

However, one should decide which definition of stiffness is to be used, either secant stiffness, or tangent stiffness. Papailiou (1995) uses the secant stiffness, which yields a continuous variation from one element to the next. On the contrary, Dastous (2005) uses the tangent stiffness B_0, B_1, B_2 etc., that is, the slope of the segments in the polygonal approximate diagram (M, κ). This last approach is valid in an incremental numerical procedure in terms of (dM, dκ). When the procedure uses (M, κ) values, the secant stiffness should be used. In the loading process, it is obtained as follows.

<u>Phase I</u> : $0 \le P \le P_1$

No slip. Bending stiffness is uniform and a maximum: $B = B_0 = B_{max}$. The secant and tangent stiffness are identical (at least in the case of an initial loading starting from a "virgin" state).

When $P = P_1$, curvature absolute value at critical points A, B et C reaches $\kappa_{m,1}$ and then, the outer layer starts slipping on the second layer.

<u>Phase II</u> : $P_1 \le P \le P_2$

The region of outer layer slip propagates at critical points A, B and C. In these regions, the curvature of a given elementary conductor element has increased from 0 to $\kappa(x)$ where $\kappa_{m,1} \le \kappa(x) \le \kappa_{m,2}$. For two neighbouring elements, the corresponding points on the (M,κ) diagram are slightly different. In this region, the (M vs κ) relationship is:

$$M(x) = M_{rf,1} + B_1 \kappa(x) \tag{4.15}$$

Thus, the secant stiffness at curvature κ is:

$$B_{sec}(\kappa) = \frac{M}{\kappa} = \frac{M_{rf,1}}{\kappa} + B_1 \tag{4.16}$$

This secant stiffness decreases as κ increases. There is a discontinuity in the tangent stiffness at the no-slip and slip region boundary. Near the clamped end point A, this boundary has an abscissa x_1 which is a function of applied force P.

<u>Phase III</u> : $P_2 \le P \le P_3$

When $P = P_2$, the absolute value of curvature at critical points A, B and C becomes $\kappa_{m,2}$ and slip starts on the second layer. For $P > P_2$ this slip region propagates. Near the clamped end A, its boundary is at point of abscissa x_2. In domain $0 \le x \le x_2$, the (M vs κ) relationship is:

$$M(x) = M_{rf,2} + B_2 \kappa(x) \tag{4.17}$$

The secant bending stiffness at curvature κ is:

$$B_{sec}(\kappa) = \frac{M}{\kappa} = \frac{M_{rf,2}}{\kappa} + B_2 \qquad (4.18)$$

The same type of reasoning applies when layer i = 3 starts slipping, and so on.

4.5   NUMERICAL METHODS

For the system shown in Fig. 4.1, with variable bending stiffness, center point deflection δ_C as a function of applied transverse force P, has to be determined numerically. The FEA method has been used by Papailiou (1995). However, the problem being basically one-dimensional (one space variable x), and the moment-curvature equations being linear, the Transfer Matrix Method (TMM), such as presented by Pilkey (2002), may also be used. One of its interesting features is that it is easily programmed.

Transfer Matrix derivation for conductor element (i) is detailed in Appendix D. In order to test the accuracy of this method, Example 4.1 is solved again, this time, using the TMM.

Example 4.4

For the Cardinal ACSR, the theoretical minimum and maximum bending stiffness have been found to be, respectively, $B_{min} = 27.75 \times 10^6$ N.mm^2 and $B_{max} = 1.7846 \times 10^9$ N.mm^2. Now, referring to the set up shown in Fig. 4.1, conductor specimen AB length is taken L = 1 m. The applied axial load is T = 40 kN, and a transverse force P = 4 kN is applied at point C. It is assumed the specimen behaves as a standard beam with uniform stiffness B. Using the TMM, determine the center deflection δ_C obtained with the two limit values of stiffness B.

Available Matlab® file: Example_4_4.m

Results:
With 20 elements:
Minimum stiffness B = B_{min} δ_C = 22.366 mm
Maximum stiffness B = B_{max} δ_C = 7.499 mm

The same values were found in Example 4.1. These results hold with any number of elements. Indeed, within the bounds of the classical beam bending theory, the TMM is an "exact" method.

4.6   APPLICATION TO THE VARIABLE STIFFNESS CASE

When limit curvature $\kappa_{m,1}$ is reached at points A, B and C, and assuming the elements behave as in the uniform curvature case, the outer layer starts slipping as force P is increased beyond the limit value P_1. Some elements enter the Phase II described in section 4.4. Here, like the FEA method, the TMM method becomes approximate. The algorithm has to determine which elements have entered Phase II. Then, their bending stiffness has to be modified to B_1, and a residual friction moment $M_{rf,1}$ must also act on these elements (Eqs (4.15) and (4.16)). For a given element, one value of curvature has to be

considered, which will be taken as the average of the nodal curvatures (the ends of each element). In order to follow the slip propagation, one has to increment the transverse force by steps ΔP, up to the required maximum force P_{max}.

The problem with the boundary conditions

In the Fig. 4.1 set-up, specimen is clamped at points A and B. This is contradictory with the above hypothesis that elements in these regions behave as in the constant curvature bending where inter-layer slip is directly related with the local curvature. Instead, one would expect slip to be completely impeded at points A and B, with a transition in adjacent elements. This local effect will be first neglected and, following Papailiou's hypothesis, it will be assumed elements at the clamped ends behave as in the constant curvature case of Chapter 3.

Example 4.5

In the Fig. 4.1 set up, conductor specimen is the Cardinal ACSR. Length of specimen AB is L = 1 m. Applied axial force is T = 40 kN. It is loaded transversely at point C by a force P_{max} = 4 kN. Using the approximate polygonal (M,κ) diagram of the conductor, and the TMM, determine the center point deflection δ_C vs P, as P increases monotonously from 0 to P_{max} .

In Matlab® file Example_4_5.m, for each load step ΔP, total values in nodal bending moment, slopes and displacements are computed at each step for the incremented total load.

In order to define the polygonal (M,κ) diagram, median limit values, which have been found in Chapter 3 have to be given as input in the file. Here the selected case corresponds to data obtained in Example 3.8 with coefficient of friction $\mu = 0.7$ and slip conditions SC2. They are:

Median limit curvatures: $\kappa_m = [1.57 \; 6.43 \; 16.38 \; 25.95] \; 10^{-5} \; (1/mm)$
Median limit moments: $M_m = [2.808 \; 6.124 \; 8.176 \; 8.929] \; 10^4 \; N.mm$

Slopes of the polygonal (M,κ) diagram are:
Zero-slip phase : $B_0 = B_{max} = 1.7846 \times 10^9 \; N.mm^2$, and for each slip phase:
$B = [6.8280 \quad 2.0612 \quad 0.7873 \quad 0.2775] \; 10^8 \; N.mm^2$

Total residual friction moments in each phase are $M_r = [1.734 \; 4.799 \; 6.886 \; 8.209] \; 10^4 \; N.mm$

Here, the selected number of elements in half-span AC is n = 100. They all have the same length $L_i = 5$ mm. Load P is incremented by steps ΔP = 100 N. After each increment, the mean value of nodal moments acting on element (i) is compared with limit values given in M_m. Then, element stiffness $B_{,i}$ and residual friction moment $M_{rf,i}$ for each element (i) are modified accordingly. With these updated element parameters, the TMM is applied, yielding transverse displacement, slope and moment at each node. Value of center point deflection δ_C is obtained for the current value of force P.

When the requested maximum value P_{max} has been reached, the Matlab® function generates a curve P vs δ_C (output figure 1). It also generates the following curves, as a function of abscissa x, over the half length AC: node deflection v(x) (output figure 2), slope $v'(x) \cong \varphi(x)$ (output figure 3), curvature $\kappa(x)$ (output figure 4), secant bending stiffness B_{sec} (output figure 5), as defined in Eq.(4.16). On these figures, Papailiou's (1995) results, for the same conductor and load parameters are also shown, as well

as his test data. Output figure 6 shows the slip stage of the beam elements, from stage 0, no slip, to stage 4, with all layers slipping.

Curve P vs δ_C (output figure 1) is shown in Appendix D (Fig. D.3). At P_{max} = 4 kN the TMM model yields $\delta_C = 16.8$ mm. This value is higher than the one found in Papailiou's tests (10.2 mm). His own calculations, based on the FEA method yield about 11 mm.

The main difference comes apparently from slip conditions at points A and C. TMM results show near-minimum bending stiffness B_{min} applies in the clamped end and center regions. As already mentioned, this contradictory with the clamped end boundary condition. Indeed, in these regions, layers are constrained and cannot slip freely. In fact, at point A, there should be no slip at all, and element stiffness should be B_{max} (0 stage). Papailiou's numerical results also show partial slip (apparently, stage 3 slip) at these points. It is not clear how the clamping conditions can be made compatible with such slip state. Also, it is doubtful slip states can be assumed to be identical at points A and C, since center point C is not a clamp and slip can be expected to develop there.

The current model could be improved by assuming that at points A and C, element stiffness has to remain at its B_{max} value. It is not clear however, how a transition zone could be programmed between these blocked elements and the free elements.

Instead, the current TMM results might be of some interest for a slightly different experimental set up, where rigid clamps are replaced by simple supports (Fig. 4.4).
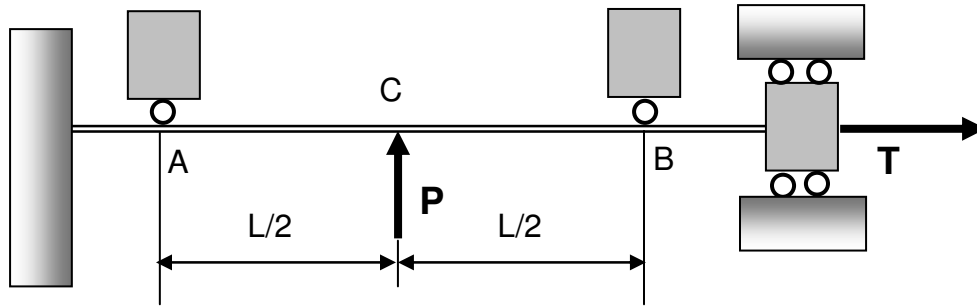

Figure 4. 4

Then, conditions at A and B are somewhat similar to those found at a standard suspension clamp.

From the curve P vs δ_C (Fig. D.3) it is seen that, as load P increases, the curve becomes practically parallel to the B_{min} straight line which is similar to the curves obtained by McConnell & Zemke (1980). Assuming the equivalent stiffness B_{eq} can still be obtained from Eq. (4.12) (as do these authors) and taking for example the result yielded by the function Example_4_5, and using the Example_4_2.m file (with $\delta_C = 16.8$ mm), one gets $B_{eq} = 9.93\,B_{min}$. That equivalent bending stiffness, while lower than the one obtained from Papailiou's data, is higher than the one found by McConnell & Zemke (1980) for various conductors (with a set-up similar to the one shown in Fig. 4.4). Also, the P vs δ_C TMM curve of Fig. D.3 compares well with the one shown in Foti & Martinelli (2011); starting with the B_{max} slope, it then curves, as P increases, to become parallel to the B_{min} straight line.

Conclusions
It has been shown in the above free bending problem, that variable bending stiffness has to be considered in the calculations. Uniform curvature results have been used to get approximate results through the TMM numerical method. Problems arise, obviously, at clamped ends where, by definition, inter-layer slip is blocked, contradicting results which show minimum stiffness elements in these regions. Consequently, one should not use this approximate analysis to get local quantities such as stresses.

4.7 SMALL-AMPLITUDE CYCLING NEAR A CLAMP

The conductor-suspension clamp system
Rather than the square-faced clamps which are implied in the Fig. 4.1 system, a more practical situation is the one found in overhead electric transmission conductors. The simplest case arises when the conductor is held with standard clamps made of a supporting body and a bolted keeper (Fig. 4.5)
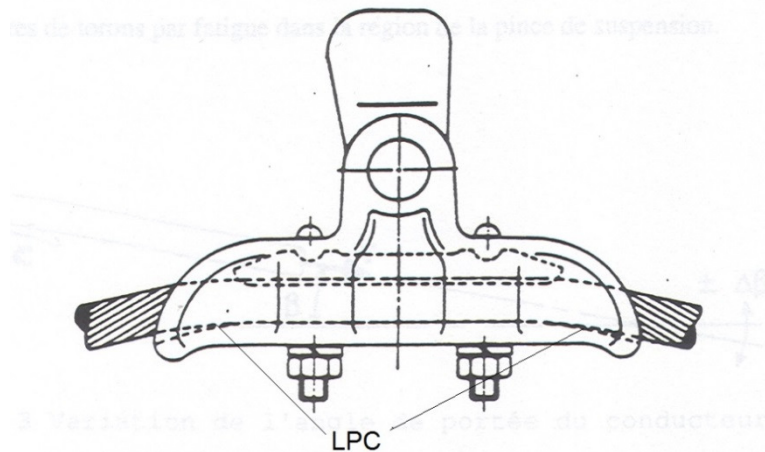

Figure 4. 5 (Cloutier & Hardy, 1988)

The shape of the conductor, where most of the span is concave upward, with a local downward concavity at each suspension clamp, calls for a point of inflexion somewhere in the vicinity of the clamp. The situation is thus similar to the one encountered in the preceding section and it is to be expected that in the laying operation of the conductor, total interlayer slip will occur near the exit points from the clamp, usually called the "Last Point of Contact", or LPC, for short. Outside the clamp, conductor curvature varies from a maximum at the LPC to zero at the point of inflexion, and it is thus a case of varying bending stiffness.

Some experimental evidence about the static shape of a conductor in the vicinity of a suspension clamp has been obtained by Dalpé (1999). In the immediate vicinity, it has been found the curve follows closely a constant stiffness curve with stiffness B = B_{min} . It is even found that, in some cases, for the selected axial tension T of 25% RTS (conductor Rated Tensile Strength), the corresponding B is slightly lower than B_{min}, which could be explained by a plastic behaviour in some wires. Such plasticity

62

has indeed been found by Ramey *et al.* (1981) when measuring strain on the outer layer of a bent conductor at a clamp.

Thus, it is doubtful the above variable stiffness calculations based on the constant curvature elastic models are of any help in explaining the free bending shape of a conductor near a clamp. The constant curvature model should rather be viewed as a tool which can be helpful in explaining conductor inner mechanics and interpreting some experimental results obtained in the Aeolian vibration field.

Small amplitude bending cycles

It is well known that conductor Aeolian vibration is a small amplitude phenomenon which occurs once the conductor is in place and has undergone large quasi-static bending. According to the moment-curvature curve seen in Chapter 3, as explained with the stick-slip model (Appendix C), small amplitude vibration will be represented by a small straight line A_0A_1, whose slope will be the maximum stiffness B_0 (Fig. 4.6), with no subsequent slip. This is a purely elastic cycle which induces relatively small amplitude alternate bending stresses in the conductor strands, and it is such stress cycling which has been used traditionally to estimate the fatigue strength of a conductor.

Figure 4. 6
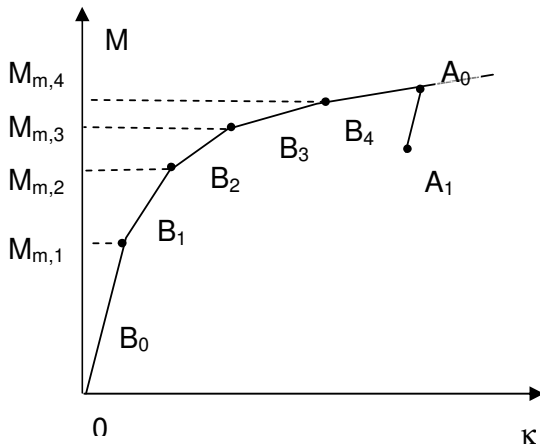
Thus, if one is interested in the fatigue problem, rather than in the conductor overall deflected shape, the analysis may be restricted to the uniform stiffness bending situation. Indeed, in the clamp vicinity, between the LPC and the point of inflexion, whatever the slip stage in a given section, the small amplitude bending cycle will be a B_0 slope straight line.

Note also that, with this model, the A_0A_1 cycling is a straight line, with zero energy loss, and thus zero damping. It is obviously inadequate for vibration studies (on this topic, see: Rawlins, 2009).

Instead of the practical conductor-suspension clamp, consider again the clamped-clamped specimen shown in Fig. 4.1. The center point deflection under a transverse load $P = P_{max}$ has been computed numerically in Example 4.5. In the following example, attention is given to the behavior of a conductor section located not too far from the left-hand clamp A when load P decreases by ΔP.

Example 4.6

In Example 4.5, using the TMM, the displacement at center point C, under maximum load $P_{max} = 4$ kN is $\delta_C = 16.84\,\text{mm}$. At a distance a = 90 mm from clamped end A, the corresponding displacement is found to be $v = 2.4211\,\text{mm}$ (displacement of node No i = 18, with 5 mm elements). Now, if there is a small decrease $\Delta P = 100\,\text{N}$, displacement Δv has to be calculated based on a uniform B_0 bending stiffness of the specimen AB. Deflection v(x) is given by Eq. (4.10).

Available Matlab[®] file: Example_4_6.m

Result:

$\Delta v(a) = 0.00167$ mm

Departure from initial deformed curve (under $P_{max} = 4$ kN), is quite small, even with unloading amplitude $\Delta P = 1 kN$.

It has been found in Example 4.3 that, in the load phase, slip begins in the outer layer when $P_1 = 250.8$ N . According to the stick-slip rheological model (Appendix C), the preceding calculation (purely elastic unloading behaviour) is valid up to $\Delta P = 2P_1 = 2 \times 250.8 = 501.6$ N . Beyond this value, there will be a reverse slip. This would correspond to a displacement at node 18 (a = 90 mm) greater than $\Delta v(a) = 0.0084$ mm . If ΔP is now applied in the reverse direction, in order to reach again the P_{max} level, the (P vs δ_C) cycle will be an hysteretic cycle

Fatigue criteria: displacement, curvature or stress
Rather than the displacement at the center point C, it is often more convenient to consider the displacement at a point A' at some distance *a* from clamp A, such as in Example 4.6. And if a constant amplitude cyclic load ΔP is imposed at C, it is equivalent to consider the $\Delta v(a)$ at A'. If fatigue tests are performed by repeating the cycle ΔP, it is also more convenient to express the fatigue results in terms of the $\Delta v(a)$ amplitude. In principle, another parameter could be used, the curvature cycle $\Delta \kappa(0)$ at or very close to clamp A. Curvature $\kappa(0)$ follows qualitatively the same type of curve when drawn versus load P and versus bending moment M_A. Thus, in the ΔP cycle, both $\kappa(0)$ and v(a) undergo a closed cycle (if ΔP is large enough). Amplitudes $\Delta v(a)$ and $\Delta \kappa(0)$ are directly related and fatigue test data may be expressed in terms of either one of these parameters.

While these parameters are probably better suited for fatigue strength evaluation, being related to global section behaviour, people generally prefer to express strength problems in terms of stress, rather than displacement amplitude or, worse, curvature. Hence, the problem arises of relating the $\Delta v(a)$ and $\Delta \kappa(0)$ amplitudes and cycles to some kind of $\Delta \sigma$ amplitude. For small amplitudes, as in the $A_0 A_1$ cycle of Fig. 4.6, this is not too difficult, as the stick-slip model predicts a purely elastic behaviour with maximum stiffness B_0. If the amplitude is larger, however, slip occurs in some contact regions, and one may wonder which $\Delta \sigma$ should be selected. This question is examined in the next chapter.

CHAPTER 5

STRESS CALCULATIONS IN SMALL AMPLITUDE CYCLIC BENDING

5.1 INTRODUCTION

In the vicinity of a suspension clamp, Aeolian vibration is a small amplitude phenomenon which is superimposed on the quasi-static conductor equilibrium curve. While the dynamic response of an actual conductor span in the field is rather complex (EPRI 2006), laboratory fatigue tests use relatively short specimens under traction. These specimens are vibrated using an electrodynamic shaker (Lévesque *et al*., 2011), and it is the resulting transverse motion which is used to study the fatigue performance of a given conductor-clamp combination. In this chapter, the problem is restricted to the quasi-static case, in which the conductor own inertia is neglected, and bending is supposed to result from the application of a transverse force. Again, uniform bending stiffness is assumed.

5.2 SMALL AMPLITUDE BENDING CYCLE

Consider again the clamped-clamped specimen shown in Fig. 4.1. Conductor inertia is neglected, and the bending cycle can be obtained by assuming the center transverse load P undergoes a ΔP cycle. A decrease ΔP of transverse force P will correspond to an unloading displacement $\Delta v(x)$ given by Eq. (4.10) (purely elastic no-slip case):

$$\Delta v(x) = \frac{\Delta P}{2\lambda T} \left[(\lambda x - \sinh \lambda x) + \frac{\cosh \dfrac{\lambda L}{2} - 1}{\sinh \dfrac{\lambda L}{2}} (\cosh \lambda x - 1) \right] \tag{5.1}$$

with $\lambda^2 = T/B$. Now, assume displacement $\Delta v = Y_b$ is known at a distance *a* from clamped end A. Corresponding force decrease ΔP can be obtained from Eq. (5.1), and bending moment variation at A is given by:

$$\Delta M_0 = \frac{\Delta P}{2\lambda} \left[\frac{\cosh \dfrac{\lambda L}{2} - 1}{\sinh \dfrac{\lambda L}{2}} \right] \tag{5.2}$$

Thus, ΔM_0 can be directly obtained through:

$$\Delta M_0 = T Y_b \frac{\cosh \dfrac{\lambda L}{2} - 1}{\sinh \dfrac{\lambda L}{2} (\lambda a - \sinh \lambda a) + \left(\cosh \dfrac{\lambda L}{2} - 1 \right)(\cosh \lambda a - 1)} \tag{5.3}$$

Curvature variation $\Delta\kappa$ is given by $\Delta M_0/B_0$. For small amplitudes, <u>the conductor is supposed to behave like a solid beam </u>(Fig. 4.6). The corresponding strain at top most fibres is $\varepsilon_x = D_{O1}\,\Delta\kappa/2$, D_{O1} being the conductor outer diameter. As explained in Chapter 1, corresponding strain in the wire axis direction is $\varepsilon_w = \varepsilon_x \cos^2\alpha_1$. Thus, the maximum cyclic stress amplitude $\Delta\sigma$ which occurs in the wire most remote from the strand neutral axis is:

$$\Delta\sigma = \frac{ED_{O1}\cos^2\alpha_1}{2}\frac{TY_b}{B_0}\frac{\cosh\dfrac{\lambda L}{2}-1}{\sinh\dfrac{\lambda L}{2}(\lambda a - \sinh\lambda a)+\left(\cosh\dfrac{\lambda L}{2}-1\right)(\cosh\lambda a-1)} \tag{5.4}$$

Example 5.1

Again, consider the case of conductor Cardinal ACSR, under axial load T = 40 kN. Length of specimen is 1 m. Assume amplitude Y_b has been measured at distance a = 89 mm (3.5 in.). Determine stress amplitude $\Delta\sigma$ at the clamp for an amplitude Y_b = 0.2 mm.

Available Matlab® file: Example_5_1.m.

Result:
It is found that $\Delta\sigma = 55.6$ MPa . This is a peak to peak value. Thus if one considers a vibrating conductor, the cyclic stress amplitude is $\sigma_a = \Delta\sigma/2 = 27.8$ MPa

Also of interest is the strain peak to peak amplitude, $\Delta\varepsilon = \Delta\sigma/E$. Expressed in micrometer/meter, in this example, one finds $\Delta\varepsilon = 855\,\mu m/m$.

The length L of specimen AB has some influence on the result. In the case of a conductor near a suspension clamp, it should be eliminated by letting L go to infinity.

Long specimen case
In such case, Eq. (5.4) may be approximated as:

$$\Delta\sigma \simeq \frac{ED_{O1}\cos^2\alpha_1}{2}\frac{TY_b}{B_0}\frac{1}{(\lambda a - \sinh\lambda a)+(\cosh\lambda a-1)} \tag{5.5}$$

Example 5.2

Same as Example 5.1, except that, now the approximate $\Delta\sigma$ given by Eq. (5.5) is calculated and may be compared with the "exact" value given by Eq. (5.4). Solve the problem with L = 1 m and L = 2 m.

Available Matlab® file: Example_5_2.m (adjust parameter L)

Results:
a) L = 1 m $\Delta\sigma = 55.56$ MPa   and $\Delta\sigma_{ap} = 53.69$ MPa

b) $L = 2$ m $\Delta\sigma = 53.85$ MPa   and $\Delta\sigma_{ap} = 53.69$ MPa

It is seen the limit value is reached rather quickly as the specimen length increases.

Eq. (5.5), which holds for long enough specimens, may be recast by replacing the hyperbolic functions by their exponential equivalent, and also recall that, by definition, $\lambda^2 = T/B$. This yields:

$$\Delta\sigma \simeq \frac{ED_{O1}\cos^2\alpha_1}{2}\frac{\lambda^2}{e^{-\lambda a}+\lambda a-1}Y_b \tag{5.6}$$

This expression is similar to the one derived by Poffenberger and Swart (1965), with the difference that, in Eq. (5.6), the conductor is supposed to behave as a solid beam, with bending stiffness B_{max}. Also, the lay angle effect is kept in Eq. (5.6), while being neglected by Poffenberger and Swart.

5.3   THE POFFENBERGER AND SWART STRESS

The classical bending stress due to Poffenberger and Swart (1965) is easily obtained from Eq. (5.6). It is based on the complete slip assumption where all wires are independent. In such case, $B = B_{min}$, and the conductor outer diameter D_{O1} has to be replaced by a wire diameter, d_w. Also, as already mentioned, wire lay angle is neglected. The cyclic stress amplitude $\sigma_a = \Delta\sigma/2$ is thus given by:

$$\sigma_a = \frac{Ed_w}{4}\frac{\lambda^2}{e^{-\lambda a}+\lambda a-1}Y_b \tag{5.7}$$

in which $\lambda^2 = T/B_{min}$.

Example 5.3

Again, consider the case of conductor Cardinal ACSR, under axial load $T = 40$ kN. Assume amplitude Y_b has been measured at distance $a = 89$ mm (3.5 in.). Determine the Poffenberger and Swart cyclic stress amplitude σ_a for an amplitude $Y_b = 0.2$ mm.

Available Matlab[®] file: Example_5_3.m.

Result: $\sigma_a = 6.45$ MPa

Compare this value to $\sigma_a = 26.8$ MPa yielded by the zero slip hypothesis (with $B = B_{max}$). Note also that the corresponding cyclic strains are given by $\varepsilon_a = \sigma_a/E$ and, with the preceding data: $\varepsilon_a = 99\,\mu m/m$ for $B = B_{min}$ and $\varepsilon_a = 413\,\mu m/m$ for $B = B_{max}$

5.4   STRESS EVALUATION IN THE STICK-SLIP REGIME

In the preceding cases, based on uniform bending stiffness B_{max} or B_{min} (Poffenberger and Swart), using stress amplitude $\Delta\sigma$ is equivalent to using amplitudes $\Delta\kappa(0)$ or $\Delta v(a) = Y_b$. Which are actually extreme values.

When amplitude ΔP is not so small, slip regions do occur, starting in the outer layer near the conductor section "neutral axis". They start at critical points A and C of the clamped-clamped specimen (Fig. 4.1). While the exact slip process is gradual, starting at or near the "neutral axis", Papailiou's simplified model neglects the transition phase and assumes that complete or total slip occurs at once in the outer layer, leading to the polygonal (M vs κ) diagram.
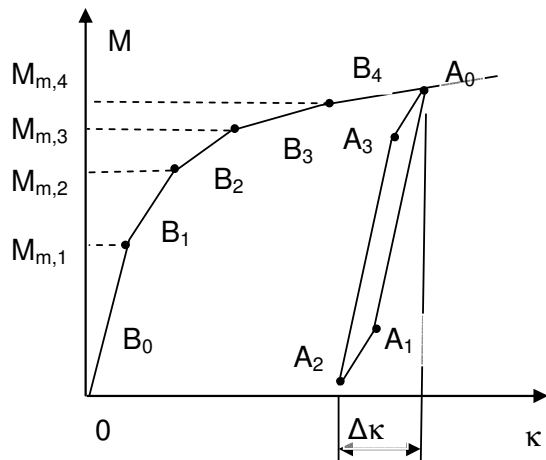

Figure 5. 1

In the cycle of amplitude ΔP, the (M vs κ) cycle at or near the clamp is shown in Fig. 5.1. According to the present stick-slip model, there is a small reverse slip cycle corresponding to lines A_1A_2 and A_3A_0. Along A_1A_2, wire material in the outer layer, undergoes a small displacement from the tension side to the compression side (considering only the bending effect). Along A_3A_0, there is a reverse displacement in the opposite direction.

In such a wire, variation of stress arises from: a) variation of curvature $\Delta\kappa$; b) variation ΔF_1 of tensile force on the wire cross-section. Thus :

$$\Delta\sigma = \Delta\sigma_a + \Delta\sigma_b \qquad (5.8)$$

Component $\Delta\sigma_a = E_1 d_1 \Delta\kappa/2$ coincides with the Poffenberger and Swart formula (Eq. 5.7), when slip is complete at all interfaces (all wires bend independently). Component $\Delta\sigma_b$ is due to the slip reversal along the contact line. In the slip state, with slip conditions (SC4), F_1 is given by Eqs. 3.41 and 3.42, and ΔF_1 is:

$$\Delta F_1 = F_{T1}\left(e^{\lambda_1 \pi/2} - e^{-\lambda_1 \pi/2}\right) = 2F_{T1}\sinh\left(\lambda_1 \pi/2\right) \qquad (5.9)$$

where $\lambda_1 = \mu_1 \sin\alpha_1$.

Example 5.4

Again, consider the case of conductor Cardinal ACSR, under axial load T = 40 kN. The clamped-clamped specimen shown in Fig. 4.1 is loaded by transverse load P up to $P_{max} = 4$ kN . It is then unloaded by ΔP such that $\Delta\kappa = 4.8\,10^{-5}$ mm^{-1} , then reloaded to P_{max}. From Example 3.5b, this means that there is reverse slip on the outer layer. The cycle is as shown in Fig. 5.1. Friction coefficient is 0.7. Determine stress amplitude $\Delta\sigma$.

Available Matlab® file: Example_5_4.m.
Matlab® file Example_1_2a.m is used to get force F_T in wires of layer 1: $F_T = 63.5$ N

Results:
$$\Delta\sigma_a = 3.57\,\text{MPa} \qquad \Delta\sigma_b = 8.41\,\text{MPa}$$

If curvature variation amplitude $\Delta\kappa$ is increased, inner layers may slip and $\Delta\sigma_a$ has to be calculated accordingly. However, component $\Delta\sigma_b$ remains a constant in the cycle (with these slip conditions). This small friction component is neglected in the Poffenberger and Swart formula (Eq. 5.7). Besides, in Eq. 5.7, tangent bending stiffness B_{min} is used instead of the secant stiffness.

5.5   PRACTICAL CONSIDERATIONS

5.5.1   Comparison with available experimental data

Much attention has been paid to the level of cyclic strain in vibrating conductors in the vicinity of a suspension clamp. An exhaustive survey and comparison of results can be found in Goudreau *et al.* (2010).

In general, these measurements are made on long, taut vibrating specimens of a conductor and in order to compare the strain levels, a given vibration amplitude is imposed on the specimen. For example, eight conductors were tested by Claren and Diana (1969). Specimens were 25 m long. They were rigidly held with square-faced aluminum clamps, instead of suspension clamps. Strain gages were positioned close to one clamp (exact distance is not given, authors say "placed just out of the clamp"), on the extreme fibres of the conductor, when considered as a uniform solid beam, that is, on wires located at distance $D_{O1}/2$ from the section neutral axis. In the ensuing discussion by Poffenberger and Komenda (1969), some of their results were redrawn for comparison with the theoretical curve given by Eq. (5.7), based on the $B = B_{min}$ hypothesis. It is clear from the corresponding figure (Fig. 14 of the paper) the strain measurements do not follow that curve. The discussers attribute the scatter to the very low bending amplitudes imposed in those tests, lower than "10 mils", i.e. lower than 0.25 mm.

Indeed, the stick-slip model predicts that for small amplitudes, there should be no interlayer slip, and bending stiffness should be $B = B_{max}$. Unfortunately, while Claren and Diana (1969) define a "slippage parameter", its variation with bending amplitude is not shown. They only give its variation with axial load T. Compared with the maximum stiffness hypothesis, the actual measured strains are smaller than predicted. This holds even for small bending amplitudes or, with the present notation, stiffness $B < B_{max}$. Most probably, this discrepancy comes from the complex state of stress and strain arising at each wire contact point. This fact cannot be neglected when the objective is to predict conductor fatigue strength under bending.

5.5.2   On the usefulness of bending stress or strain evaluation

It is well known that conductor fatigue failures in small amplitude vibration such as Aeolian vibration originate most of the time at contact points (EPRI, 2006) that is, at places where the state of stress, strain and displacement (with a possible corresponding slip) is complex, and rather difficult to evaluate. Yet, conductor fatigue prediction is usually based on bending stress and strain levels which are obtained either from analytic models, which can be as simple as Eq. (5.7) (Poffenberger and Swart, 1965), or as sophisticated as Papailiou's model (1995), or from experimental techniques, such as strain

gage measurements on individual wires. These stress and strain levels are certainly good indicators of the vibration amplitude severity, and there should be a strong correlation between such levels and conductor fatigue performance, even if the calculated levels cannot be related with the intrinsic fatigue properties of the wire material itself. A conductor bending fatigue evaluation based on these indicators should not be compared with the corresponding evaluation found in the machine design field where, for example, a given shaft fatigue strength is based on the material S/N curve.

Yet, even if this approach is practical, more information can be obtained by looking at the actual conditions prevailing in the contact regions.

5.5.3   Elastic compliance at contact points

In the stick-slip model presented in Chapters 2 to 4, relative motion of contacting wires may occur only when the tangential force at a contact point reaches a maximum given by Coulomb's law. It has been shown by Mindlin (1949) that, when contacting bodies in contact are elastic, relative displacements do occur even below this limit tangential force.

The problem has been studied in detail for elastic spheres in contact by Mindlin and Deresiewicz (1953). In this case, an exact analytical solution can be obtained because of the simple circular contact zone. The notion of tangential compliance has later been applied to cables by Raoof (1983). It has been applied to conductor bending near a termination by Leblond and Hardy (2005).

Here, it can simply be said, when looking at a conductor global behaviour, such a tangential compliance is equivalent to adding a spring in series with the slider in the rheological models presented in Chapter 2 and in Appendix C. The result is that maximum bending stiffness B_{max} can never be reached (Leblond and Hardy, 2005). This may explain why, in very small amplitude vibration experiments, the measured bending stiffness is somewhere around $B_{max}/2$, depending on the axial load on the conductor (Claren and Diana, 1969), while the simple stick-slip models would predict a stiffness equal to B_{max}.

As shown by Mindlin (1949), the tangential compliance is coupled with a microslip region and, when the contact region is subjected to small amplitude cycling, fatigue cracks may indeed appear and lead to complete wire fracture, under what is called fretting fatigue (EPRI, 2006). Unfortunately, no analytical model is currently available in order to predict its occurrence and only empirical laws based on experimental data have been proposed.

In actual conductor-clamp systems (Fig. 4.5), the contact problem is even more complex, as the outer layer wires are in contact with the clamp itself. It is also found that under practical conditions, wire material, generally soft electrical grade aluminum, undergoes small plastic deformation in the contact regions. Needless to say, no analytic solution exists for this situation and, in order to make numerical predictions, one has to resort to approximate techniques such as the Finite Element Analysis (Lévesque *et al.*, 2011).

Thus, stick-slip models which have been proposed in the literature for the conductor bending problem, the features of which have been summarized in this work, should not be expected to provide quantitative answers in fatigue strength evaluation situations. Yet, compared with the purely elastic approach (Costello, 1997) they provide a useful insight on the phenomenon, as well as a basis for a better interpretation of experimental results.

REFERENCES

Baticle, E. (1912). *Le calcul du travail du métal dans les câbles métalliques*. Annales des Ponts et Chaussées. 1912(1); pp. 20-40.

Cardou, A. (2006). *Taut helical strand bending stiffness*. Tech. Report. July 2006. 9 pages PDF file Available at: http://www.umformtechnik.net/rub/UTFscience/124/UTF+2006/145/archiv/1/2006.

Cardou, A. and Jolicoeur, C. (1997).*Mechanical models of helical strands*. App. Mech. Rev. Jan 1997; 50(1):1-14.

Chouinard, G. (1994). *Analyse des caractéristiques de dissipation d'énergie aux points de contact entre les couches 1 et 2 d'un toron 1 x n_1 x n_2* . M.Sc. Thesis. Université Laval, Québec, Canada. 1994. 120 pages.

Claren, R. and Diana, G. (1969). *Dynamic strain distribution on loaded stranded cables*. IEEE Trans. on Power App. and Syst. Nov 1969; PAS-88, pp. 1678-1690.

Cloutier, L.; Goudreau, S., and Cardou, A. (2006). *Fatigue of overhead electrical conductors*. In *EPRI. Transmission Line Reference Book : Wind Induced Conductor Motion: Second Edition*. Palo-Alto, CA: Electric Power Research Institute; 2006 and 2009; 1018554; pp. 3-1 to 3-56.

Cloutier, L., and Hardy, C. (1988). *Effect of suspension clamp design on conductor fatigue life (a position paper)*. Montreal, Canada. Canadian Electrical Association. CEA report No ST-178. June 1988; 53 pages.

Costello, G. A. (1997). *Theory of wire rope*. 2nd ed. N.Y.: Springer-Verlag; 1997. ISBN: 0-387-97189-0.

Dowling, N. E. (1993). *Mechanical Behavior of Materials : Engineering Methods for Deformation, Fracture and Fatigue*. Englewood Cliffs, NJ: Prentice Hall; 1993; ISBN: 0-13-579046-8.

EPRI (2006). *Transmission Line Reference Book : wind Induced Conductor Motion*. Palo-Alto, CA: Electric Power Research Institute; 2006 Dec; 1012317.

Ernst, H. (1933a). *Beitrag zur Beurteilung der behörlidchen Vorschriften für die Seile von Personenschwebebahnen*. Ph.D. Thesis. T.H. Danzig. Danzig (presently: Gdansk, Poland). 1933, 32 pages.

--- (1933b). *Beitrag zur Beurteilung der behörlidchen Vorschriften für die Seile von Personenschwebebahnen*. Fördertechnik und Frachtverkehr. 1933.

Feyrer, K. (2007). *Wire ropes : tension, endurance, reliability*. Berlin, New York: Springer-Verlag; 2007; ISBN: 9783540338215.

Foti, F., and Martinelli, L. (2011). *A model for the cyclic biaxial bending of stranded ropes*. Abstract in Conference proceedings of the 20th congress of the AIMETA, Bologna, Italy, 12-15 september 2011, p. 240. Full paper (10 pages) available at: http://ww2.integer.it under its Italian title: *Un modello per la flessione biassiale ciclica di funi a trefoli.* (Last accessed in March 2013).

Goudreau, S.; Lévesque, F.; Cardou, A., and Cloutier, L. (2010). *Strain measurements on ACSR conductors during fatigue tests II - Stress fatigue indicators*. IEEE Trans. on Power Delivery. Oct 2010; 25(4); pp. 2997-3006.

Hong, K-J.; Der Kiuregian, A., and Sackman, J. L. (2005). *Bending behavior of helically wrapped cables*. ASCE J. Eng. Mech. May 2005; 131(5); pp. 500-511.

Hruska, F. H. (1951). *Calculation of stresses in wire ropes*. Wire and Wire Products. Sep 1951; 26(9); pp. 766-767 and 799-801.

--- (1952). *Radial forces in wire ropes*. Wire and Wire Products. May 1952; 27(5); pp. 459-463.

Jolicoeur, C. and Cardou, A. (1991). *A numerical comparison of current mathematical models of twisted wire cables under axisymmetric loads*. ASME J. of Energy Resources Tech. 1991; 113(4); pp. 241-249.

Lanteigne, J. (1985). *Theoretical estimation of the response of helically armored cables to tension, torsion and bending*. ASME J. of Appl. Mech. June 1985; 52; pp. 423-432.

Leblond, A. and Hardy, C. (2005). *Assessment of the fretting-fatigue-inducing stresses within vibrating stranded conductors in the vicinity of clamps*. Sixth Intl Symp. On Cable Dynamics; Charleston, S.C. Sep 2005; 10 pages on cd-rom.

Leider, M. G. (1975). *Die Bestimmung der Zusatzspannungen bei der Biegung von Drahtseilen und ihr Einfluss auf die Seillebensdauer*. Thesis. Fakultät für Maschinenbau, Universität Karlsruhe. Karlsruhe, Germany. 1975.

Lévesque, F.; Goudreau, S.; Cardou, A., and Cloutier, L. (2010). *Strain measurements on ACSR conductors during fatigue tests I - Experimental data*. IEEE Trans. on Power Delivery. Oct 2010; 25(4); pp. 2825-2834.

Lévesque, F.; Goudreau, S.; Cloutier, L., and Cardou, A. (2011). *Finite element model of the contact between a vibrating conductor and a suspension clamp*. Tribology International. Aug 2011; 44(9); pp. 1014-1023.

Love, A. E. H. (1944). *A Treatise on the Mathematical Theory of Elasticity*. Dover Publications, New York. 1944.

Mindlin, R. D. (1949). *Compliance of elastic bodies in contact*. ASME J. of Appl. Mech. 1949; 16; pp. 259-268.

Mindlin, R. D. and Deresiewicz, H. (1953). *Elastic spheres in contact under varying oblique forces*. ASME J. Appl. Elas. Sep. 1953; 20; pp. 327-344.

Papailiou, K. O. (1995). *Die Seilbiegung mit einer durch die innere Reibung, die Zugkraft und die Seilkrümmung veränderlichen Biegesteifigkeit*. Ph.D. Thesis. E.T.H. Zurich, Switzerland. 1995; 158 pages.

Pilkey, W.D. (2002). *Analysis and Design of Elastic Beams. Computational Methods.* J. Wiley & Sons, New York. 2002. ISBN 0-471-38152-7

Poffenberger, J. C. and Komenda, R. A. (1969). *Discussion to Claren and Diana 1969 paper "Dynamic Strain Distribution etc."* IEEE Trans. on Power Apparatus and Systems. Nov 1969; PAS-88; pp. 1686-1688.

Raoof, M. (1992). *Free bending fatigue of axially pre-loaded spiral strands*. J. of Strain Anal. for Eng. Des. Jul 1992; 27(3); pp. 127-136.

--- (1983). *Interwire contact forces and the static, hysteretic and fatigue properties of multi-layer structural strands*. Ph.D. Thesis. Imperial College of Science and Technology, London, U.K. 1983; 509 pages.

Rawlins, C. B. (2005). *Analytical Elements of Overhead Conductor Fabrication*. Fultus Corporation; 2005; ISBN: 1-59682-072-1.

--- (2009). *Flexural self-damping in overhead electrical transmission conductors*. J. of Sound and Vib., June 2009, 323(1-2), pp. 232-256.

Timoshenko, S. (1963). *Strength of materials, part II*. D. Van Nostrand, New York; 1963.

APPENDIX A

TYPICAL CONDUCTOR DATA

Note: <u>layers are numbered starting from the outer layer inwards</u>. Here, layer 1 is always the outer layer.

A.1 Bersimis ACSR (Lanteigne, 1985)

Layer No	Young's Modulus MPa	Number of wires	Lay length mm	Lay angle degrees	Lay radius mm	Radius of wire mm
core	200×10^3	1	n/a	n/a	n/a	1.270
4	200×10^3	6	171	5.33	2.540	1.270
3	69×10^3	8	258	8.44	6.096	2.286
2	69×10^3	14	299	12.64	10.668	2.286
1	69×10^3	20	380	14.14	15.240	2.286

Table A. 1

Overall diameter of conductor: 35.05 mm
Rated Tensile Strength: 154.57 kN
Three aluminum layers (i = 1 to 3) and steel core (i = 4 and core wire)

A.2 Cardinal ACSR (Papailiou, 1995)

Layer No	Young's Modulus MPa	Number of wires	Lay length mm	Lay angle degrees	Lay radius mm	Radius of wire mm
core	210×10^3	1	n/a	n/a	n/a	1.67
4	180×10^3	6		6.06	3.34	1.67
3	65×10^3	12		11.99	6.67	1.66
2	65×10^3	18		12.64	9.99	1.66
1	65×10^3	24		14.14	13.31	1.66

Table A. 2

Also, from (EPRI, 2006):
Overall diameter of conductor: 30.378 mm
Rated Tensile Strength: 150.35 kN (Std. Weight Coating)
Three aluminum layers (i = 1 to 3) and steel core (i = 4 and core wire)

A.3   Drake ACSR

Layer No	Young's Modulus MPa	Number of wires	Lay length mm	Lay angle degrees	Lay radius mm	Radius of wire mm
core	200×10^3	1	n/a	n/a	n/a	1.735
3	200×10^3	6		5.0		1.735
2	69×10^3	10		12.96		2.221
1	69×10^3	16		15.67		2.221

Table A. 3

Overall diameter of conductor: 28.14 mm
Rated Tensile Strength: 140.12 kN
Two aluminum layers (i = 1 and 2) and steel core (i = 3 and core wire)

APPENDIX B

MISCELLANEOUS THEORETICAL PROOFS

B.1 DISTANCE BETWEEN CONTACT POINTS (STRAIGHT CONDUCTOR)

Lay angles on contact cylinders

Contact between layers (i) and (i+1) takes place on the contact cylinder, radius R_{Ci}. Points of contact are the intersection points of wire extreme "fibres": the inner one for layer (i), and the outer one for layer (i+1). These fibres are helical curves having practically the same lay length as the center line helix. However, because the contact cylinder radius is slightly different than the lay cylinder radius, the helix angle is also different.

Take for example layer (i) :

$$\tan \alpha_i' = \frac{2\pi(R_i - r_i)}{h_i} = \frac{2\pi R_i}{h_i} - \frac{2\pi r_i}{h_i}$$

$$\tan \alpha_i' = \tan \alpha_i - \frac{2\pi r_i}{h_i} = \left(1 - \frac{r_i}{R_i}\right)\tan \alpha_i$$

(B.1)

Since ratio r_i/h_i is small, the difference between α_i' and α_i is also small (at least for the outer layers.

Example B.1

Outer layer (i = 1) of Bersimis ACSR (Appendix A) :
$r_1 = 2.286$ mm
$h_1 = 380$ mm
$\alpha_1 = 14.14$ deg.

Figure B. 1

Eq. (B.1) yields $\alpha_1' = 12.09\,\text{deg}$.
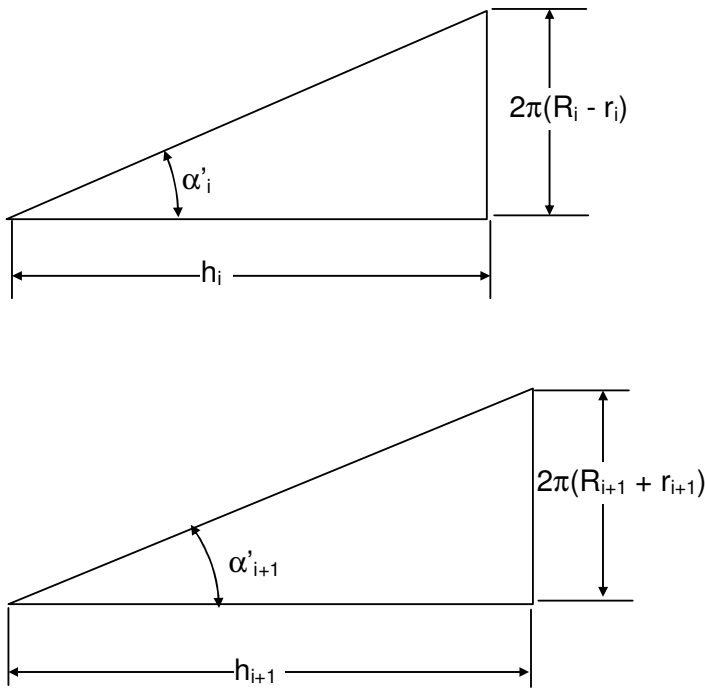
For complete results, use Matlab® file Example_B_1.m

Results:
Lay angle of wire centerline (deg.): [14.14 12.64 8.44 5.33]
Radius of contact cylinders (mm) :   [15.24 10.67 6.10 2.54]
Corrected lay angle of inside contact fiber (deg.) : [12.09 9.99 5.30 2.67]
Corrected lay angle of outside contact fiber (deg.) : [16.16 15.23 11.53 7.97]

Distance between points of contact on a given wire

Consider, for example, the case i = 1. Radius of contact cylinder $R_{C1} = R_1 - r_1 = R_2 + r_2$

Layer (1) contact fibres are, say, right-hand lay helices, while layer (2) contact fibers are left-hand helices. The problem is to find the distance between the intersection points of helix (1) with two adjacent helices (2).

It can be solved in the plane by "slitting" the contact cylinder along one of its generators and laying it flat (Fig. B.2). Helices are now straight lines. Line AA' is one of the helices (1). Assume A is a point where it is intersected by one helix (2). The next point of intersection will occur with the helix which is offset by a distance $AC = 2\pi R_{C1}/n_2$, n_2 being the number of wires in layer (2) on the vertical edge of the rectangle. Point B is the next point of intersection on AA'. Since the angles α'_1 and α'_2 are known, calculating the length of AB is now an elementary geometry problem.
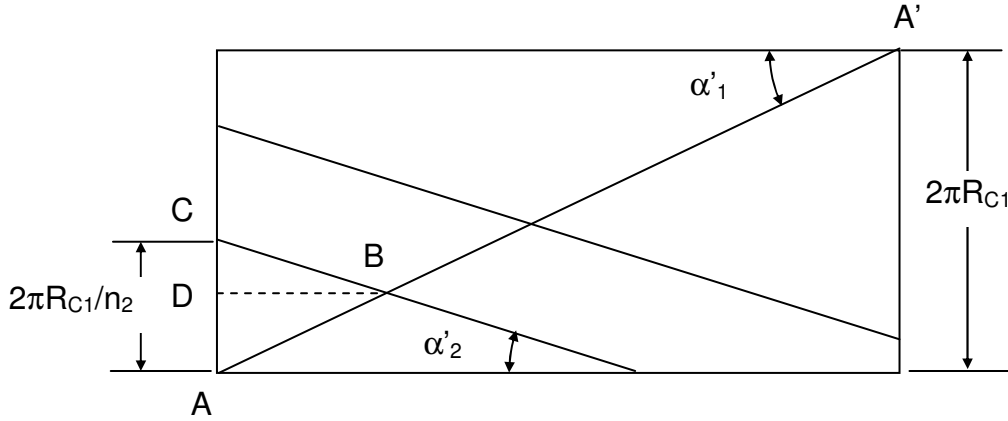
Figure B. 2

Calling D the orthogonal projection of point B on AC, one has:

$$DB = AB\cos\alpha'_1 = CB\cos\alpha'_2 \tag{B.2}$$

$$AC = \frac{2\pi R_{C1}}{n_2} = AB\sin\alpha'_1 + CB\sin\alpha'_2 \tag{B.3}$$

Combining Eqs (B.2) and (B.3), one gets:

$$AB = \frac{2\pi R_{C1}}{n_2}\frac{\cos\alpha'_2}{\sin(\alpha'_1 + \alpha'_2)} \tag{B.4}$$

It is easy to generalize it to any layer (i):

$$AB = d_{Ci} = \frac{2\pi R_{Ci}}{n_{i+1}}\frac{\cos\alpha'_{i+1}}{\sin(\alpha'_i + \alpha'_{i+1})} \tag{B.5}$$

where α'_i is the corrected lay angle for the inside contact fiber of layer (i) while α'_{i+1} is the corrected lay angle for the outside contact fiber of layer (i+1). This is the same equation as in Chouinard (1994),

except for the fact that, in his equation, the lay angles α_i and α_{i+1} have to be replaced by their corrected values α'_i and α'_{i+1}, given by Eq. (B.1).

Papailiou's Equation (Papailiou, 1995)

In Papailiou's thesis (1995), the number of contact points between layers (i) and (i+1), over a lay length of a wire in layers (i) and (i+1) is given in his Eqs (3.1) (layer i) and (3.2) (layer i+1) (page 46). For example, in layer (i), this number n_{Ci} is, using our notations:

$$n_{Ci} = n_{i+1} \left(\frac{R_i}{R_{i+1}} \frac{\tan \alpha_{i+1}}{\tan \alpha_i} + 1 \right) \tag{B.6}$$

where the plus sign has been selected in Eq. (3.1), corresponding to the usual alternate lay structure. Unfortunately, no details are given in (Papailiou, 1995) on how Eq. (B.6) was derived.

Now, accordingly, the axial distance (measured on the conductor x axis) of these contact points is:

$$d_{xi} = \frac{h_i}{n_{Ci}} = \frac{2\pi R_i}{\tan \alpha_i} \frac{1}{n_{i+1}} \frac{R_{i+1} \tan \alpha_i}{R_i \tan \alpha_{i+1} + R_{i+1} \tan \alpha_i} \tag{B.7}$$

which yields:

$$d_{xi} = \frac{1}{n_{i+1}} \frac{2\pi R_i R_{i+1}}{R_i \tan \alpha_{i+1} + R_{i+1} \tan \alpha_i} \tag{B.8}$$

The actual distance of contact points, measured on the wire centre line is:

$$d_{Ci} = \frac{d_{xi}}{\cos \alpha_i} = \frac{1}{n_{i+1}} \frac{1}{\cos \alpha_i} \frac{2\pi R_i R_{i+1}}{R_i \tan \alpha_{i+1} + R_{i+1} \tan \alpha_i} \tag{B.9}$$

Assuming layers (i) and (i+1) have equal wire radius r_i,

$$R_i = R_{Ci} + r_i \quad \text{and} \quad R_{i+1} = R_{Ci} - r_i \tag{B.10}$$

Letting the ratio $\gamma_i = r_i / R_{Ci}$, Eq. (B.9) yields:

$$d_{Ci} = \frac{2\pi R_{Ci}}{n_{i+1}} \frac{(1-\gamma^2) \cos \alpha_{i+1}}{(1+\gamma) \sin \alpha_{i+1} \cos \alpha_i + (1-\gamma) \sin \alpha_i \cos \alpha_{i+1}} \tag{B.11}$$

which can be compared with Eq. (B.5). Eq. (B.11) agrees with Chouinard's when γ is very small.

Example B.2

Consider the outer layer (layer 1) of the Bersimis ACSR conductor. Determine the distance between contact points on a given wire of this layer. Compare results given Eqs. (B.5) and (B.11).

<u>Results:</u>

From Example B.1: $\quad n_1 = 20 \quad n_2 = 14 \quad \alpha_1 = 14.14° \quad \alpha_2 = 12.64°$

$\quad R_{C1} = 15.24 \text{ mm} \quad \alpha_1' = 12.087° \quad \alpha_2' = 15.233°$

Eq. (B.5) yields $\quad d_{C1} = 14.38 \text{ mm}$ (Chouinard's equation yields 14.54 mm)

While in Eq. (B.11) $\quad \gamma_1 = r_1/R_{C1} = 2.286/15.24 = 0.15$ and $d_{C1} = 5.72 \text{ mm}$

B.2   NUMBER OF CONTACT POINTS

Number of contact points over a lay length of layer (i)

According to Eq. (B.5), the number of contact points n_{Cwi} between a wire of layer (i) and all wires of layer (i+1) over a lay length h_i of layer (i) is:

$$n_{Cwi} = \left\lfloor \frac{L_i}{d_{Ci}} + 1 \right\rfloor = \left\lfloor \frac{h_i}{\cos(\alpha')_i} \frac{n_{i+1}}{2\pi R_{Ci}} \frac{\sin(\alpha_i' + \alpha_{i+1}')}{\cos \alpha_{i+1}'} + 1 \right\rfloor \tag{B.12}$$

where L_i is the wire length . The notation $\lfloor x \rfloor$ is used to represent the integral part of x. It is also called the "floor function". The "1" term is added because there is one more contact point than the number of intervals $\lfloor L_i/d_{Ci} \rfloor$. This equation reduces to:

$$n_{Cwi} = \left\lfloor \frac{n_{i+1} \sin(\alpha_i' + \alpha_{i+1}')}{\sin \alpha_i' \cos \alpha_{i+1}'} + 1 \right\rfloor \tag{B.13}$$

It is the same as the one found by Chouinard (1994), apart from his use of helix angles α_i and α_{i+1} instead of α_i' and α_{i+1}' , and his neglect of the "floor function", leading to a number of points which is not an integer. Eq.(B.13) may also be written as:

$$n_{Cwi} = \left\lfloor 1 + n_{i+1}\left(1 + \frac{\tan \alpha_{i+1}'}{\tan \alpha_i'}\right) \right\rfloor \tag{B.14}$$

The total number of contact points at the interface between layers (i) and (i+1), over a lay length h_i of layer (i) is of course $n_i \times n_{Cwi}$.

Number of contact points over a conductor unit length at interface (i)

This calculation is performed in order to compare these results with a formula used by Rawlins (2009). The number of contact points on interface (i), over a conductor unit length is:

$$n_{Cui} = n_i \times \left| \frac{1}{h_i} \left(1 + n_{i+1} \left(1 + \frac{\tan \alpha'_{i+1}}{\tan \alpha'_i} \right) \right) \right| \tag{B.15}$$

which yields:

$$n_{Cui} = n_i \times \left| \frac{\tan \alpha'_i}{2\pi R_{Ci}} \left(1 + n_{i+1} \left(1 + \frac{\tan \alpha'_{i+1}}{\tan \alpha'_i} \right) \right) \right| \tag{B.16}$$

and:

$$n_{Cui} = n_i \times \left| \left(1 + n_{i+1} \right) \frac{\tan \alpha'_i}{2\pi R_{Ci}} + n_{i+1} \frac{\tan \alpha'_{i+1}}{2\pi R_{Ci}} \right| \tag{B.17}$$

Finally, in terms of the lay lengths, one gets:

$$n_{Cui} = n_i \times \left| n_{i+1} \left(\frac{1}{h_i} + \frac{1}{h_{i+1}} \right) + \frac{1}{h_i} \right| \tag{B.18}$$

Comparison with Rawlins (2009)

The number of contact points between a wire of layer (i) and wires of layer (i+1) over one lay length of layer (i) is given by Eq. (B.14), which can also be written in terms of lay lengths h_i and h_{i+1} as follows:

$$n_{Cwi} = \left| 1 + n_{i+1} \left(1 + \frac{\tan \alpha'_{i+1}}{2\pi R_{Ci}} \frac{2\pi R_{Ci}}{\tan \alpha'_i} \right) \right| = \left| 1 + n_{i+1} \left(1 + \frac{h_i}{h_{i+1}} \right) \right| \tag{B.19}$$

Using the present notations, corresponding Eq. (6) of Rawlins' paper may be written as follows:

$$n_{Cwi} = n_{i+1} \left(1 + \frac{h_i}{h_{i+1}} \right) \tag{B.20}$$

Apart from the floor brackets, it differs by 1 with Eq. (B.19). It is recalled this term has been justified above by the fact there is one more contact point than intervals between such points.

Also, the total contact points per unit length between layers (i) and (i+1), given by Eq. (B.18) may be compared with Rawlins' Eq. (10). Using the present notations, this equation may be written as follows:

$$\overline{n}_{Cui} = n_i n_{i+1} \left(\frac{1}{h_i} + \frac{1}{h_{i+1}} \right) \tag{B.21}$$

Apart from the floor brackets, Eqs (B.18) and (B.21) differ by a term n_i / h_i which comes from the one contact point difference mentioned above. It may or may not be considered as negligible, depending on the number of wires in layers (i) and (i+1).

Example B.3

Data for the conductor Bersimis ACSR are found in Appendix A. Compare the number of contact points between layers (1) and (2).

From Appendix A : $n_1 = 20 \quad n_2 = 14 \quad h_1 = 0.380\,\mathrm{m} \quad h_2 = 0.299\,\mathrm{m}$.

Results:
Eq. (B.18) yields: $n_{Cu1} = 1720\,\mathrm{m}^{-1}$
Eq. (B.21) yields: $\bar{n}_{Cu1} = 1673\,\mathrm{m}^{-1}$, a 2.7% difference.

Now, consider layers (3) and (4) with $n_3 = 8 \quad n_4 = 6 \quad h_3 = 0.258\,\mathrm{m} \quad h_4 = 0.171\,\mathrm{m}$
Eq. (B.18) yields: $n_{Cu3} = 496\,\mathrm{m}^{-1}$
Eq. (B.21) yields: $\bar{n}_{Cu3} = 466\,\mathrm{m}^{-1}$, a 6% difference.

B.3   A TRIGONOMETRIC IDENTITY

In the calculation of the complementary bending stiffness of a single layer, and also in a multi-layer strand, one encounters the following summation, resulting from the contribution of the n wires of a given layer: $\sum_{k=1}^{n} \sin^2 k\theta_n$ with $\theta_n = \dfrac{2\pi}{n}$. It can be shown the summation can easily be obtained from the following identity:

$$\sum_{k=1}^{n} \sin^2 k\theta_n = \frac{n}{2} \tag{B.22}$$

(Here, we dispense with noting n_i, the number of wires in layer (i)).

Papailiou (1995) has given a proof of identity (B.22). We propose the following approach based on the complex number geometrical representation in the Argand-Gauss plane. First, recall the identity:

$$\sin^2 \theta = \frac{1}{2}(1 - \cos 2\theta) \tag{B.23}$$

Thus:

$$\sum_{k=1}^{n} \sin^2 k\theta_n = \sum_{k=1}^{n} \frac{1}{2}(1 - \cos 2k\theta_n) = \frac{n}{2} - \frac{1}{2}\sum_{k=1}^{n} \cos 2k\theta_n \tag{B.24}$$

Consider now the second term in the right-hand side. It is the real part of the exponential analytic function $e^{i(2k\theta_n)}$. In the complex plane, it is represented by a vector joining the origin to a point on the unit circle. This vector makes an angle $\theta = 2k\theta_n = 2k\dfrac{2\pi}{n}$ with the real axis. Thus, the sum $\sum_{k=1}^{n} e^{i(2k\theta_n)}$ may be considered as the sum of n unit vectors making equal angles.

If the number n of wires in a layer is even (the usual case), the n vectors reduce to n/2 vectors making a $4\pi/n$ angle (Fig. 3, with n = 12). The sum of these vectors is clearly the null vector, which means both the real and the imaginary parts of $\sum_{k=1}^{n} e^{i(2k\theta_n)}$ are zero. The second term of Eq. (B.24) right-hand side vanishes, and Eq. (B.22) is proved.

If the number n is odd, it is easy to check that the n terms in the sum $\sum_{k=1}^{n} e^{i(2k\theta_n)}$ are represented by n distinct vectors making a $2\pi/n$ angle, and the same result holds.
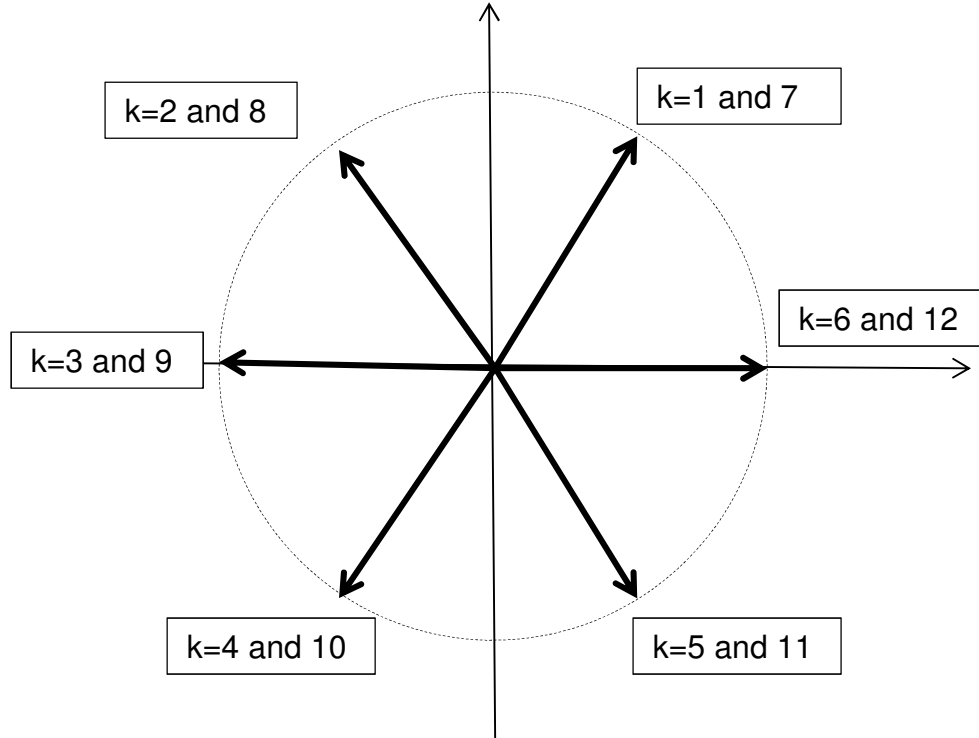
Figure B. 3   Example : n = 12, $\theta_n = \pi/3$

APPENDIX C

RHEOLOGICAL MODEL FOR A MULTILAYER CONDUCTOR IN BENDING

C.1   INTRODUCTION

It is shown in Chapter 3 that the moment-curvature diagram of a multilayer conductor in bending may be adequately represented by a polygonal line. This linearization eliminates the slip propagation phases and assumes slip of one layer on the adjacent one takes place instantaneously.

In such linearized diagram, the slope of the first segment (which starts at the origin) is $B_0 = B_{max}$, the conductor maximum bending stiffness, which is obtained by assuming strands behave as in a solid bar, with zero slip at contact points. When the imposed curvature reaches value $\kappa_{m,1}$, the first layer slips on the adjacent one. Symmetry conditions impose zero displacement at points located on the extrados (convex side) and intrados (concave side) of the bent conductor. Slip allows a small displacement of strand material from the compression zone to the tension zone. Beyond this value of curvature, slope of the second segment is B_1, which applies up to curvature $\kappa_{m,2}$ etc. This slope is the conductor tangential stiffness. When layer (m) is also in the slip regime, slope becomes $B_m = B_{min}$, obtained by assuming wires are completely free to bend independently from one another.

For a given conductor, transition curvatures do depend on the imposed axial load T, on the coefficient of friction μ_i between layers, and also on the type of hypothesis which is made on the influence of outer layers on the inner ones.

C.2   RHEOLOGICAL MODEL

It has been shown in the single layer case, Chapter 2, that the (M vs κ) diagram could be linearized using a rheological model based on a system consisting of springs and sliders (Figs 2.8 and 2.9). The multilayer conductor case may be treated in the same way. For example, a four-layer conductor may be represented with the model shown in Fig. C.1. It is made of four spring-slider couples (SP_i)-(SL_i) plus a single spring whose stiffness is $k_0 = B_{max}$ the zero-slip stiffness of the conductor, when bending starts. Each slider (SL_i) has a limit moment $M_{m,i}$ below which it is rigid. Each spring (SP_i) has a stiffness k_i which is calculated as follows.

When limit curvature $\kappa_{m,1}$ is reached, layer (1) slips, which means slider (SL_1) is activated. As shown in Chapter 2, spring stiffness k_1 is given by:

$$\frac{1}{k_1} = \frac{1}{B_1} - \frac{1}{B_0} \tag{C.1}$$

When limit curvature $\kappa_{m,i}$ is reached, slider (SL_i) starts slipping. Total curvature is:

$$\kappa = \frac{M}{k_0} + \frac{M - M_{m,1}}{k_1} + \frac{M - M_{m,2}}{k_2} + \cdots + \frac{M - M_{m,i}}{k_i} \tag{C.2}$$
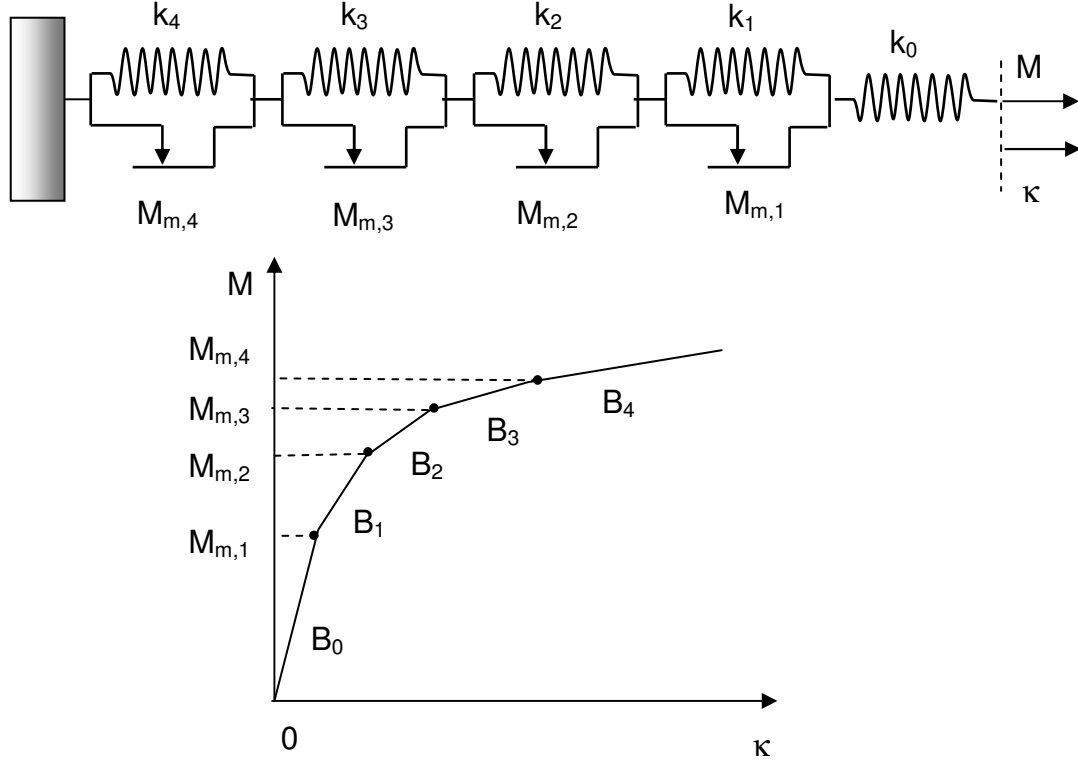

Figure C. 1

The slope of the corresponding segment is given by :

$$\frac{d\kappa}{dM} = \frac{1}{B_i} = \frac{1}{k_0} + \frac{1}{k_1} + \frac{1}{k_2} + \cdots + \frac{1}{k_i} = \sum_{j=0}^{i} \frac{1}{k_j} \tag{C.3}$$

yielding :

$$\frac{1}{k_i} = \frac{1}{B_i} - \sum_{j=0}^{i-1} \frac{1}{k_j} \tag{C.4}$$

Which leads to the simpler equation :

$$\frac{1}{k_i} = \frac{1}{B_i} - \frac{1}{B_{i-1}} \tag{C.5}$$

Because of the sequential slip process, layer (i) slips after layer (i-1) and condition $B_i < B_{i-1}$ is always satisfied. Thus, one has $k_i > 0$.

Example C.1a

Consider the Bersimis ACSR with the same hypotheses as in Example 3.7: uniform coefficient of friction between layers, $\mu_i = 0.7$; axial load T = 30% RTS; slip conditions (SC5). In order to apply the above rheological model, determine each spring element stiffness k_i (i = 0,…,4).

Available Matlab® file : Example_C_1.m (case 1)
Results:
Stiffness B_i after layer (i) complete slip is (Example 3.7)
$B = [1.0842 \quad 0.2458 \quad 0.0828 \quad 0.0635] \, 10^9 \, \text{N.mm}^2$

Spring element stiffness k_i (Eq. (C.5)) are :
$k_0 = B_0 = B_{max} = 3.4832 \times 10^9 \, \text{N.mm}^2$ (Example 3.1a)
$k = [1.5742 \quad 0.3179 \quad 0.1249 \quad 0.2724] \, 10^9 \, \text{N.mm}^2$

Example C.1b

Consider the Cardinal ACSR with the same hypotheses as in Example 3.8: uniform coefficient of friction between layers, $\mu_i = 0.7$; axial load T = 40 kN; slip conditions (SC2). In order to apply the above rheological model, determine each spring element stiffness k_i (i = 0,…,4).

Available Matlab® file : Example_C_1.m (case 2)

Results:
Stiffness B_i after layer (i) complete slip is (Example 3.8)
$B = [6.8280 \ 2.0612 \ 0.7873 \ 0.2775] \, 10^8 \, \text{N.mm}^2$

Spring element stiffness k_i (Eq. (C.5)) are :
$k_0 = B_0 = B_{max} = 1.7846 \times 10^9 \, \text{N.mm}^2$ (Example 3.1b)
$k = [1.7846 \ 1.1059 \ 0.2952 \ 0.1274 \ 0.0429] \, 10^9 \, \text{N.mm}^2$

C.3   APPLICATION OF RHEOLOGICAL MODEL

The spring-slider model is particularly useful to study non-monotonous loadings such as those found in vibration. The properties of this model have been described in detail by Dowling (1993) in the context of elasto-plastic material behaviour. Some of these properties will be briefly summarized. It will be found that they lead to Papailiou's results in his thesis (1995), which have been derived for the particular case of conductor bending.

It is assumed a conductor has been imposed a monotonous curvature loading, up to complete slip of layer (i). On the (M vs κ) diagram, the conductor is at point A_0 (M_0, κ_0), on segment (i), slope B_i. Then, assume the applied moment is slowly decreased. The sliders which had been activated are then blocked in their current position. The spring-slider couples (SP_i)-(SL_i) are again rigid and elongation κ_i in spring (SP_i) is frozen.
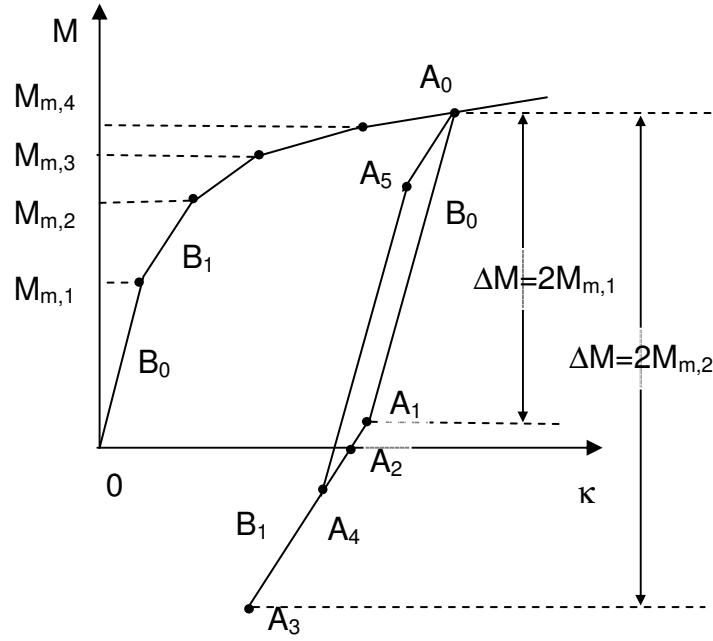
Figure C. 2

Moment decrease ΔM affects only spring (SP_0), leading to a curvature decrease $\Delta\kappa = \Delta M/B_0$. Thus, the unloading curve is a straight line, with a slope B_0. On couple (1), this moment unloading is entirely absorbed by the slider (as the spring elongation is maintained constant, as well as the corresponding moment M_0-$M_{m,1}$). At any time, the force on the slider is $M_{m,1} - \Delta M$ and it remains rigid as long as the condition $|M_{m,1} - \Delta M| < M_{m,1}$ is satisfied. Whenever $\Delta M = 2M_{m,1}$, the slider is released and there is incipient slip in the opposite direction, which allows spring (SP_1) to contract. In the conductor on which the imposed curvature is undergoing a decrease, this corresponds to a reverse slip of the outer layer (layer 1). The subsequent moment decrease follows a straight line with slope B_1, up to the point where $\Delta M = 2M_{m,2}$ (Fig. C.2, point A_3). Then, slider (SL_2) is released, and the unloading curve is the straight line with slope B_2. The same process will apply eventually to the other spring-slider couples. When $\Delta M = M_0$ (point A_2), the moment imposed onto the conductor vanishes. However, there is a residual, or permanent, curvature κ_2.

Now, assume that at point A_4 (M_4,κ_4), for $2M_{m,1} < \Delta M < 2M_{m,2}$, moment M is increased. Slider (SL_1) again becomes rigid and curvature variation comes from spring (SP_0) only, and follows a B_0 slope straight line. If moment variation amplitude is $\Delta M = M_0 + |M_4|$ (ΔM being taken from the A_4 level), slider (SL_1) is unlocked, and the load diagram is now a B_1 slope segment A_5A_0, back to the unloading point A_0. The unload-load diagram is a closed cycle. As shown by Papailiou (1995), the area enclosed in this cycle corresponds to the dissipated energy from the friction forces.

In a sustained vibratory motion, the load point follows a trajectory such as ($A_0A_1A_4A_5A_0$) and the energy dissipated might be used to evaluate a damping factor.

For small amplitude vibrations, the load-unload cycle is merely a segment A_0A_1, with slope B_0. Thus, in principle, the cycle area vanishes, and such cyclic bending vibrations should correspond to zero damping. It is well known this is not the case. Damping is present, even at very small amplitudes.

Such deviation of the model with respect to the actual conductor behaviour arises from the fact it is based on a simple macroscopic expression of Coulomb's law of friction. That is, it does not take into account the fact that, at contact points, which are contact regions, there always is some microslip occurring as soon as a tangential load is applied to the contacting bodies (here, the contacting strands), even when this tangential load is too small to induce gross slip between these bodies. This matter is quite important, as it is related to the fretting fatigue process, which often leads to conductor strand breaks.

APPENDIX D

THE TRANSFER MATRIX METHOD (TMM)
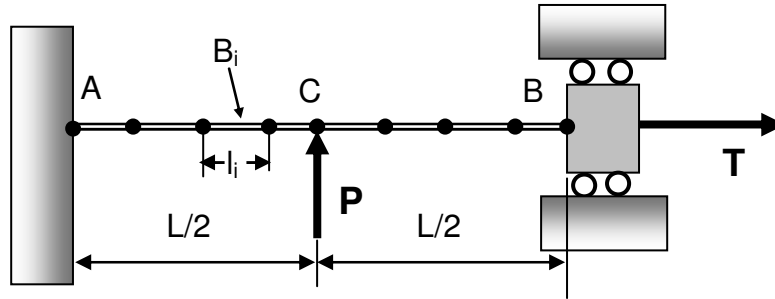
Figure D. 1

Specimen AB is replaced with a series of beam elements, length l_i and bending stiffness B_i. Consider element (i) free-body diagram. In the present case, the only external loads are forces T and P, at nodes A, B, and C. Shear force has a constant value in AC and CB.

D.1   EQUILIBRIUM EQUATIONS FOR ELEMENT (i) (2D PROBLEM)

In order to obtain the general form of the equilibrium equations for a plane problem, the possible nodal forces and moments acting on nodes (i) and (i+1) are shown in Fig. D.2. Since only static cases are considered, there are no "inertia forces" on the element.
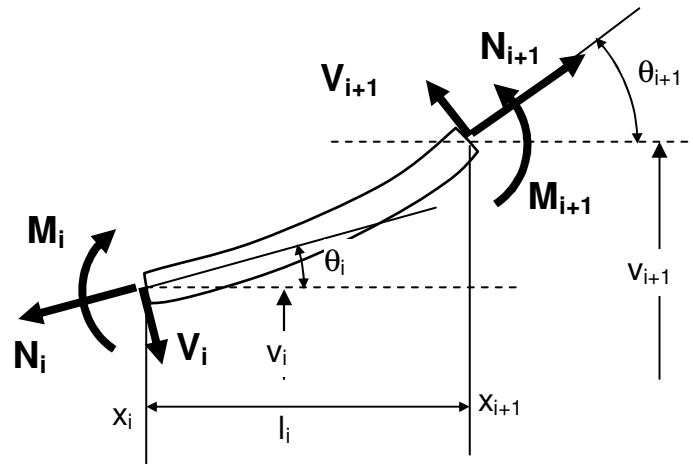
Figure D. 2

For element (i), length l_i, node (i) displacement is v_i, and rotation of the tangent of the bent element at the same node is θ_i. Nodal forces and moment are: normal force N_i, shear force V_i, and bending moment M_i. At node (i+1), corresponding components are $(v_{i+1}, \theta_{i+1}, N_{i+1}, V_{i+1}, M_{i+1})$. The three equilibrium equations are:

$$N_{i+1} \cos \theta_{i+1} - V_{i+1} \sin \theta_{i+1} + V_i \sin \theta_i - N_i \cos \theta_i = 0$$
$$N_{i+1} \sin \theta_{i+1} + V_{i+1} \cos \theta_{i+1} - V_i \cos \theta_i - N_i \sin \theta_i = 0 \qquad \text{(D.1)}$$
$$M_{i+1} - M_i + N_{i+1} \sin \theta_{i+1} \ell_i + V_{i+1} \cos \theta_{i+1} \ell_i - N_{i+1} \cos \theta_{i+1} (v_{i+1} - v_i) + V_{i+1} \sin \theta_{i+1} (v_{i+1} - v_i) = 0$$

The first two equations are used to simplify the moment equation, yielding:

$$M_{i+1} = M_i - N_i \ell_i \sin \theta_i - V_i \ell_i \cos \theta_i + N_i \cos \theta_i \Delta v_i - V_i \sin \theta_i \Delta v_i \qquad \text{(D.2)}$$

where $\Delta v_i = v_{i+1} - v_i$

Now, it is assumed angles θ_i and θ_{i+1} are small, as are displacements (or, at least, the relative displacement Δv_i). This hypothesis yields:

$$N_{i+1} - V_{i+1} \theta_{i+1} \cong -V_i \theta_i + N_i$$
$$N_{i+1} \theta_{i+1} + V_{i+1} \cong +V_i + N_i \theta_i \qquad \text{(D.3)}$$
$$M_{i+1} \cong M_i - N_i \ell_i \theta_i + N_i \Delta v_i - V_i \ell_i$$

D.2   TRANSFER MATRIX FOR ELEMENT (i)

In order to use the TM method, equations have to be linear. Thus, variation of the normal force on the element, which depends on cosines of angles θ_i and θ_{i+1}, is assumed to be negligible. Thus:

$$N_i \cong N_{i+1} \cong T \qquad \text{(D.4)}$$

For a section located at abscissa x, between nodes (i) and (i+1), the bending moment M(x) is thus approximately (keeping N_i in the equation):

$$M(x) = M_i - N_i (x - x_i) \theta_i + N_i (v(x) - v_i) - V_i (x - x_i) \qquad \text{(D.5)}$$

In the case of a conductor, moment M(x) is the combination of two components. One comes from the elastic bending behaviour. The other comes from the friction residual moment $M_{rf,i}$ (moment with respect to the section neutral axis, of strand residual axial force when the corresponding layer is in the slip phase). The classical beam bending equation between curvature and moment applies only to the elastic component. It yields:

$$B_i \kappa(x) = B_i \frac{d^2 v}{dx^2} = M(x) - k_i M_{rf,i} \qquad \text{(D.6)}$$

in which $k_i = \text{sign}(M)$. Indeed, the $M_{rf,i}$ has to decrease the absolute value of M(x). Also, in the Fig. D.1 system, there is no ambiguity on the sign of the M(x) function for any element. In the inflexion point region, where such ambiguity could exist, there is obviously no slip, and no residual friction moment.

Thus, from Eq. (D.5) :

$$B_i v'' - N_i v = (M_i - M_{rf,i} - N_i v_i + V_i x_i + N_i \theta_i x_i) - (N_i \theta_i + V_i) x \qquad (D.7)$$

Residual friction moment $M_{rf,i}$ will be assumed to be uniform in element (i). That is, the whole element is assumed to be in the same slip stage, as if having a uniform curvature.

Now, Eq. (D.7) may be written in the simpler following form:

$$v'' - \lambda_i^2 v = a_i - b_i x \qquad (D.8)$$

where:

$$\lambda_i^2 = \frac{N_i}{B_i} \qquad a_i = \frac{1}{B_i}(M_i - k_i M_{rf,i} - N_i v_i + V_i x_i + N_i \theta_i x_i) \qquad b_i = \frac{1}{B_i}(V_i + N_i \theta_i) \qquad (D.9)$$

One particular solution to Eq. (D.9) is:

$$v_{pi}(x) = C_{1i} + C_{2i} x \qquad (D.10)$$

where:

$$C_{1i} = -\frac{a_i}{\lambda_i^2} = -\frac{1}{N_i}(M_i - k_i M_{rf,i} - N_i v_i + V_i x_i + N_i \theta_i x_i)$$

$$C_{2i} = \frac{b_i}{\lambda_i^2} = \frac{V_i}{N_i} + \theta_i \qquad (D.11)$$

The complete solution to Eq. (D.8) may be written as follows:

$$v(x) = C_{1i} + C_{2i} x + C_{3i} \sinh \lambda_i x + C_{4i} \cosh \lambda_i x \qquad (D.12)$$

Constants C_{3i} and C_{4i} can be expressed using node (i) parameters v_i, θ_i. After rearranging terms, one gets:

$$C_{3i} = -\frac{1}{N_i}(M_i - k_i M_{rf,i}) \sinh \lambda_i x_i - \frac{V_i}{\lambda_i N_i} \cosh \lambda_i x_i$$

$$C_{4i} = \frac{1}{N_i}(M_i - k_i M_{rf,i}) \cosh \lambda_i x_i + \frac{V_i}{\lambda_i N_i} \sinh \lambda_i x_i \qquad (D.13)$$

Similarly, node (i+1) parameters, v_{i+1}, θ_{i+1}, are given by:

$$v_{i+1} = C_{1i} + C_{2i} x_{i+1} + C_{3i} \sinh \lambda_i x_{i+1} + C_{4i} \cosh \lambda_i x_{i+1}$$

$$\theta_{i+1} = 0 + C_{2i} + \lambda_i C_{3i} \cosh \lambda_i x_{i+1} + \lambda_i C_{4i} \sinh \lambda_i x_{i+1} \qquad (D.14)$$

Using the classical hyperbolic sine and cosine identities, parameters v_{i+1}, θ_{i+1} may be expressed in terms of node (i) parameters v_i, θ_i :

$$v_{i+1} = v_i + \theta_i \ell_i + \frac{\ell_i}{N_i}\left(1 - \frac{\sinh \lambda_i \ell_i}{\lambda_i \ell_i}\right)V_i + \frac{1}{N_i}(\cosh \lambda_i \ell_i - 1)(M_i - k_i M_{rf,i})$$

$$\theta_{i+1} = 0 + \theta_i - \frac{1}{N_i}(\cosh \lambda_i \ell_i - 1)V_i + \frac{\lambda_i}{N_i}\sinh \lambda_i \ell_i (M_i - k_i M_{rf,i})$$

(D.15)

Also, looking at the linearized equilibrium equations D.3, it is found V_{i+1} et M_{i+1} may be expressed in terms of node (i) parameters:

$$V_{i+1} = \cosh \lambda_i \ell_i \, V_i - \lambda_i \sinh \lambda_i \ell_i (M_i - k_i M_{rf,i})$$

$$M_{i+1} - k_i M_{rf,i} = -\frac{\sinh \lambda_i \ell_i}{\lambda_i}V_i + \cosh \lambda_i \ell_i (M_i - k_i M_{rf,i})$$

(D.16)

Thus, the four state variables $(v_{i+1}, \theta_{i+1}, V_{i+1}, M_{i+1})$ at node (i+1) are seen to be linearly related to the corresponding variables at node (i) $(v_i, \theta_i, V_i, M_i)$ through four equations D.15 and D.16. These equations may be written in matrix form as follows (Pilkey, 2002) :

$$\{s\}_{i+1} = [U]_i \{s\}_i$$

(D.17)

Vectors $\{s\}_i$ et $\{s\}_{i+1}$ are the value of the state vector at nodes (i) and (i+1), which is defined as:

$$\{s\} = \begin{bmatrix} v \\ \theta \\ V \\ M \\ 1 \end{bmatrix}$$

(D.18)

and $[U]_i$ is the 5×5 transfer matrix of element (i) :

$$[U]_i = \begin{bmatrix} u_{11} & u_{12} & u_{13} & u_{14} & u_{15} \\ u_{21} & u_{22} & u_{23} & u_{24} & u_{25} \\ u_{31} & u_{32} & u_{33} & u_{34} & u_{35} \\ u_{41} & u_{42} & u_{43} & u_{44} & u_{45} \\ u_{51} & u_{52} & u_{53} & u_{54} & u_{55} \end{bmatrix}_i$$

(D.19)

Matrix elements are:

$$u_{11} = u_{22} = u_{55} = 1 \quad u_{21} = u_{31} = u_{32} = u_{41} = u_{42} = u_{51} = u_{52} = u_{53} = u_{54} = 0$$

$$u_{12} = \ell_i \quad u_{13} = \frac{\ell_i}{N_i}\left(1 - \frac{\sinh\lambda_i\ell_i}{\lambda_i\ell_i}\right) \quad u_{14} = \frac{1}{N_i}\left(\cosh\lambda_i\ell_i - 1\right) \quad u_{15} = -\frac{k_i}{N_i}\left(\cosh\lambda_i\ell_i - 1\right)M_{rf,i}$$

$$u_{23} = -\frac{1}{N_i}\left(\cosh\lambda_i\ell_i - 1\right) \quad u_{24} = \frac{\lambda_i}{N_i}\sinh\lambda_i\ell_i \quad u_{25} = -\frac{k_i\lambda_i}{N_i}\sinh\lambda_i\ell_i\, M_{rf,i} \tag{D.20}$$

$$u_{33} = \cosh\lambda_i\ell_i \quad u_{34} = -\lambda_i\sinh\lambda_i\ell_i \quad u_{35} = k_i\lambda_i\sinh\lambda_i\ell_i\, M_{rf,i}$$

$$u_{43} = -\frac{1}{\lambda_i}\sinh\lambda_i\ell_i \quad u_{44} = \cosh\lambda_i\ell_i \quad u_{45} = -k_i\left(\cosh\lambda_i\ell_i - 1\right)M_{rf,i}$$

In principle, it is thus possible to proceed sequentially from node (1) values, to node (2), and then node (3) etc. However, one parameter is unknown at the built-in end point A, which is the value of the end moment $M_1 = M_A$. The missing condition is found at center point C where, by symmetry, the vanishing slope yields $\theta(L/2) = 0$. With n elements in the domain $0 \le x \le L/2$, a relationship between M_1 et θ_{n+1} has to be found. It is obtained through the product of the n matrices $[U]_i$. The resulting matrix $[U]$ is given by :

$$[U] = \prod_{i=n}^{1}[U]_i \tag{D.21}$$

which has the form :

$$[U] = \begin{bmatrix} u_{vv} & u_{v\theta} & u_{vV} & u_{vM} & f_v \\ u_{\theta v} & u_{\theta\theta} & u_{\theta V} & u_{\theta M} & f_\theta \\ u_{Vv} & u_{V\theta} & u_{VV} & u_{VM} & f_V \\ u_{Mv} & u_{M\theta} & u_{MV} & u_{MM} & f_M \\ 0 & 0 & 0 & 0 & 1 \end{bmatrix} \tag{D.22}$$

Thus, the sought for relation between node (1) and node (n+1) state variables is:

$$\{s\}_{n+1} = [U]\{s\}_1 \tag{D.23}$$

where :

$$\{s\}_{n+1} = \begin{bmatrix} v_{n+1} \\ \theta_{n+1} \\ V_{n+1} \\ M_{n+1} \\ 1 \end{bmatrix} = \begin{bmatrix} \delta_C \\ 0 \\ V_C \\ M_C \\ 1 \end{bmatrix} \qquad \{s\}_1 = \begin{bmatrix} v_1 \\ \theta_1 \\ V_1 \\ M_1 \\ 1 \end{bmatrix} = \begin{bmatrix} 0 \\ 0 \\ P/2 \\ M_A \\ 1 \end{bmatrix} \tag{D.24}$$

Thus, Eq. (D.23) yields :

$$\delta_C = u_{vV}\frac{P}{2} + u_{vM}M_A + f_v$$

$$0 = u_{\theta V}\frac{P}{2} + u_{\theta M}M_A + f_\theta$$

$$V_C = u_{VV}\frac{P}{2} + u_{VM}M_A + f_V \tag{D.25}$$

$$M_C = u_{MV}\frac{P}{2} + u_{MM}M_A + f_M$$

The second equation yields an expression for the built-in moment M_A :

$$M_A = -\frac{f_\theta}{u_{\theta M}} - \frac{u_{\theta V}}{u_{\theta M}}\frac{P}{2} \tag{D.26}$$

Replacing M_A in the first equation yields an expression for the center point deflection δ_C :

$$\delta_C = \left(u_{vV} - u_{vM}\frac{u_{\theta V}}{u_{\theta M}}\right)\frac{P}{2} - \frac{u_{vM}}{u_{\theta M}}f_\theta + f_v \tag{D.27}$$

D.3 MONOTONOUSLY INCREASING TRANSVERSE FORCE P

In order to obtain the δ_C vs P curve (or, equivalently, P vs δ_C), one should evaluate the matrix $[U]_i$ for each element and take the product $[U]$ as in Eq. (D.21). Once the elements of matrix $[U]$ are known, deflection δ_C is found from Eq. (D.27).

The difficult part is in finding the $[U]_i$ matrices, since they depend on which slip phase is the corresponding element. As slip propagates from points A and C, an increment method has to be used. Starting from P = 0, the transverse force is increased by steps ΔP. After each increment, boundaries between slip zones are found and bending stiffness B_i for each element is determined from the uniform curvature bending diagram of the conductor. With stiffness B_i , the element transfer matrix $[U]_i$ is found.

Because the element properties vary during the loading process, one has to analyze the conductor specimen deflection step by step. At each level of loading, P, one has to determine the slip stage of each element. Then, using the corresponding stiffness, calculate the supplementary deflection from the load increment ΔP. These deflection and moment increments are then added to their current values and element slip stages are then updated.

The algorithm should check first what is the limit force P_1 for which outer layer slip starts. If $P_{max} > P_1$, the deflection at P = P_1 is easily obtained which provides the initial value of deflection v_i as well as node moments M_i . From this level on, the calculation has to proceed step by step.

At a given stage, stiffness matrices $[U]_i$ are known, as well as their product $[U]$. The increments $\{\Delta s\}_i$ and $\Delta \delta_C$ arising from ΔP can be calculated from Eq. (D.27). Vectors $\{s\}_i$ are then updated, as well as the $[U]_i$ element matrices.

D.4 TAKING INTO ACCOUNT NORMAL FORCE N VARIATION

Because of the slope of the bent specimen, normal force N varies slightly when the axial force applied at the end B is kept a constant T. Thus, in the TMM, a corrected value may be used in the following way.

Element (i) transfer matrix is first determined with value N_i = T. Then, new values are found for each element, starting with N_1 = T, using the first equilibrium equation in Eqs (D.3) (the last two are used to determine M_{i+1}):

$$N_{i+1} = N_i + V_{i+1}\theta_{i+1} - V_i\theta_i \tag{D.28}$$

After the first iteration, parameters (θ_i, V_i) have been found. Starting at node (1), where N_1 = T, and using Eq. (D.28), a corrected value of N_i can be obtained in each element. This value can be used in the next load increment to calculate the current $[U]_i$ stiffness matrices.

D.5 APPLICATION: CURVE P vs δ_C FROM Example 4.5

Figure D. 3

Example 4.5 – P vs δ_C

94

INDEX

torus (circular)   16,33
Transfer Matrix Method (TMM)   59,87
trellis contact patch   2,33
Young's modulus   73,74